

Quantification of single-tree structure in mountain forests using terrestrial laser scanning

Di Wang

June 7, 2018
Vienna, Austria

Die approbierte Originalversion dieser
Dissertation ist in der Hauptbibliothek der
Technischen Universität Wien aufgestellt und
zugänglich.

<http://www.ub.tuwien.ac.at>



The approved original version of this thesis is
available at the main library of the Vienna
University of Technology.

<http://www.ub.tuwien.ac.at/eng>



Dissertation

Quantification of single-tree structure in mountain forests using terrestrial laser scanning

Ausgeführt zum Zwecke der Erlangung des akademischen Grades eines
"Doktor der technischen Wissenschaften (Dr.techn.)"

Unter der Leitung von
Univ.Prof. Dipl.-Ing. Dr.techn. Norbert Pfeifer

und der Mitbetreuung von
Dipl.-Ing. Dr.techn. Markus Hollaus

E120.7
Department für Geodäsie und Geoinformation
Forschungsgruppe Photogrammetrie

Eingereicht an der der Technischen Universität Wien
Fakultät für Mathematik und Geoinformation

von

MSc. Di Wang

Matrikelnummer: 01528356



Dissertation

**Quantification of single-tree structure in
mountain forests using terrestrial laser
scanning**

A thesis submitted in fulfillment of the academic degree of
"Doktor der technischen Wissenschaften (Dr.techn.)"

Under the supervision of
Univ.Prof. Dipl.-Ing. Dr.techn. Norbert Pfeifer

and the co-supervision of
Dipl.-Ing. Dr.techn. Markus Hollaus

E120.7
Department of Geodesy and Geoinformation
Research Group Photogrammetry

Research conducted at TU Wien
Faculty of Mathematics and Geoinformation

by

MSc. Di Wang

Matriculation number: 01528356

Reviewer:

Prof. Christian Heipke

Institute of Photogrammetry and GeoInformation
Leibniz Universität Hannover

Reviewer:

Dr. Kenneth Olofsson

Department of Forest Resource Management
Swedish University of Agricultural Sciences

Di Wang

Quantification of single-tree structure in mountain forests using terrestrial laser scanning

Dissertation, June 7, 2018

Supervisors: Prof. Norbert Pfeifer and Dr. Markus Hollaus

Technische Universität Wien

Photogrammetry Group

Faculty of Mathematics and Geoinformation

Department of Geodesy and Geoinformation

Gußhausstraße 27-29

1040 Vienna, Austria

Abstract

Mountain forests provide a great deal of values, ranging from protection against natural hazards, timber production, biodiversity conservation, to carbon storage and climate change mitigation. Understanding and monitoring the detailed structure information at the single-tree level in mountain forests is equally important as area-wide assessments to sustainably managing these mountain forest services. Fine-scale three dimensional (3D) forest structures can be assessed by using terrestrial laser scanning (TLS) systems, which provide accurate and high-resolution measurements (i.e., 3D point clouds) of objects. TLS has greatly advanced single-tree quantifications by successfully extracting attributes such as tree stem location, diameter, stem curve, stem volume and biomass components. However, existing approaches are mainly developed for managed forests or those in flat environments. Due to factors such as site fertility, spacing and light conditions, wind, and landslide events, mountain forests have more complex below-canopy structures mainly featuring multifarious understory, stems with non-vertical orientations and cross-sections that differ significantly from a circular shape. These impacts make it difficult to directly apply existing methods in mountain forests. This dissertation tackles such challenges by developing novel methods that overcome the high degree of complexity in processing TLS data acquired in mountain forests. The work in this dissertation focuses on methodology developments specifically associated to three scientific objectives; (a) separation of tree wood and leaf components; (b) tree stem detection and modeling in mountain landslide-affected forests; and (c) reconstruction of stem cross-sections. A side focus is also paid on smart point cloud structuring in order to assist the processing of large volume point cloud data. Firstly, an empirical study is carried out to examine the feasibility of four popular supervised machine learning methods and the impact of feature calculation. A follow-up work develops a novel approach that is fully automatic and unsupervised. Experiments confirm its strength in separating wood and leaf components for plot-level mountain forests. Second, a new method is introduced that detects and reconstructs tree stems with irregular vertical orientations. The reconstructed stems reach high accuracy compared to field references. Lastly, a new method is developed to model the actual shape of stem cross-sections, which breaks down the assumption that the cross-section of tree stems is circular. These works conducted in this dissertation provide practical examples and guidelines for understanding

mountain forest structures at the single-tree level, and at the same time demonstrate that the required data processing can be largely automated. These contributions can help to achieve more intelligent and sustainable mountain forest managements in the future.

Kurzfassung

Gebirgswälder stellen für eine Vielzahl von Bereichen einen Nutzen dar, von Schutz vor Naturgefahren über die Holzproduktion, den Erhalt der Biodiversität bis hin zu Kohlenstoffspeicherung und Milderung des Klimawandels. Für eine nachhaltige Bewirtschaftung der Gebirgswälder ist dabei das Verständnis und die Überwachung der detaillierten Struktur auf Einzelbaum-Niveau von ebenso großer Bedeutung wie deren flächenbasierte Bewertung. Die feinskalige, drei-dimensionale (3D) Waldstruktur kann mittels terrestrischem Laserscanning (TLS) ausgewertet werden, was genaue, hochauflösende Messungen (3D-Punktwolken) der Objekte liefert. Durch TLS konnten bisher große Fortschritte bei der Einzelbaum-Quantifizierung erzielt werden, da sich damit erfolgreich Attribute wie die Position des Stammes, der Durchmesser, die Stammkurve, das Stammvolumen und Biomasse-Komponenten ableiten lassen. Bisherige Ansätze wurden primär für bewirtschaftete Wälder oder Wälder in flachem Gelände entwickelt. Aufgrund von Faktoren wie der Fruchtbarkeit eines Standorts, den Abständen zwischen den Bäumen, den Lichtbedingungen, Wind und Hangrutschungsereignissen weisen Gebirgswälder jedoch eine komplexere Schicht unterhalb der Kronenschicht auf, welche durch einen mannigfaltigen Unterwuchs, Stämme mit nicht-vertikaler Ausrichtung und durch Stammquerschnitte von nicht-kreisförmiger Form gekennzeichnet sind. Diese Einflüsse erschweren die direkte Anwendung bestehender Methoden für Gebirgswälder. Diese Dissertation richtet sich auf die Bewältigung dieser erschwerenden Bedingungen, indem neue Methoden entwickelt werden, welche den hohen Komplexitätsgrad in der Verarbeitung von TLS Daten aus Gebirgswäldern meistern können. Die Arbeit der Dissertation fokussiert auf die Entwicklung von Methoden mit drei wissenschaftlichen Zielsetzungen; (a) der Unterscheidung zwischen Holz- und Blattkomponente des Baumes; (b) der Baumstamm-Detektion und -Modellierung in Gebirgswäldern, welche von Hangrutschungen beeinflusst sind; und (c) der Rekonstruktion der Stammquerschnitte. Ein Nebenfokus wird dabei auf eine kluge Punktwolkenstrukturierung gelegt, um die Verarbeitung von Punktwolken von großem Datenvolumen zu ermöglichen. Zuerst wird eine empirische Studie durchgeführt um die Verwendbarkeit von vier verbreiteten überwachten Methoden

aus dem Machine-Learning sowie deren Einfluss auf die Merkmalsberechnung zu untersuchen. In einer anschließenden Arbeit wird dazu ein neuer, vollautomatischer und unüberwachter Ansatz entwickelt. Experimente bestätigen dessen Stärke in der Unterscheidung zwischen Holz- und Blattkomponenten auf Parzellenebene in Gebirgswäldern. Zweitens wird eine neue Methode eingeführt, welche Baumstämme unregelmäßiger vertikaler Ausrichtung detektieren und rekonstruieren kann. Für die rekonstruierten Stämme lassen sich damit hohe Genauigkeiten erzielen im Vergleich zu im Feld erhobenen Referenzdaten. Zum Schluss wird eine neue Methode entwickelt, welche die tatsächliche Form der Stammquerschnitte modelliert und damit mit der Annahme runder Querschnitte der Baumstämme bricht. Die Arbeiten, welche in dieser Dissertation durchgeführt werden, liefern praktische Beispiele und Leitlinien für das Verständnis der Waldstruktur von Gebirgswäldern auf Einzelbaum-Niveau und demonstrieren gleichzeitig, dass die erforderliche Datenverarbeitung weitgehend automatisiert werden kann. Diese Beiträge können dabei helfen, in Zukunft eine intelligentere und nachhaltigere Bewirtschaftung von Gebirgswäldern zu erzielen.

Erklärung zur Verfassung der Arbeit - Author's Statement

Hiermit erkläre ich, dass ich diese Arbeit selbstständig verfasst habe, dass ich die verwendeten Quellen und Hilfsmittel vollständig angegeben habe und dass ich die Stellen der Arbeit einschließlich Tabellen, Karten und Abbildungen -, die anderen Werken oder dem Internet im Wortlaut oder dem Sinn nach entnommen sind, auf jeden Fall unter Angabe der Quelle als Entlehnung kenntlich gemacht habe.

I hereby declare that I independently drafted this manuscript, that all sources and references are correctly cited, and that the respective parts of this manuscript - including tables, maps, and figures - which were included from other manuscripts or the internet either semantically or syntactically are made clearly evident in the text and all respective sources are correctly cited.

Vienna, Austria, June 7, 2018

Di Wang

Acknowledgement

The journey has come to an end. I am truly indebted to all the help and support I have had in this journey. My Phd work and personal life for past three years in Vienna have been a great ride. It is truly my privilege to have the opportunity to be part of the outstanding Photogrammetry group at TU Wien.

Particular thanks go to my supervisors Norbert Pfeifer and Markus Hollaus, for the great guidance. I am truly thankful for the freedom that I have been granted by you so that I can focus on developing my own research interests. I have made immense progresses under your invaluable guidance, not only on research but also on comprehensive quality. I would like to thank all members at the Photogrammetry group for making such a unique work environment and extraordinary teamwork. I have learned so much from each of you. Thank you Martin, for helping and guiding me in the field measurements in Düns. You are truly an expert! Thank you Ana, Andreas, Nan, Livia, Moritz and many more for the great talks and help! I also would like to thank Felix for his kind assist.

Many thanks also go to Cao Senmao, Li Nan, Lu Hao and other friends that make up the Chinese lunch group. It has been always a warm experience to feel at home. I owe special thanks to Lu Hao who helps to establish the work relationship between me and CAF. The collaboration has resulted in a joint publication already. Also, thank you for the help in my difficult times during your stay in Vienna.

Heart of gratitude, I am grateful to my parents for never-ending care and support. Time flies, it has been ten years since I left home to pursue my education, and I feel very remorse for rarely having chances to go back home and company you. Your love is great and selfless. I cannot express even in words.

– 漠虚静以恬愉兮，澹无为而自得。 –

Contents

1	Introduction	1
1.1	Mountain Forests	1
1.2	Forest Monitoring	2
1.2.1	Laser Scanning Technique	3
1.2.2	Area-wide Assessment Using Airborne Systems	4
1.2.3	Single-tree Level Quantification Using Terrestrial Systems	5
1.3	Motivation and Study Objectives	8
1.3.1	Research Statements	8
1.3.2	Specific Objectives	10
1.4	List of Publications	12
1.4.1	Summary of the Publications	13
1.4.2	Author Contributions	17
2	Point Cloud Structuring Assisted Data Processing	19
2.1	Point Cloud Querying and Spatial Partition	19
2.2	Applications	22
2.2.1	Accelerated Range Search	22
2.2.2	3D Compactness Measurement	24
2.2.3	Parallelized Tile Processing	25
2.3	Conclusion	27
3	Publication I: Feasibility of Machine Learning Methods for Separating Wood and Leaf Points from Terrestrial Laser Scanning Data	29
3.1	Introduction	29
3.2	Materials	31
3.2.1	<i>Erytrophleum fordii</i>	31
3.2.2	<i>Betula pendula</i>	31
3.3	Methods	33
3.3.1	Feature Calculation	33
3.3.2	Feature Selection	33
3.3.3	Machine Learning Classifiers	34
3.3.4	Evaluation	36
3.4	Experiments and Results	37
3.5	Discussion	38

3.5.1	Classifier Performance	38
3.5.2	Feature Importance	40
3.5.3	Training Sample Delineation	41
3.6	Conclusion	41
4	Publication II: Separating Tree Photosynthetic and Non-Photosynthetic Components from Point Cloud Data Using Dynamic Segment Merging	43
4.1	Introduction	43
4.2	Study Data	46
4.2.1	Single Tree Data—SD-1	46
4.2.2	Plot-Level Data—PD-1	47
4.2.3	Plot-Level Data—PD-2	48
4.2.4	Plot-Level Data—PD-3	49
4.2.5	Plot-Level Data—PD-4	49
4.2.6	Validation Data	49
4.3	Methods	50
4.3.1	Dynamic Segment Merging	50
4.3.2	Post Processing	55
4.3.3	Segment Feature	56
4.3.4	Tile Processing	57
4.3.5	Random Forest Classification	58
4.3.6	Evaluation	60
4.4	Results	60
4.4.1	Single Tree Data	60
4.4.2	Plot-Level Data	62
4.5	Discussion	63
4.5.1	Calculation of Normal Vectors	63
4.5.2	Algorithm Performance	65
4.5.3	Challenges in Components Separation	67
4.5.4	Future Applications of the DSM Method	67
4.6	Conclusions	68
5	Publication III: Automatic and Self-Adaptive Stem Reconstruction in Landslide-Affected Forests	71
5.1	Introduction	71
5.2	Study Data	73
5.3	Methods	75
5.3.1	Down Sampling	76
5.3.2	Terrain Model Derivation	77
5.3.3	Stem Location Detection	77
5.3.4	Stem Reconstruction	80
5.3.5	Post Processing	85

5.3.6	Evaluation	86
5.4	Results	87
5.5	Discussion	89
5.5.1	Parameters	89
5.5.2	Error Analysis	90
5.5.3	Algorithm	93
5.5.4	Applicability of TLS in Landslide-Affected Forest	97
5.6	Conclusions	97
6	Publication IV: Reconstructing Stem Cross Section Shapes from Terrestrial Laser Scanning	99
6.1	Introduction	99
6.2	Study Area and Data	100
6.2.1	Study Site I	100
6.2.2	Study Site II	101
6.3	Method	101
6.3.1	Stem Mapping	101
6.3.2	DBH Estimation	102
6.3.3	Evaluation	106
6.4	Results	107
6.5	Discussion and Conclusion	108
7	General Conclusions	111
	Bibliography	115

List of Figures

1.1	Airborne laser scanning over trees. Image modified from the original work by Anthony Beck, used under a CC-BY 3.0 license from Wikimedia commons.	4
1.2	Top view of the luxuriant understory and tree structures (up to 2 meters above ground) of a forest in an Austrian Alpine mountain range. Tree stem locations are marked by black rectangles.	9
1.3	Stem irregularity. (a) Non-vertical tree stems. (b) Irregular stem cross-section shape, making the conventional circle fitting unacceptable. . .	10
2.1	A visualization of a 2D KD-tree on six points. Image modified from the original work by user ID KindDragon33, used under a CC-BY 3.0 license from Wikimedia commons.	20
2.2	Uniform voxelization of a forest point cloud. The boundaries of each bin and its contained points are equally rendered with random colors. The voxel size is set to 5 meters in this example.	21
2.3	Octree voxelization of a forest point cloud. The boundaries of each bin and its contained points are equally rendered with random colors. The Maximum bin capability is set to 50,000 points, which results in a bin depth of 1617 in this example.	21
2.4	2D tiling of a ALS point cloud. The boundaries of each bin and its contained points are equally rendered with random colors. The tile size is set to 50 meters in this example.	22
2.5	A voxel has 26 neighboring voxels in a 3D uniform space.	23
2.6	Runtime benchmarking of range querying with and without spatial partitions. Color jungle green represents the runtime with spatial partitions. a) Uniform voxels constructed on a point cloud with 1,170,489 points. Processing parallelized with 7 CPU threads. b) Voxels constructed a point cloud with 4,933,336 points. Processing parallelized with 24 CPU threads. c) 2D tiles constructed on a point cloud with 122,829 points. Processing parallelized with 7 CPU threads. d) 2D tiles constructed on a point cloud with 332,480 point. Processing parallelized with 7 CPU threads.	24
2.7	Spatial occupancy array of a tree crown point cloud. (a) Uniform voxelization. (b) The original unorganized point cloud.	25

2.8	Tile processing for forest segmentation. Each segment is randomly colored. (a) Segmentation results on each tiles.(b) Results after tile merging.	26
3.1	Point cloud of the <i>Erytrophleum fordii</i>	31
3.2	Point cloud of the <i>Betula pendula</i> , silver birch.	32
3.3	Evaluation of number of classification trees to be grown.	35
3.4	Performance of four classifiers for the <i>Erytrophleum fordii</i> as a function of the different feature sets. Feature sets were determined based on the <i>Fisher</i> filter method described in section 3.2	38
3.5	Performance of four classifiers for the silver birch as a function of the different feature sets. Feature sets were determined based on the <i>Fisher</i> filter method described in section 3.2	38
3.6	A crown subset (i.e., 16 - 20 m) of the <i>Erytrophleum fordii</i> . Branches and leaves heavily interact.	39
3.7	Classification results of RF model for <i>Erytrophleum fordii</i> . Left part shows the wood components and right part shows the leaf points. . . .	40
3.8	Classification results of RF model for silver birch. Left part shows the wood components and right part shows the leaf points.	40
4.1	Five datasets used in this study. (a) SD-1. (b) PD-1. (c) PD-2. (d) PD-3. (e) PD-4. The left column shows the original point clouds. Manually classified point clouds are shown in the middle column (non-photosynthetic components) and right column (photosynthetic components). These manually classified points served as validation sets in this study.	47
4.2	Distribution of reflectances of photosynthetic and non-photosynthetic components after radiometrical calibration.	48
4.3	Initial segments by over-segmentation. Each segment is randomly colored. The stem surface has large size segments because it is geometrically homogeneous, while bushes have smaller segments as they are more irregular in shape.	53
4.4	Identifying adjacency relations. (a) Original point cloud. (b) Overly partitioned segments. The middle segment with black color is the target segment. Its adjacent segments are founded by the adaptive search radius, and are randomly colored. (c) <i>Superpoints</i> representation of (b).	54

4.5	Adjacency graph of segments in Figure 4.4. The identified graph is initially unweighted (left), while it is further weighted by SL values defined in Equation (4.3) (right). Segment 13 is unqualified as in Equation (4.3), thus it has 0 weight to the target segment 1. For this example, segment 10 has the largest weight, meaning that it is the most similar qualified segment. Therefore, it will merge with the target segment 1 in this step.	55
4.6	An example of tree branches grouped into one segment with the Dynamic Segment Merging (DSM) method (a) and then separated with the top-shift procedure (b).	56
4.7	An example of a Heat map of acquired accuracy for the PD-2 dataset to locate proper TH_l and TH_n values.	57
4.8	Point cloud tiling. (a) Uniform voxels. (b) Octree partition. (c) 2D tiles on XY plane.	58
4.9	Point cloud tile processing and merging. (a) DSM results on tiles. (b) Results after tile merging.	58
4.10	Separation results with adaptive neighborhoods from the DSM method for (a) SD-1, (b) PD-1, (c) PD-2, (d) PD-3, and (e) PD-4. Photosynthetic and non-photosynthetic components are colored by green and brown, respectively.	62
4.11	Normal vector estimation. (a) Normal vectors estimated with fixed neighborhoods, and colored by N_z . (b) Optimal neighborhood size for each point. (c) Normal vectors estimated with optimal neighborhoods, and colored by N_z	64
4.12	Comparison of segmentation for the SD-1 dataset. Each segment is randomly colored. (a) Segmentation from the proposed DSM method. (b) Segmentation from the conventional region growing method. . . .	66
4.13	A close inspection of results for the PD-3 dataset.	67
4.14	An example of our DSM method applied to detect wood points of the entire <i>Erythrophleum fordii</i> tree (a). Detected wood components are shown in (b), and the corresponding Quantitative Structure Model (QSM) is given in (c).	68
5.1	Landslide-affected forest in the Austrian Alps. Trees are inclined after shallow landslide caused soil movements. The red rectangle covers the area in this study. Coordinates in WGS84 UTM Zone 32N.	73
5.2	The area of the study site approximately equals 31 m \times 16 m. Seven scan locations are marked by white rectangles. Tree positions are marked by solid circles. The size is scaled by the DBH, and color is scaled by the percentage of TLS coverage (i.e., 0–1 (100%)). Contours are derived from the DTM.	75

5.3	Workflow of our algorithms. Terrain removal is a preliminary procedure; thus, it is not shown here.	76
5.4	(a) An example of the projection density map of a point cloud subsection, which contains six trees. The map is generated by 2 cm × 2 cm grids. (b) Corresponding map of the average z-normal vectors. Red rectangles show six trees identified by our method.	78
5.5	The relation between the density and z-normal for all cells. The thresholds are determined by finding the maximum curvature, at which the curve becomes flat. The cells framed by the red dotted line rectangle are identified as stems.	79
5.6	Example of the region growing method used in this study. Two groups are generated. The “X” denotes the starting seeds for each group. . . .	82
5.7	The asymmetric thresholds for circle fitting. The black circle is the one determined by our algorithm. The dotted green circle is over fitted and determined by symmetric thresholds. When using symmetric thresholds, the points in the red rectangle have weak effects; thus, the fitted circle is biased by the unbalanced weights introduced by the point distribution.	83
5.8	Cylinder growing strategy. The cylinder is shifted (a); vertically tilted (b); and horizontally rotated (c).	85
5.9	(a) A moving window technique to smooth the connection part of two consecutive cylinders; (b) after smoothing, a truncated cone is generated.	86
5.10	Scatter plot of DBH automatically estimated from TLS and reference measurements in the field. The R^2 is 0.99.	87
5.11	Bias of diameter estimation and its distribution with height. Results are evaluated from all trees.	88
5.12	Bias of stem location estimation and its distribution with height. Results are evaluated from all trees.	89
5.13	(a) Point cloud of a proportion of the forest; (b) a visualization of the corresponding reconstructed stems in (a); (c) an example tree shows that our method is able to handle the curvature of the deformed stem.	89
5.14	The results of DBH plotted again TLS coverage. The DBH in the left axis denotes the filed-measured DBH. dDBH refers the absolute bias. Color is scaled by the TLS coverage.	91
5.15	The cross-section of a tree at 1.3 m above the ground. The severe irregularity leads to an underestimation of the diameter using our algorithm.	92
5.16	An example of the effectiveness of RASANC algorithm in circle fitting. The outliers in original points (a) are first filtered by the region growing method (b).	93
5.17	An example of our method applied to a deciduous tree. The point cloud was acquired from TLS and UAV laser scanning, respectively. . . .	95

6.1	Study site I: the red rectangle covers a small transection roughly equal to an area of 31 m × 19 m. The blue dots indicate the locations of seven TLS scans.	101
6.2	Study site II: a mature Scots pine forest scanned with TLS in single-scan mode.	102
6.3	Transformation of coordinates from Cartesian (x, y) to polar (r, θ). The angular domain in the polar frame is $[-\pi, \pi]$	102
6.4	Fourier approximation of points (full coverage) on the angular domain. The actual domain is $[-\pi, \pi]$, which is duplicated to $[-\pi, 3\pi]$ to show the periodicity. The thick red line indicates the final approximated curve, and the thin red lines denote the threshold boundaries of 2 cm. The points outside the boundaries are iteratively excluded.	103
6.5	The effective domain clamped by the dotted red lines is determined by clustering connected points. On the domain of $[-\pi, \pi]$, the points are disconnected by the $-\pi/\pi'$ axis. The presented example is from a stem with 60% TLS coverage.	105
6.6	The proportion of the effective domain to 2π is determined by the corrected center location. The new center location is identified by a circle fitting on filtered points.	105
6.7	Scatter plot of the DBH estimated from TLS by using three approaches and the reference values for the stems in study site I.	107
6.8	Scatter plot of the DBH estimated from TLS by using three approaches and the reference values for the stems in study site II.	107
6.9	Comparison of various fitting routines. The dashed blue circle indicates the initial circle estimation used to determine the center location within the cross section. The B-spline is troubled by outliers. Fourier series fitting creates an accurate perimeter estimate.	108

List of Tables

3.1	Features extracted from the point cloud. <i>EV</i> denotes the eigenvalue and <i>NV</i> is the normal vector. <i>EVs</i> are sorted in a descend manner. "R-" is the abbreviation of "Ranking" form feature selection. "R-Combined" means that the feature set is a combination of data from both trees. Top 5 ranked features are underlined.	32
3.2	Statistical evaluation of machine learning classifiers for wood-leaf separation.	35
3.3	Statistical evaluation of machine learning classifiers for the crown subset of the <i>Erytrophleum fordii</i> with 5, 10, 15, 20, and 26 features. . . .	39
3.4	Comparison of performances with different training data on the crown subset. Sample <i>f</i> denotes the manually selected 10% training set. Sample <i>s</i> refers to a training set with 1m height intervals.	42
3.5	Performances of all classifiers trained with a combined training set from both trees.	42
4.1	Thirty-two features extracted from the point cloud. <i>EV</i> denotes the eigenvalue and <i>NV</i> is the normal vector. Three <i>EVs</i> are sorted in descending order. <i>EV</i> ₁ defines the first eigenvalue, and so on.	59
4.2	Results summary of various methods on all datasets. Bold numbers are the best results among methods. (F) denotes the results acquired with fixed neighborhood sizes, and (A) stands for adaptive neighborhood sizes. * Training and validation points have an equal split of photosynthetic and non-photosynthetic components.	61
5.1	Specifications of the Riegl VZ-2000 scanner.	74
5.2	Results of the stem detection rate and reconstruction rate.	87
5.3	Bias and RMSE of automatically estimated DBH, diameter, location and volume. * Results are evaluated from all heights along all stems. . .	88
5.4	Summary of several selected studies on automatic stem detection and modeling from TLS data. Only the first authors are shown to save space. Some of the contents and values are visually inspected or calculated from corresponding publications. S and M in scan mode stand for single scan and multiscan, respectively. M(p) means that multiscan is only performed partially.	96

6.1 Bias and RMSE of the estimated DBH 108

Introduction

” *May The Forest Be With You.*

1.1 Mountain Forests

Mountain forests occupy almost a quarter of all forest cover worldwide (Price et al., 2011). Their ecosystems provide a great deal of values, ranging from protection against natural hazards, timber production, biodiversity conservation, to carbon storage and climate mitigation (Blatter et al., 2017).

In recent decades, there has been an increased occurrence of soil erosion in many alpine regions (Alewell, 2014). Climate change adaptation and natural disasters in these regions are receiving considerable attention (Forbes and Broadhead, 2013). Forests in mountain ranges serve as physical obstacles that impede downslope mass movements such as rockfalls, landslides, debris flows, and avalanches (Price et al., 2011). This phenomenon is well documented in studies that confirm the stabilizing effect of all forest classes on landslide occurrences (Schmaltz et al., 2017).

Mountain forests also hold a great value in producing wood, either to support the people living in mountain ranges for energy supply, or for the global timber industry. Wood fuel is largely required to fulfill energy demand in many regions (Ali and Benjaminsen, 2004). Woody biomass is an important contributor to satisfying the increased energy demand (Valente et al., 2014). In addition, mountain farms profit from forestry and timber production, by managing a large area (Price et al., 2011). In recent years, there have been increased efforts on a better mountain forest timber mobilization (Hollaus et al., 2015). These efforts help to better identify and qualify areas accessible by forest tractors, thus in long term help to develop a sustainable wood harvesting strategy.

Mountain forests are home to a unique collection of plant and animal species. A third of world's protected areas are located in mountains (Price et al., 2011). On the global scale, mountain ranges are biodiversity hot spots with high biological

richness, because the rapid altitudinal change of climatic conditions (Körner, 2004). Large-scale patterns of plant distribution in mountains continue to be of interest (Spehn et al., 2011). On the other hand, global awareness is raised to wildlife habitat in mountain forests (Russell et al., 2007). A particular focus is on the assessment of mountain forest change and its impact on biodiversity destabilization (Martinuzzi et al., 2009). In Europe, negotiations between the European Commission and the EU's Member States have resulted in a list of 231 habitat types to be protected under the Habitats Directive (Evans, 2012). These habitat types include many mountain forests.

Global climate change has major impacts on our living environment. Forests have an important role in climate protection as they are major contributors to the carbon sink of the whole terrestrial ecosystems (Canadell and Raupach, 2008). Among them, mountain forests hold a vast quantity of carbon (Price et al., 2011). Recent studies (Spracklen and Righelato, 2014) revealed that mountain forests ecosystems may provide 40 percent more carbon storage than previously estimated worldwide. In Austria, mountain forests have six times more forests older than 140 years than that of lowland forests (Price et al., 2011), indicating that mountain forests have a more sustaining role in mitigating climate change.

1.2 Forest Monitoring

Understanding and monitoring the detailed structure information of mountain forests are key to sustainably managing those mountain forest services mentioned in section 1.1. However, such needed assessments are still rare in practice. Conventional field measurements are labor intensive and can hardly cover attributes that are indirectly measurable without felling the trees, such as wood biomass and stem profiles. In practice, such attributes that cannot be measured non-destructively in field are often estimated and extrapolated by using allometric models (e.g., Repola, 2008; Repola, 2009; Raumonon et al., 2013; Hackenberg et al., 2014) that are constructed based on other forest inventory data such as tree height and diameter at the breast height (DBH). However, these functions are not always valid, because they were developed from specific local morphological or climate conditions, thus their applicability is usually restricted to specific species and sites (Návar, 2009). Moreover, field inventory data are not always available in many developing countries with rich natural forest resources, due to the geographical remoteness, lack of capacity, data paucity or armed conflicts (Rodríguez-Veiga et al., 2017).

In past decades, remote sensing has achieved extraordinary advances in the mapping and understanding the global ecosystems (Lefsky et al., 2002). A broad range

of application examples have proven the capability of remote sensing techniques for forest monitoring. Remote sensing sensors can be grouped to active and passive ones based on their measurement techniques. A more intuitive and common practice to category remote sensing data for ecological applications is based on three data sources; passive optical imagery, microwave, and laser scanning (also known as Light Detection and Ranging, LiDAR) (Rodríguez-Veiga et al., 2017). Passive optical imagery and active microwave radar data are primarily used by researchers to analyze forests in a broad scale. For example, satellite based passive optical sensors such as Sentinel-2 (Drusch et al., 2012) and Landsat-8 (Roy et al., 2014) can contribute in identifying the distribution, richness, change and habitats of tree species from landscape to worldwide level (Kerr and Ostrovsky, 2003). Active radar sensors such as Advanced Land Observing Satellite Phased Array L-band Synthetic Aperture Radar (ALOS PALSAR) (Rosenqvist et al., 2007) can predict above ground biomass across different landscapes (Mitchard et al., 2009). However, the limitations of these types of data are apparent – they only map the forests in two dimension (2D), which impedes the assessment of below-canopy structures in three dimension (3D).

1.2.1 Laser Scanning Technique

Laser scanning technique is an active measurement technique that transmits laser pulses to targets in order to measure distances and reflectance properties of objects of interests. The recorded 3D points by a scanner is called a *point cloud*. Due to its great capability of accurate 3D mapping and radiometric information measure, it has been widely used in ecosystems studies since the introduction of commercial available sensors (Lefsky et al., 2002). Typically, instruments for locating the return signals in geo-coordinates including Global Positioning System (GPS) and Inertial Navigation Systems (INS) are integrated with the laser scanner, especially for airborne systems. These instruments measure the position of the platform and the attitude of the sensor. Laser scanning systems differ from each other based on their scanning mechanism, emission power, laser wavelength, pulse duration and repetition rate, beam size and divergence angle, and information recording (discrete or full waveform) (Lefsky et al., 2002). The same as many other remote sensing techniques, laser scanning systems can also be categorized according to the platform in which they are mounted; space-borne, airborne, ground-based, hand-held or mobile.

In Figure 1.1, an example of forest measurement using an airborne laser scanning (ALS) system is given. The emitted laser pulses hit some components of trees, such as branches and leaves. A portion of the laser pulses are reflected back to the sensor. Some pulses continue traversing downwards with the presence of gaps, or if the

firstly hit objects are smaller than the beam size, or only partial of the laser footprint hit objectives. These mechanisms result in the fact that multiple reflections may be recorded from one laser pulse. The distribution of backscattered energy creates a waveform, which is resulted as the convolution of the emitted waveform and objects. The recored waveform is a product from the backscattered energy and the receiver electronics (Figure 1.1). The energy itself is know as *intensity*. For a discrete recording system, only peak returns in the waveform profile are recorded. In practice, only several (e.g., up to 4) discrete returns are stored. Full waveform systems record the complete backscattered signal, thus provides more information compared to discrete return systems. Full waveform are usually further processed by decomposing the signal to individual *echoes* (Wagner et al., 2006). The extracted *echoes* are associated with range and radiometrical properties such as *echo width* and *echo amplitude*. These additional attributes quantitatively measure the scattering properties of objects, and provide promising benefits for ecosystem studies such as forest species classification (Reitberger et al., 2008).

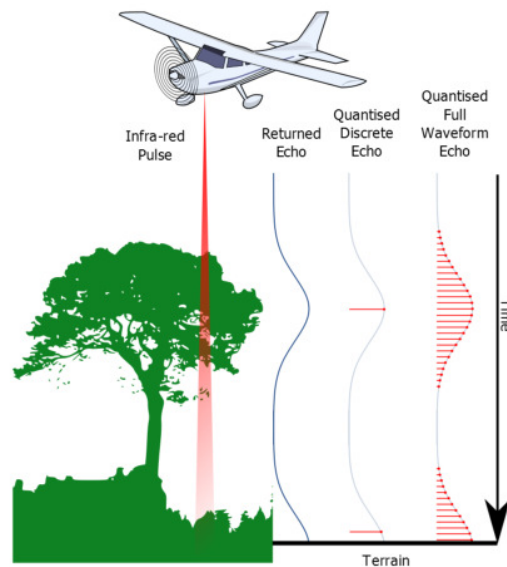


Fig. 1.1: Airborne laser scanning over trees. Image modified from the original work by Anthony Beck, used under a CC-BY 3.0 license from Wikimedia commons.

1.2.2 Area-wide Assessment Using Airborne Systems

In past decades, laser scanning has made striking advances in quantifying forest structures. The Canadian Forestry Service showed the applicability of laser scanning for estimating forest stand heights, crown cover density and ground elevation below the forest canopy in the early 1980s (Aldred and Bonnor, 1985). Since then, laser scanning has been widely used to derive many vital forest attributes including above-ground biomass, basal area, mean stem diameter, vertical foliage profiles

and canopy volume (Lim et al., 2003). Over the last decade, forest assessment using laser scanning has progressed from concerns on data acquisition and processing to current interests on generating mature local, regional, continental and global products (Wulder et al., 2013).

The different level of details in forest quantification requires using different laser scanning systems. ALS, and recently developed Unmanned Aerial Vehicle (UAV) based laser scanning (ULS), are generally targeted to region to country-wide studies (Nord-Larsen and Schumacher, 2012). The derived forest attributes are often assisted by field data in order to upscale the derived information to more detailed scales, or to extrapolate the field data to a wider area by mathematical or physical models. The robustness and repeatability of ALS data for forest quantification and attribute estimation have been well demonstrated (Wieser et al., 2016; Mücke et al., 2013; Levick et al., 2016; Kim et al., 2009). Recent developments of ALS systems are leaning towards lightweight hardware and expanding the spectrum measure to multispectral capability. Lightweight sensors mounted on UAV (i.e., ULS) emerge as a new candidate for fast and reliable region level forest quantification. The high density and accuracy of ULS data provide a high level of completeness with respect to the top canopy layer and a promising level of data coverage on tree stems, which in combination overcome the deficiency of ALS on its sparse data coverage and relatively large footprint (Wieser et al., 2016). On the other hand, multispectral laser scanning (e.g., Dalponte et al., 2018) provides much richer spectral information of objects. This augmented capability clearly has the potential to provide structural and physiological information simultaneously and facilitate the formulation of new products such as true effective leaf area index (LAI) and Normalized Difference Vegetation Index (NDVI) (Wulder et al., 2013).

However, a major limitation of ALS and ULS systems is that they can hardly reliably estimate below-canopy structures such as stem diameters and biomasses. Current solution is to use multi-source single tree inventory data such as field measurements and terrestrial laser scanning (TLS) to aid the ALS analysis.

1.2.3 Single-tree Level Quantification Using Terrestrial Systems

Nevertheless, several considerably most vital attributes that are defined in forest inventory such as stem curve, stem volume and biomass components (total, stem and branches) (Liang et al., 2016) can only be assessed by using ground-based laser scanning systems. The apparent reason is that derivation of these attributes requires detailed 3D information of below-canopy structures. TLS (Liang et al., 2014a), mobile laser scanning (MLS) (Liang et al., 2014c), and personal laser scanning

(PLS) (Liang et al., 2014b) are capable of capturing point clouds that have almost complete representations of tree stems and branches. The maturity of TLS for forest quantification remains some years behind that of ALS systems (Wulder et al., 2013). Early works related to TLS tree attribute estimation were reported around 2000 (Lovell et al., 2003). Since then, it quickly becomes a promising technique for forest studies with the hardware and methods continue to develop. To this day, TLS has become a common practice in plot-wise forest inventory in some countries (Liang et al., 2016).

A community convention of using the term TLS specifically refers the scanning approach that a scanner is mounted on a tripod. It by far provides the most accurate and high-resolution point clouds. According to different scanning setups, TLS can be either a single-scan or multi-scan mode. Single-scan stands for a setup that the scanning is only performed at one location, while multi-scan means that scanning are carried out from several locations. Data generated from multi-scan need to be co-registered so that the point clouds can be merged into a common coordinate system. The success of both single-scan and multi-scan TLS in single-tree level quantification are widely documented (Liang et al., 2012; Liang et al., 2014a). Naturally, multi-scan provides more complete data coverage, and is less affected by occlusions inside forests. However, it requires significantly more manpower and time to carry out the measurement.

Single-tree level quantification mainly applies on tree woody structures, although many efforts are made on ecological aspects such as LAI (Zheng et al., 2013) and leaf water content (Zhu et al., 2015). More narrowly, stem location, DBH, stem curve, and biomass components are the prime attributes that TLS are targeting at for single-tree quantification. In past years, community efforts are paid to the development of intelligent algorithms that can confidently extract these attributes, which are robust to different data acquisition setups, forest conditions, and large data volumes. A recent benchmark project: Benchmarking of Terrestrial Laser Scanning for Forestry Applications (*Project Benchmarking on Terrestrial Laser Scanning for Forestry Applications*) endeavors to systematically examining the real power of TLS in forest inventory against varied data acquisition approaches, processing methodology, and forest conditions.

In order to reduce the uncertainty in TLS-derived estimates of stem location, DBH, stem curve, and biomass, a prerequisite is to filter out 3D points coming from leaves and other objects (Disney et al., 2018). Theoretically, stem detection can be regarded as a sub-question of wood filtering, although they may be finalized using completely different methods. However, filtering woody components is a very much ongoing challenge. Comparing to the efforts made on stem detection and diameter estimation, less attentions are made to detect complete woody compo-

nents, although it is of vital importance in estimating biomass. Existing methods for filtering the woody components from point cloud data can be categorized into two groups: intensity based and geometry based. A different third approach uses the combination of radiometric and geometric features (Zhu et al., 2018). Intensity-based methods (Pfennigbauer and Ullrich, 2010; Béland et al., 2014) use radiometric information of objects captured by a laser scanner, based on the fact that wood and leaf components have different optical properties at the operating wavelength of the laser scanner (Tao et al., 2015a). However, these optical properties are influenced by the distance, partial hit, and laser incident angle (Kaasalainen et al., 2009). Therefore, a key challenge of using intensity values is that they have to go through instrument-specific radiometrical calibration before being included in further processing (Calders et al., 2017; Höfle and Pfeifer, 2007; Kaasalainen et al., 2011). Geometry-based methods only use the 3D coordinates of the point cloud captured by a laser scanner. A commonly deployed approach is to use supervised machine learning classification, together with geometrical features extracted for each point. This method only needs the 3D point clouds, and does not require the calibration of intensity information. However, a major drawback of supervised machine learning classification is the requirement of training data, thus it can be impractical for processing large numbers of trees. The trained models are also difficult to be generalized to data acquired by other platforms and from different forest conditions.

Estimation of stem location, diameter and stem curve needs to firstly isolate individual stems. A straightforward method is to remove points other than stems, and then group stems points into isolated stems. The procedure for removing other points is also known as *stem denoising* (Conto et al., 2017). A common method is to identify stem points by evaluating some feature saliencies that are derived from local neighboring points around each points (Liang et al., 2012; Ma et al., 2016). Assumptions are often made on the shape prior such as stems are mainly vertical in orientation. Similar mentality is used in another group of method that transforms point clouds to 3D voxel spaces and use morphological operations to filter out unwanted points (Gorte and Winterhalder, 2004). A third approach uses the Hough Transformation, which can be applied to detect circular shapes on 2D horizontal layers of the point clouds, by assuming that stem cross-sections are circular (Conto et al., 2017). It is noted that stem detection using Hough Transformation directly isolates individual stems, as stems are detected as isolated circles. Nevertheless, other stem denoising approaches need a following step which further groups denoised stem points into individual stems. Simple methods are used such as Euclidean distance based clustering (Hackenberg et al., 2014) and mean-shift clustering (Weinmann et al., 2017).

Estimating DBH and stem curve requires a certain method to retrieve the thickness information of tree stems. A simple manual method is to measure the distance between two points farthest off (Kankare et al., 2016). A similar routine measures the distance from two directions and use the average value as the estimated diameter. Another type of automated method utilizes geometric primitive fitting. The most commonly used approach is to approximate the stem by cylinders (Liang et al., 2014a) or its cross-section by circles (Pueschel et al., 2013). Both approaches can be augmented by incorporating some advanced techniques to increase the fitting quality, such as using iteratively reweighted least squares (Liang et al., 2012; Liang et al., 2014a) and using the Random Sample Consensus (RANSAC) method to surpass outliers (Olofsson et al., 2014). For DBH estimation, the primitive fitting is carried out around the height of 1.3 meters above ground, following the definition of DBH. It has to be pointed out that a digital terrain model (DTM) is needed in this case to normalize the point cloud, so that the height of each point corresponds to the height above ground. Such a DTM can be robustly modeled from the point cloud itself (Pfeifer and Mandlbürger, 2008). Stem curve, which describes the diameter at different heights along the stem, needs diameter estimation at various heights. Some studies use advanced curve fitting (e.g., Pfeifer and Winterhalder, 2004; You et al., 2016) instead of assuming the circular shape of stem cross-sections in 2D or the cylindrical shape of stems in 3D.

1.3 Motivation and Study Objectives

1.3.1 Research Statements

There is a great interest in quantifying forest structures at the single-tree level in mountain forests. Apart from the same interests for managed forests on topics such as forest inventory, timber production and monitoring of tree growth, a particular attention for mountain forests is to better understand their roles in ecosystems, including keeping moisture in the ground by holding the soil in place to protect erosion and carbon sequestration as a role in the global climate system. Accurate assessment of single tree structures especially the woody components is needed to reach such a goal. For example, dynamic slope stability models (e.g., Steger et al., 2015; Kuriakose et al., 2009) were developed to study the interdependencies of different ecosystem processes, including deforestation or afforestation. Detailed stem volume and biomass information at the single-tree level can greatly benefit and facilitate such studies (Schmaltz et al., 2016). Moreover, quantification of stem shapes can help to understand the growth anomaly and the impacts from soil movements (Razak et al., 2013). The spatial pattern resulted from these information may assist further ecosystem managements.

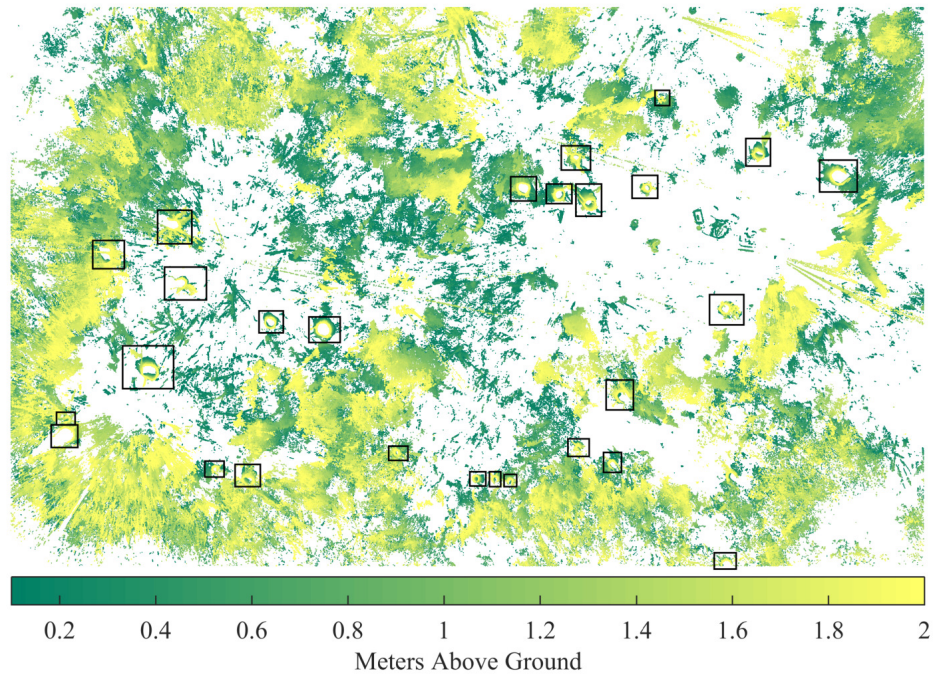


Fig. 1.2: Top view of the luxuriant understory and tree structures (up to 2 meters above ground) of a forest in an Austrian Alpine mountain range. Tree stem locations are marked by black rectangles.

A great challenge of directly applying existing approaches presented in section 1.2.3 in mountain forests is that mountain forests have far more complex structures than managed forests. It is obvious that many available approaches developed for single tree quantification are based on several fundamental assumptions such as tree stems are vertical and the cross-sections are circular. However, these assumptions are often invalid in mountain forests, making it difficult to use existing methods without modifications or improvements. An example is given in Figure 1.2, in which the complexity of a forest in Austrian Alps is shown. Comparing to many managed forests and those in flat environments, mountain forests feature littery understory, which increases the difficulty of finding stems from severe surrounding disturbances (Figure 1.2). Tree stems often have non-vertical orientations, and the cross-section can differ significantly from a circle (Figure 1.3). The wood formation mechanism is often influenced by factors such as the site fertility, spacing and light conditions, wind, snow pressure, and landslide events (Plomion et al., 2001). The probability of the occurrence of growth anomaly is much higher in mountain natural forests than it in managed forests. Consequently, currently available approaches for quantifying tree structures using TLS data can not be directly applied in many mountain forests. There is an urgent need to explore the applicability of TLS in quantifying mountain forest structures, and to develop reliable methods that can deal with the added complexity in data processing.

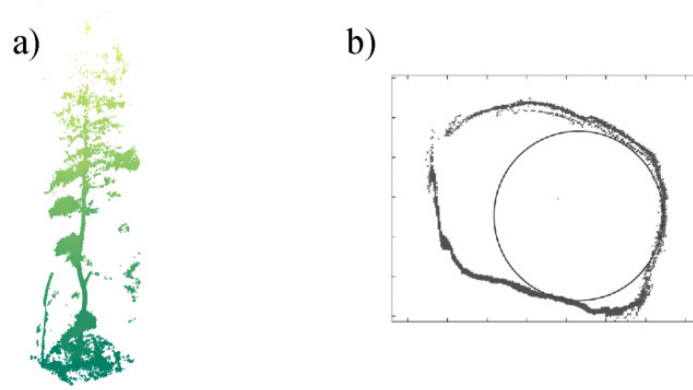


Fig. 1.3: Stem irregularity. (a) Non-vertical tree stems. (b) Irregular stem cross-section shape, making the conventional circle fitting unacceptable.

In addition, a general challenge of TLS data processing is how to efficiently handle large volumes of point cloud data. A comparable issue has been addressed for ALS data processing (Pfeifer et al., 2014). However, rare efforts are paid to TLS data processing, especially for forest studies. Forest point cloud data acquired by TLS may easily consist of millions to billions discrete and unorganized points (Liang et al., 2016). How to efficiently manage and process these data need to be investigated, at least to some extent, to facilitate the usage of TLS technique to a broader audiences.

1.3.2 Specific Objectives

Given the research gaps described above, this dissertation aims to expand the success of using 3D point cloud data – especially TLS – in forest inventory to mountain forests with more complex conditions. Specifically, the study objectives of this dissertation cover three research aspects and one technical topic that are represented in the four research articles that make up this cumulative dissertation.

· Separation of tree wood and leaf components.

- Evaluating the potential of machine learning classifiers for separating wood and leaf components using point cloud data. (Publication I)
- Investigating the importance of different geometric features for machine learning classification. (Publication I)
- Developing and implementing a fully automatic and unsupervised method for separating wood and leaf components. (Publication II)

- Testing the developed method for various forest types and data sources, and comparing it with supervised machine learning approaches. (Publication II)

· **Tree stem detection and modeling in mountain landslide-affected forests.**

- Performing TLS acquisition in high mountain forests and evaluating its overall applicability. (Publication II, III, IV)
- Reviewing the state-of-the-art methods for stem detection and modeling from TLS point clouds. (Publication III)
- Developing and implementing a fully automatic method that can cope with the complexities such as multi-layered canopy structure, dense understory, mixed tree species and deformed stem shapes in mountain forests. (Publication III)
- Testing the developed method for a landslide-affected forests in Austrian Alps. (Publication III)

· **Reconstruction of stem cross-sections.**

- Reviewing existing methods for tree stem cross-section modeling from TLS point clouds. (Publication III, IV)
- Identifying the deficiency of commonly used circle and cylinder fitting in cross-section modeling. (Publication III, IV)
- Developing and implementing a robust method that can accurately reconstruct the actual stem cross-section. (Publication IV)
- Testing the developed method for a landslide-affected forests in Austrian Alps and a managed forest in Finland. (Publication IV)

· **Point cloud structuring assisted data processing.**

- Developing an efficient data structuring approach that can assist and accelerate the processing of TLS data for forest applications. (Publication II, and other unpublished work on crown segmentation)

1.4 List of Publications

This cumulative dissertation is base on three peer-reviewed journal papers and one peer-reviewed conference paper, which include:

- **Publication I** Wang, D., Hollaus, M., & Pfeifer, N. (2017). Feasibility of machine learning methods for separating wood and leaf points from terrestrial laser scanning data. *ISPRS Annals of Photogrammetry, Remote Sensing and Spatial Information Sciences*, IV-2/W4, 157-164.
- **Publication II** Wang, D., Brunner, J., Ma, Z., Lu, H., Hollaus, M., Pang, Y., & Pfeifer, N. (2018). Separating tree photosynthetic and non-photosynthetic components from point cloud data using dynamic segment merging. *Forests*, 9(5), 252.
- **Publication III** Wang, D., Hollaus, M., Puttonen, E., & Pfeifer, N. (2016). Automatic and self-adaptive stem reconstruction in landslide-affected forests. *Remote Sensing*, 8(12), 974.
- **Publication IV** Wang, D., Kankare, V., Puttonen, E., Hollaus, M., & Pfeifer, N. (2017). Reconstructing stem cross section shapes from terrestrial laser scanning. *IEEE Geoscience and Remote Sensing Letters*, 14(2), 272-276.

The work in this dissertation has been conducted as part of the following research projects:

The project "The influence of Biomass and its change on landSLIDE activity" (BioSLIDE) within the research program Earth System Sciences (ESS) of the Austrian Academy of Science (Österreichische Akademie der Wissenschaften, ÖAW).

The project "Feasibility Studie: Gewinnung von Baum- und Waldparametern aus Laserscanningdaten von Multicopterflügen" funded by the Austrian Research Promotion Agency (FFG) under gran agreement No. 860021.

1.4.1 Summary of the Publications

Publication I: Feasibility of Machine Learning Methods for Separating Wood and Leaf Points from Terrestrial Laser Scanning Data

The first publication (Wang et al., 2017a) is an empirical study that evaluates four common machine learning classifiers for their effectiveness on separating wood and leaf points using geometrical features derived from TLS point clouds.

Classification of wood and leaf components of trees is an essential prerequisite for deriving vital tree attributes, such as wood mass, leaf area index (LAI) and woody-to-total area. Past two decades have witnessed great progresses of laser scanning in quantifying tree structures. TLS has widespread applications in estimating tree attributes, such as stem location (Liang et al., 2012), DBH (You et al., 2016), basal area and volume (Chen et al., 2007). However, separating tree wood and leaf components in TLS data is still challenging (Disney et al., 2018).

Intensity based approaches are widely proposed, as different components of a tree can feature discriminatory optical properties at the operating wavelengths of a sensor system. However, these optical properties are influenced by the distance, partial hit, and laser incident angle (Kaasalainen et al., 2009). Therefore, a key challenge of using intensity values is that they have to go through instrument-specific radiometrical calibration before being included in further processing (Calders et al., 2017; Höfle and Pfeifer, 2007; Kaasalainen et al., 2011). A more common method is to deploy supervised machine learning classification for such a task. Geometrical features are extracted for each point, and training samples are often manually delineated to guide a classifier. However, it remains unclear how the chosen machine learning classifier and features used would influence classification results.

This publication compares four popular machine learning classifiers, namely Support Vector Machine (SVM), Naïve Bayes (NB), Random Forest (RF), and Gaussian Mixture Model (GMM), for separating wood and leaf points from TLS data. Two trees, an *Erythrophleum fordii* and a *Betula pendula* (silver birch) are used to test the impacts from classifier, feature sets, and training samples. The results showed that RF is the best model in terms of accuracy, and local density related features are important. Experimental results confirmed the feasibility of machine learning algorithms for the reliable classification of wood and leaf points.

The main finding of this publication is that RF model is recommended in future studies for its efficiency and simplicity. This finding provides a baseline for future studies in separating wood and leaf points using supervised machine learning

classification. However, a limitation is that this study was based on isolated individual trees. More comprehensive investigations for plot-level forest data need to be performed in subsequent studies.

Publication II: Separating Tree Photosynthetic and Non-Photosynthetic Components from Point Cloud Data Using Dynamic Segment Merging

This publication (Wang et al., 2018) is a follow-up work of the publication I. A major drawback of supervised machine learning classification is the requirement of training data. First of all, manual delineation of various components from point cloud data can be extremely tedious. Rendering and manipulating the high density TLS data is also an intensive task for hardware. Furthermore, manual selection of training points is impractical for processing large numbers of trees (Disney et al., 2018). Second, the spatial distribution of training data greatly impacts the overall performance of machine learning methods. Points on main stems, small branches, leaves, bushes, and so on have to be carefully covered, which impedes the feasibility of manual manipulation.

This publication develops a fully unsupervised approach that is free of user intervention and manual training data, for separating tree photosynthetic (e.g., leaf, grass, and flower) and non-photosynthetic (e.g., stem and branch wood) components from various point cloud data with varied acquisition sources. The core observation applied in this method is that non-photosynthetic components such as stems and branches appear to be linear at various scales. The essential method developed in this publication is a robust and dynamic point cloud segmentation routine, namely Dynamic Segment Merging (DSM). This method overcomes the inefficiency of conventional region growing method in segmenting data in gradual changing regions. Then, the linear segments are identified by examining segments' feature saliency. In addition, a point cloud structuring technique is explored to accelerate data processing.

Experiments were carried out by using one single tree dataset, and four plot-level datasets. These datasets covered varied data acquisition strategies, scene complexities, and scanning instruments. One plot additionally featured calibrated intensity information. For comparison, a supervised random forest model suggested by the publication I was also performed. The results showed that the overall accuracy ranged from 81.8% to 92.0% with an average value of 87.7%.

The results in this publication indicate that separating tree photosynthetic and non-photosynthetic components from laser scanning data can be achieved in a

fully unsupervised manner without the need of training data and user intervention. The method developed in this publication is also independent from data sources, forest types, and plot sizes. This highlights a great potential in future studies, as separating wood and leaf components is often the first step needed for quantifying tree structures.

Publication III: Automatic and Self-Adaptive Stem Reconstruction in Landslide-Affected Forests

This publication (Wang et al., 2016a) focuses on tree stem detection and reconstruction in landslide-affected forests in high Alpine mountain ranges. Stem related attributes are among the most important ones for forest quantification (Liang et al., 2016). TLS has achieved promising advancements in estimating these attributes, but mainly for forests in flat environments or planned forests. The basic assumption for these types of forests is that tree stems are vertical and their cross-sections are nearly circular. This assumption directly leads to the development of methods to detect and model tree stems. For example, simple stem denoising with circle fitting (e.g., Watt and Donoghue, 2005) and cylinder fitting (e.g., Hopkinson et al., 2004; Wezyk et al., 2007) are the primary strategies often mentioned in the literatures.

A critical issue that violates the application of these available methods in mountain forests is that mountain forests are often characterized by steep terrain with a multi-layered canopy structure, including dense understory, mixed tree species and deformed stem shapes. The stem formation is often influenced by factors, such as the site fertility, spacing and light conditions, wind and landslide events (Koizumi and Hirai, 2006). Therefore, the stems are often growing in a manner deviating from the vertical direction and have irregular forms.

This publication develops a novel method to model tree stems precisely in an alpine landslide-affected forest using TLS. Tree stems are automatically detected by a two-layer projection method. A unique relationship between projected grid density and normal vector components is found that can be used to locate tree stems. This finding automates the determination of some empirical thresholds. Stems are modeled by inscribing a series of cylinders based on a 2D-3D RANSAC-based approach. The novel inscribing technique ensures a robust fitting even for tree stems that are only partially covered by laser points. The results showed that stems can be detected with a completeness of 93%, and stem curve can be successfully extracted with a high accuracy reaching a root mean square error of 2.45 cm.

Tree locations and stem related attributes were automatically generated and compared with reference data, as well as stem volumes. The results imply that the proposed method is able to map and model the stem curve precisely in complex forest conditions. The resulting stem parameters can be employed in single tree biomass estimation, tree growth quantification and other forest-related studies.

Publication IV: Reconstructing Stem Cross Section Shapes from Terrestrial Laser Scanning

The fourth publication (Wang et al., 2017b) can be regarded as a follow-up work of publication III. In publication III, cylinder fitting was still used for stem modeling due to its robustness. However, experiments showed that the fitting error can be large for cross-sections that significantly deviate from a circle (Figure 1.3). In fact, this observation can be common for mountain forests, especially for those affected by soil movements. Circle or cylinder fitting is not ideal for estimating diameters in these situations. Moreover, the cross section provides other economically important attributes related to, for example, the wood quality and growth environment. Therefore, there is a general need for knowing the actual cross-section shapes for mountain trees, instead of simply approximating them by circles and cylinders.

This publication develops a simple and robust method to reconstruct the actual cross-section shapes using TLS data. A key step is to transform a point cloud from the Cartesian coordinates to the polar coordinates. Consequently the fitting is performed in polar coordinates by using Fourier series curve approximation. The advantage of using Fourier series is that it is easy to constraint its periodicity to 2π , which corresponds to a close-form curve in the Cartesian coordinates. Iterative approximation is also deployed to remove gross errors.

The proposed approach is tested for approximating DBH with the use of two data sets: the first from an Alpine mixed and landslide-affected forest with multi-scan TLS, and the second from a mature Scots pine forest in Finland with single-scan TLS. Three different diameter approximations are tested: circle fitting, Fourier series fitting, and combined Fourier series and circle fitting. Experiment results confirmed that the developed method generated more accurate diameter estimations, especially for those trees with deformed cross-section shapes in landslide-affected forests. Specifically, the accuracy of diameter estimation is improved by 12.4% compared to that of using simple circle fitting.

The main contribution of this publication is that it develops a simple but robust method which provides a more realistic presentation of the stem cross-section

compared to the conventional circle approximation. Therefore, it is valuable for certain studies, such as in urban and mountain environments where tree forms are more complex. This publication provides a basis for quantitative studies, such as for determining the ovality and bending moment on tree cross-sections in an automatic manner.

1.4.2 Author Contributions

- **Publication I** Design of the study; crafting features and algorithm implementation; analysis of point cloud data; writing of the final article.
- **Publication II** Design of the study; partial field data collection; delineation of reference data; algorithm implementation; analysis of all five point cloud datasets; writing of the final article.
- **Publication III** Design of the study; field TLS data acquisition and reference data measurements; algorithm implementation; analysis of point cloud data; writing of the final article.
- **Publication IV** Design of the study; field TLS data acquisition and reference data measurements; algorithm implementation; analysis of point cloud data; writing of the final article.

Point Cloud Structuring Assisted Data Processing

Point cloud data acquired by laser scanners may consist of millions to billions discrete and unorganized points. Efficient spatial data structuring is often required to managing and querying over a huge number of 3D points. However, there are no systematic investigations available in the literatures, and especially for TLS point clouds of forest scenes. Therefore, efficient processing of large point clouds requires an initial step on the identification of the appropriate data structure and access mechanisms.

2.1 Point Cloud Querying and Spatial Partition

For point clouds, two aspects related to data structuring are particularly considered – point querying and spatial partition, which are needed for a number of reasons including efficient neighboring search (Elseberg et al., 2011), parallelized processing acceleration (Wang et al., 2018), generation of a continuum (Xu et al., 2017b), and measurements of 3D shape properties (Bribiesca, 2008).

Point querying, including both nearest neighborhood search and range querying are frequently performed in point cloud processing, owing to the inherent spatial property of point cloud data. For example, estimation of normal vectors often requires information on K nearest neighbors (Knn) (Rabbani et al., 2006). Range querying is a first step needed to estimate density information and structural cues surrounding a specific point (Chen et al., 2018). The most widely used spatial data structure for point querying in point clouds is the KD-tree and its modifications for the efficiency (Muja and Lowe, 2014). KD-tree, which stands for K-Dimensional tree, is a binary tree structure, whose non-leaf nodes (splitting hyperplanes) split all children along a specific dimension. For example, a hyperplane perpendicular to the X-axis firstly splits data into left sub-tree and right sub-tree, respectively (Figure 2.1). The next level divides data on the next dimension, returning to the first dimension once all others have been exhausted. For point clouds that only contain geometric coordinates, a KD-tree refers to three-dimensional. In this dissertation, the implementation of KD-tree and the corresponding neighborhood and range

querying provided in the Statistics and Machine Learning Toolbox in Matlab (The MathWorks, Inc., Natick, Massachusetts, United States) is used.

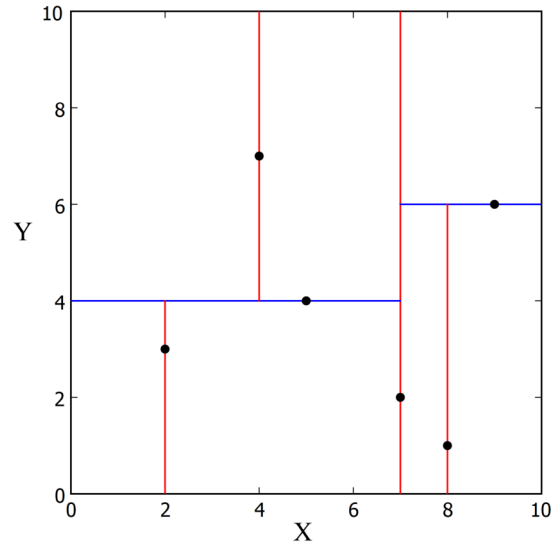


Fig. 2.1: A visualization of a 2D KD-tree on six points. Image modified from the original work by user ID KindDragon33, used under a CC-BY 3.0 license from Wikimedia commons.

Spatial partition is to divide a point cloud into a number of subdivisions (i.e., bins). The main purposes of using partition include efficient point cloud managements (Pfeifer et al., 2014), generation of a continuum which transforms unorganized point clouds to organized forms (Xu et al., 2017b), reduction of the computation cost, and suppression of negative effects of outliers and varying point densities (Xu et al., 2017a). Spatial partition methods including uniform voxelization (Papon et al., 2013), Octree voxelization (Elseberg et al., 2013), and 2D tiling (Pfeifer et al., 2014) are often used. Uniform voxelization is a commonly used approach to partition a point cloud into local spaces (e.g., Papon et al., 2013). It is fast to generate, and works with satisfaction for a point cloud with a homogeneous density distribution (Figure 2.2). On the other hand, Octree voxelization is better at balancing the needed computational resources in each sub-region and surpassing the impacts from outliers and varied point density. For example, a typical Octree implementation sets the maximum number of points a bin may contain. If more points exist, the bin will be recursively subdivided (Figure 2.3). Moreover, for point clouds covering a large spatial scale, 2D tiles on the XY plane is a proper choice since data are mainly distributed on the X and Y dimension (Figure 2.4).

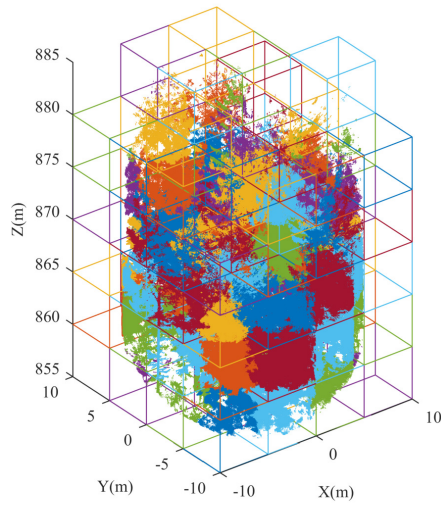


Fig. 2.2: Uniform voxelization of a forest point cloud. The boundaries of each bin and its contained points are equally rendered with random colors. The voxel size is set to 5 meters in this example.

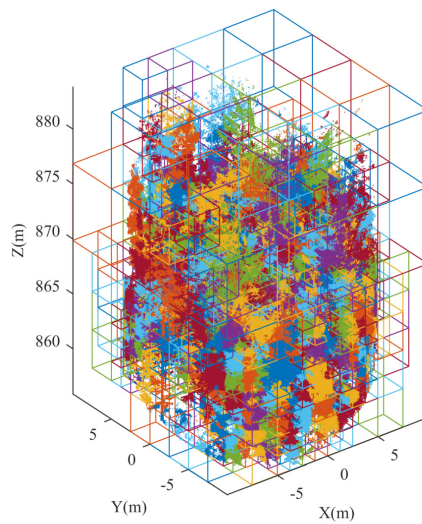


Fig. 2.3: Octree voxelization of a forest point cloud. The boundaries of each bin and its contained points are equally rendered with random colors. The Maximum bin capability is set to 50,000 points, which results in a bin depth of 1617 in this example.

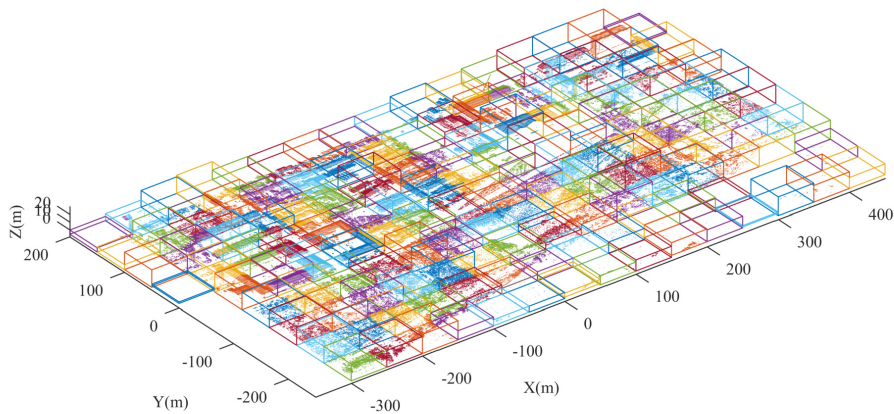


Fig. 2.4: 2D tiling of a ALS point cloud. The boundaries of each bin and its contained points are equally rendered with random colors. The tile size is set to 50 meters in this example.

2.2 Applications

The techniques presented in section 2.1 are used in the papers that are included in this dissertation, but are not explicitly mentioned. Therefore, this section further introduces several examples in details.

2.2.1 Accelerated Range Search

Range querying refers to finding all neighbors within a specified distance of querying points, and is frequently performed in point cloud processing. A base-line application is to infer local geometrical structure information surrounding a point. The assessed structure information then can be potentially used to segment or recognize objects. For example, for a point on a tree branch, the linear saliency revealed by points distributed in its surrounding within a certain range may help to identify tree branches in a forest point cloud (Wang et al., 2018). A certain number of applications also require multi-scale analysis, in order to estimate structures with varied sizes (Park et al., 2012). Therefore, an efficient routine for point cloud range querying should be investigated.

Range querying can be facilitated by using the KD-tree structure (see section 2.1). However, range querying can still be very time consuming for large datasets, and for querying a large distance that may contain a large number of points. Nevertheless,

an observation is that the queried range is often much smaller than the extent of a point cloud. This indicates that a two-level structuring strategy may help to limit the range querying in subdivisions, thus accelerates the processing.

In detail, a range querying problem can be shrunk to a local space that is constructed by a spatial partition method (see section 2.1) (Papon et al., 2013). Consequently, only a KD-tree in the local space needs to be constructed, instead of over the entire point cloud. This strategy results in two advantages. First, the range querying is performed in the local space that has a much smaller extent than the entire point cloud, thus avoids the memory consumption for a single large variable by dispersing it into multiple variables. Second, by limiting the querying in a local space, the processing can be easily parallelized for multiple local spaces. Accordingly, it provides a potential to largely reduce the computational time.

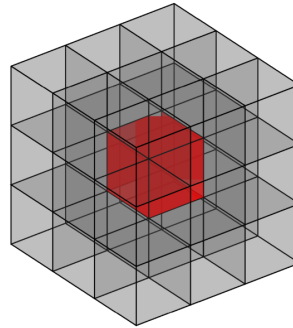


Fig. 2.5: A voxel has 26 neighboring voxels in a 3D uniform space.

For example, a 3D voxel has 26 neighboring voxels touching it in a uniform space (uniform voxelization, Figure 2.5). The range querying for a point inside a voxel can be limited within the voxel itself together with its 26 neighboring voxels, under the constraint that the voxel size is no less than the querying range. That is, the processing unit becomes a voxel instead of a point. A positive fact is that a uniform voxel space has a regular structure with a fast spatial indexing frame. Therefore, finding the neighboring voxels of a specific voxel is straightforward. Subsequently, the range querying then can be parallelized for each voxel. Figure 2.6 shows an example of runtime comparisons for point clouds range querying for various distances with and without spatial partitions in Matlab 2017a (The MathWorks, Inc., Natick, Massachusetts, United States). The queried distances ranged from the average point spacing with an increment of itself until tenfold. Parallel computing is deployed for those with spatial partitions. Uniform voxelization and 2D tiling are used for TLS forest point clouds and large-area ALS and MLS data, respectively. A general conclusion is that the computational time for structured point clouds are reduced significantly compared with those without structuring, especially when the

queried distance is large. Moreover, the seep-up is less significant for small datasets (e.g., Figure 2.6c), and for querying a small distance for a very dense point cloud (e.g., Figure 2.6a). However, the two-level structuring strategy greatly accelerates range querying for large datasets and for querying a large distance, which are the current bottlenecks in practice.

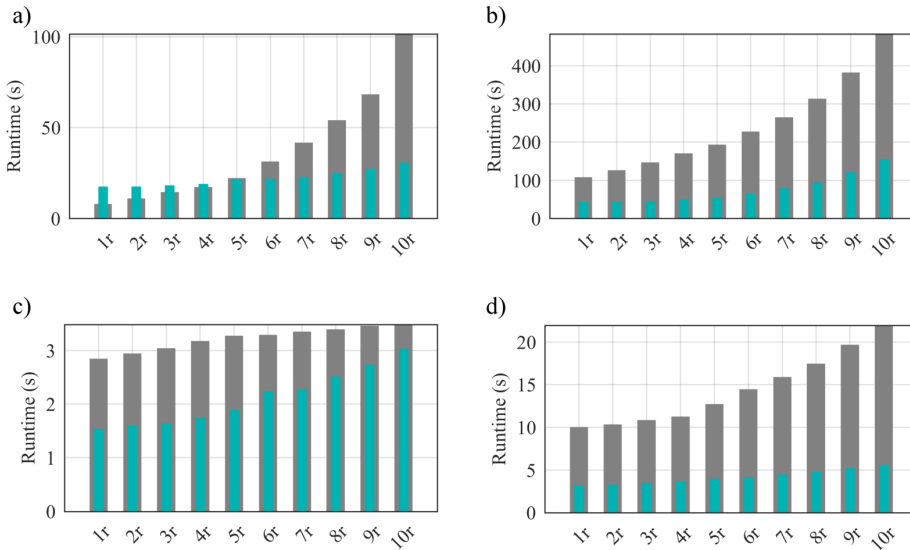


Fig. 2.6: Runtime benchmarking of range querying with and without spatial partitions. Color jungle green represents the runtime with spatial partitions. a) Uniform voxels constructed on a point cloud with 1,170,489 points. Processing parallelized with 7 CPU threads. b) Voxels constructed a point cloud with 4,933,336 points. Processing parallelized with 24 CPU threads. c) 2D tiles constructed on a point cloud with 122,829 points. Processing parallelized with 7 CPU threads. d) 2D tiles constructed on a point cloud with 332,480 point. Processing parallelized with 7 CPU threads.

2.2.2 3D Compactness Measurement

Measurement of the shape property of an unorganized point cloud is of vital importance. For example, planar shapes can be estimated to detect roofs in point clouds (Xu et al., 2017b; Pöchtrager et al., 2017). Linear shape properties help to find tree branches in forest scenes (Wang et al., 2018). These shape information derived from point clouds are directly related to the knowledge on local structures.

However, estimation of some high-level shape properties from unorganized point clouds can be untoward. The inherent challenge is that point clouds are discrete and scattered. For example, tree crown shapes can be evaluated by using approaches such as convex hull (Li et al., 2012) and alpha shape (Vauhkonen et al., 2010). However, these approaches only provide some simple measures and their approxi-

mations. Other metrics such as 3D shape compactness and symmetry are difficult to estimate directly in unorganized point clouds.

A solution is to use a proper spatial partition method to generate a volumetric representation of a point cloud. Such a volumetric representation is also known as spatial occupancy array (i.e., continuum), and is very common in computer-aided tomography (Bribiesca, 2008). A volumetric representation for 3D point clouds corresponds to a 3D uniform voxel representation, and it transforms point clouds into 3D discrete representations with a regular structure (i.e., the same as section 2.2.1). The transformed representation can be regarded as a simplified version of the original point cloud. Consequently, several shape measurements can take the advantage of the discrete analysis. For example, 3D shape compactness, which is defined by the ratio $(area^3)/(volume^2)$, is useful in evaluating the goodness of an optimization problem in tree crown segmentation from point cloud data (Véga et al., 2014) (Figure 2.7). Occupied areas (i.e., the enclosing surface area) is not directly measurable for a 3D point cloud. However, a simple measure of discrete compactness (Bribiesca, 2008) on top of the volumetric representation can be achieved by

$$C_d = \frac{n - A/6}{n - (\sqrt[3]{n})^2}, \quad (2.1)$$

where A is the area of the enclosing surface and n denotes the number of occupied 3D voxels. The discretization of unorganized point clouds into 3D voxel representations greatly reduce the computational complexity.

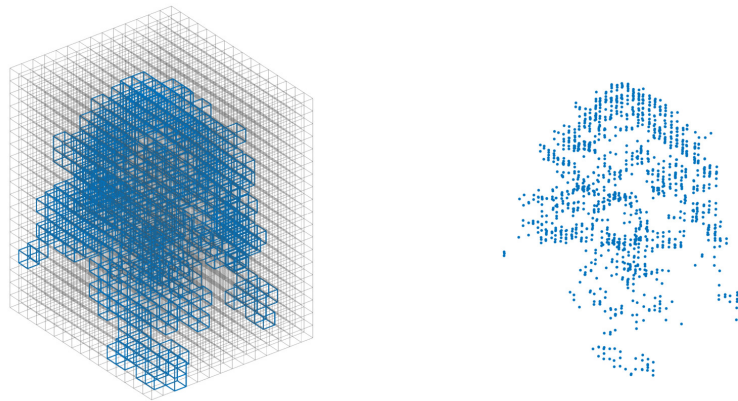


Fig. 2.7: Spatial occupancy array of a tree crown point cloud. (a) Uniform voxelization. (b) The original unorganized point cloud.

2.2.3 Parallelized Tile Processing

A bottleneck of processing large point clouds is on the tedious computation time needed for many advanced algorithms. This challenge is even prominent for

processing high density TLS datasets and large-area datasets acquired by e.g., ALS and MLS. To mitigate such as a problem, high-end hardware configurations are often required.

However, a certain types of strategies on the algorithm level can help to solve this problem, at least to some extent. A commonly used approach is the tile processing (Vosselman, 2013), which is essentially implemented based on spatial partition. Tile processing means that the processing is distributed in individual tiles (i.e., subdivisions in spatial partition), so that the entire processing can be parallelized. Moreover, results obtained on individually processed tiles often need to be merged for many applications such as point cloud segmentation. A vital benefit that tile processing provides is on the reduction of computation time, if multi-processors are available. In addition, the memory consumption is also distributed to each computer processor, avoiding memory overcommitment for a single processor.

Figure 2.8 shows an example of forest point cloud segmentation on tiles, and tile merging afterwards. Such a segmentation routine helps to identify tree stems and branches in forests (Wang et al., 2018). The parallelized tile processing greatly accelerates point cloud manipulation. A quantitative analysis shows that the runtime in this example is reduced approximately 100 times by using parallelized tile processing with 7 CPU threads. It is noted that the degree of acceleration depends on the time complexity of an algorithm, and may not be linear to the number of threads used.

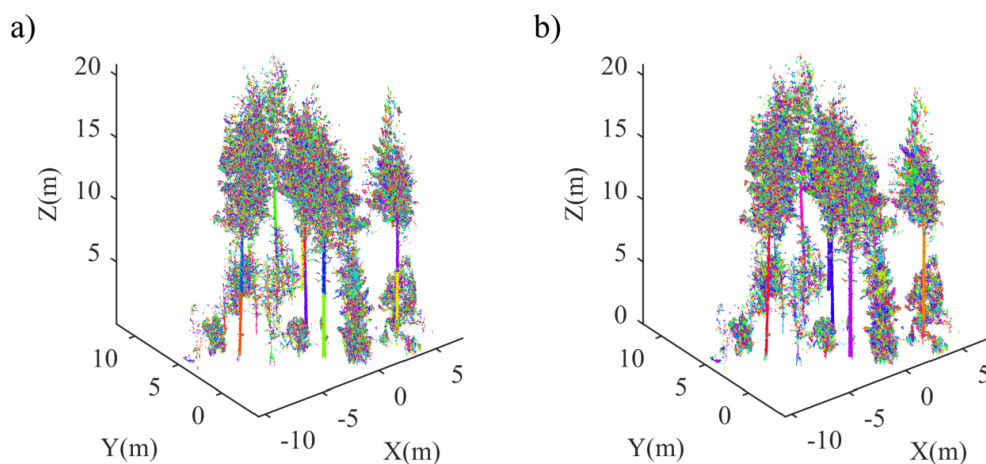


Fig. 2.8: Tile processing for forest segmentation. Each segment is randomly colored. (a) Segmentation results on each tiles.(b) Results after tile merging.

2.3 Conclusion

In this chapter, spatial partition assisted point cloud processing is explicitly demonstrated by three application examples. These examples show that point cloud spatial partition provides a number of benefits especially on the reduction of processing time and generation of a continuum (i.e., regular structure). These useful strategies are not systematically investigated for forest point cloud processing in the literatures. The potential of using proper spatial partition routines is confirmed in this chapter and other relevant works in this dissertation, thus is recommended in future studies.

Publication I: Feasibility of Machine Learning Methods for Separating Wood and Leaf Points from Terrestrial Laser Scanning Data

” *This section is a reproduced version of: Wang, D., Hollaus, M., & Pfeifer, N. (2017). Feasibility of machine learning methods for separating wood and leaf points from terrestrial laser scanning data. ISPRS Annals of Photogrammetry, Remote Sensing and Spatial Information Sciences, IV-2/W4, 157-164.*

3.1 Introduction

Quantifying forest structure is of broad importance. For example, understanding forest foliage profile can be of particular interest for biodiversity conservation and climate adaptation, as it affects the photosynthesis and evapotranspiration processes (Ma et al., 2016). Monitoring carbon stocks in forested ecosystems requires accurate quantification of the spatial distribution of wood volume (Levick et al., 2016). Moreover, description of 3D structure helps to investigate species competition, wood production, and ecosystem and agro-ecosystem dynamics (Béland et al., 2014). For mapping forest structure, laser scanning is widely used in past decades. Laser scanning technique, also known as light detection and ranging (lidar), acquires 3D coordinates of objects over a large scale. In addition, full-waveform laser scanners are able to measure the scattering properties of vegetation in a quantitative way (Wagner et al., 2008). Therefore, laser scanning generates a high potential for forest related studies.

Assessment of canopy structure at tree or branch scale can be difficult with laser scanning data acquired from satellite and airborne platforms (Tao et al., 2015a). Terrestrial Laser Scanning (TLS), on the other hand, has been established as an efficient tool for acquiring 3D data used for a range of fine-scale forest studies (Liang et al., 2016), including stem mapping (Liang et al., 2012), tree height measurement (Olofsson et al., 2014), diameter estimation (Wang et al., 2017b), stem curve retrieval (Wang et al., 2016a), biomass calculation (Kankare et al., 2013), and leaf area index (LAI) estimation (Zheng et al., 2013). To better retrieve forest ecological attributes, it is often necessary to separate wood and leaf components of trees (Tao et al., 2015a). For example, estimation of LAI requires to screen out wood points, otherwise the wood returns will artificially increase the apparent foliage content (Béland et al., 2014).

Wood-leaf point separation for TLS data is challenging. In general, existing methods can be categorized into two groups; intensity based and geometry based. Intensity based methods (Pfennigbauer and Ullrich, 2010; Béland et al., 2014) use radiometric information of objects captured by a laser scanner. The assumption is that wood and leaf components have different optical properties at the operating wavelength of the laser scanner (Tao et al., 2015a). By determining a proper intensity threshold, wood and leaf points can be separated. However, intensity captured by a laser scanner needs an instrument specific radiometrical calibration before including it in further processing (Calders et al., 2017). Recently developed multi-wavelength (e.g., hyperspectral) scanners can help to better solve such a task (Li et al., 2013; Hakala et al., 2012; Vauhkonen et al., 2013). However, these scanners are still in an early development stage, and not yet widely available. Geometry based methods only use 3D coordinates of objects captured by a laser scanner. Local structure-related saliency information are derived from 3D points and supervised machine learning methods such as Support Vector Machine (SVM) (Yun et al., 2016) and Gaussian Mixture Model (GMM) (Ma et al., 2016) are often employed to classify wood and leaf points. Some direct geometric methods were also reported (Tao et al., 2015a). Nevertheless, geometry based machine learning methods are rarely systematically examined for wood-leaf classification, although it is a well-known and widely adapted technique for other classification tasks (Weinmann et al., 2013; Weinmann et al., 2017; Brodu and Lague, 2012). There is a vast need to exploit 3D geometry based approaches for separating wood and leaf points, as 3D coordinates are the most fundamental information acquired by any laser scanners. For machine learning methods, various classifiers were used in previous studies (Yun et al., 2016; Ma et al., 2016). The lack of comparable studies calls for a specific examination on how the chosen machine learning classifier and features used would influence classification results.

This study aims to examine four machine learning algorithms, Support Vector Machine (SVM), Naïve Bayes (NB), Random Forest (RF), and Gaussian Mixture Model (GMM), in geometry-based wood and leaf points separation using TLS data. In the following section 3.2 the used data are described, in section 3.3 the machine learning models used for separating wood and leaf points are presented. Finally, in section 3.4 the results are presented and discussed in section 3.5. Conclusion is given in section 3.6.

3.2 Materials

3.2.1 *Erytrophleum fordii*

TLS data of an evergreen sub tropical tree, *Erytrophleum fordii*, were provided by Hackenberg et al., 2015. The data were acquired in October 2013 from eight scan positions. The acquired point cloud was further manually cleaned, as the tree crown interacts with other trees. Therefore, points from adjacent trees' foliage need to be removed. The cleaned point cloud for the *Erytrophleum fordii* tree contains ~ 3.9 million points. The average distance between two adjacent points is ~ 5 mm (Figure 3.1).

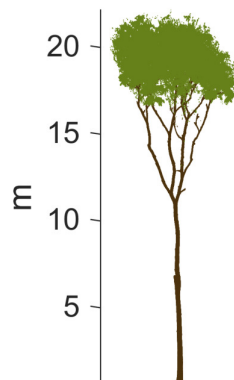


Fig. 3.1: Point cloud of the *Erytrophleum fordii*.

3.2.2 *Betula pendula*

Hyperspectral TLS data of another silver birch tree (*Betula pendula*, Figure 3.2) were provided by (Puttonen et al., 2016). The single-scan data feature radiometrical information of the scanned tree, in addition to the 3D XYZ coordinates. The average distance between two adjacent points is ~ 1 cm. Measurements were carried out using a Hyperspectral Laser Scanner (HSL) from the Finnish Geospatial Research

Institute (FGI) (Hakala et al., 2012). Laser radiometry was calibrated by setting up an external reference plate. For more information about the HSL data, readers are referred to (Puttonen et al., 2016).

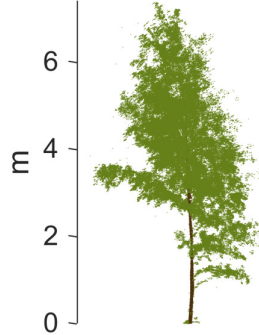


Fig. 3.2: Point cloud of the *Betula pendula*, silver birch.

Tab. 3.1: Features extracted from the point cloud. *EV* denotes the eigenvalue and *NV* is the normal vector. *EVs* are sorted in a descend manner. "R-" is the abbreviation of "Ranking" form feature selection. "R-Combined" means that the feature set is a combination of data from both trees. Top 5 ranked features are underlined.

No.	Feature	Description	R- <i>E. fordii</i>	R-Birch	R-Combined
1	linearity $L_{\lambda,3D}$	linear saliency $(EV_1 - EV_2)/EV_1$.	23	19	22
2	planarity $P_{\lambda,3D}$	planar saliency $(EV_2 - EV_3)/EV_1$.	17	26	17
3	scattering $S_{\lambda,3D}$	volumetric saliency EV_3/EV_1 .	14	14	15
4	omnivariance $O_{\lambda,3D}$	variance of the neighborhoods $\sqrt[3]{EV_1 * EV_2 * EV_3}$.	16	20	16
5	anisotropy $A_{\lambda,3D}$	$(EV_1 - EV_3)/EV_1$.	15	15	14
6	eigenentropy $E_{\lambda,3D}$	$-\sum_{n=1}^3 EV_n * \log(EV_n)$	18	22	19
7	sum_ EV_{3D}	$\sum_{n=1}^3 EV_n$.	20	10	20
8	surface_variation _{3D}	change of curvature $EV_{min}/(\sum EV)$.	12	17	12
9	Z value $Z_{\lambda,3D}$	the height of the point.	<u>1</u>	<u>2</u>	<u>1</u>
10	radius_knn $R_{knn,3D}$	radius of local neighborhood.	9	<u>4</u>	8
11	density _{3D}	local point density.	<u>3</u>	<u>1</u>	<u>3</u>
12	verticality $V_{\lambda,3D}$	$1 - NV_{S_z}$.	24	13	24
13	$\Delta Z_{knn,3D}$	height difference of local neighborhood.	10	8	10
14	$\sigma Z_{knn,3D}$	standard deviation of heights of local neighborhood.	11	7	11
15	radius_knn $R_{knn,2D}$	radius of local neighborhood.	8	<u>5</u>	7
16	density _{2D}	local point density.	<u>2</u>	9	<u>2</u>
17	sum_ EV_{2D}	$\sum_{n=1}^2 EV_n$.	21	11	21
18	EV_ratio_{2D}	EV_2/EV_1 .	7	25	9
19	cell_density _{2D}	density of projected 2D cells.	<u>4</u>	6	<u>4</u>
20	$\Delta cell_{2D}$	height difference of points in each cell.	25	<u>3</u>	25
21	$\sigma cell_{2D}$	standard deviation of heights of points in each cell.	22	12	23
22	EV_1_{3D}	first eigenvalue of 3D covariance matrix.	26	16	26
23	EV_2_{3D}	second eigenvalue of 3D covariance matrix.	19	21	18
24	EV_3_{3D}	third eigenvalue of 3D covariance matrix.	13	18	13
25	EV_1_{2D}	first eigenvalue of 2D covariance matrix.	6	24	<u>5</u>
26	EV_2_{2D}	second eigenvalue of 2D covariance matrix.	<u>5</u>	23	6

3.3 Methods

3.3.1 Feature Calculation

Twenty-six 2D and 3D geometry-based point cloud features extracted for each data set were described in Table 3.1. The features were originally proposed and used in Weinmann et al., 2015 for urban area scene analysis. Local 3D features are inferred from the distribution of neighboring points of every point. Structure saliency such as planar, linear, and scattering can be inferred from the eigenvalues of the decomposed covariance matrix (Equation 3.1).

$$Cov_p = \frac{\sum_{i=1}^K (p_i - \bar{p})(p_i - \bar{p})^T}{K}, \quad (3.1)$$

where $p_i = \{x_i, y_i, z_i\}^T$ is a 3D point and \bar{p} is the barycenter of the K nearest neighboring points. 2D feature calculation involves a projection of points onto the horizontal plane. For details of feature extraction procedures, the readers are referred to (Weinmann et al., 2015).

3.3.2 Feature Selection

The high dimensionality of the input data may exhibit redundancy and can be potentially reduced by various feature selection algorithms. Moreover, feature selection may attenuate the over-fitting problem in multivariate classification methods (Geiß et al., 2015). Feature selection methods can be grouped into three categories; wrappers, embedded, and filters (Guyon et al., 2008). Wrappers methods evaluate a subset of features by accuracy estimates and require trained classifiers. Embedded methods embed the selection process into the classifier learning. On the other hand, filter methods explore the intrinsic properties of the data, and thus operate independently with respect to classifiers. In this study, we employ the filter method for feature selection for its simplicity and efficiency, although more robust and concrete methods are used in previous studies (Weinmann et al., 2013).

A fast and effective filter method is the *Fisher* method (Gu et al., 2012). This method computes a score (*Fisher score*) according to a ratio of interclass separation and intraclass variance for each feature and ranks them. The scores reflect the discriminative power of each feature. In this study, we apply the *Fisher* method for both *Erythrophleum fordii* and silver birch datasets. The resultant rankings are given in Table 3.1. Consequently, the classifier learning was performed for 5, 10, 15, 20, and 26 features accordingly, based on the rankings.

3.3.3 Machine Learning Classifiers

Wood-leaf separation is a binary classification problem. Given m training samples, (y_i, \mathbf{x}_i) $i = 1, \dots, m$ with labels $y_i \in \{1, -1\}$ and n dimensional feature vectors, $\mathbf{x}_i \in \mathbf{R}^n$, the objective is to find a function $f(\cdot; \boldsymbol{\alpha}) : \mathbf{x} \mapsto y$ that represents the classifier $y = f(\mathbf{x}; \boldsymbol{\alpha})$, where $\boldsymbol{\alpha}$ are all the parameters of the classifier.

In this study, we examine the feasibility of four machine learning algorithms, SVM, NB, RF, GMM, for wood-leaf separation. In this section, the fundamentals and principles of the four used machine learning algorithms are briefly summarized.

Support Vector Machine

SVM was proposed by (Vapnik, 1995). For a binary classification problem, it finds a hyper-plane $\mathbf{w} \cdot \mathbf{x} + b = 0$, which maximizes the distance of the closest vectors (i.e., margin) in both classes. \mathbf{w} is the n -dimensional vector perpendicular to the hyper-plane, and b is the distance of the closest point on the hyper-plane to the origin. The classifier is then

$$f(\mathbf{x}) = \text{sgn} \left(\sum_{i=1}^m \lambda_i y_i K(\mathbf{x}_i, \mathbf{x}_j) + b \right), \quad (3.2)$$

where λ is the weight and $K(\mathbf{x}_i, \mathbf{x}_j)$ is a *kernel function* $K(\mathbf{x}_i, \mathbf{x}_j) = \Phi(\mathbf{x}_i) \cdot \Phi(\mathbf{x}_j)$, subjects to $y_i(\langle \mathbf{w}, \mathbf{x}_0 \rangle + b) - 1 \geq 0$.

Naïve Bayes

NB is a statistical approach based on Bayes's theorem (Marcot et al., 2006). It assumes that the features are conditionally independent given the class,

$$p(x|y) = \prod_{i=1}^m p(x_i|y). \quad (3.3)$$

Therefore, from the Bayes's theorem, the posterior probability of a feature vector to be part of a certain class is

$$p(y|x) = \frac{p(y) \prod_{i=1}^m p(x_i|y)}{p(x)}, \quad (3.4)$$

where $p(y)$ is the prior probability of the class. A point will be labeled as the class with the highest probability.

Random Forest

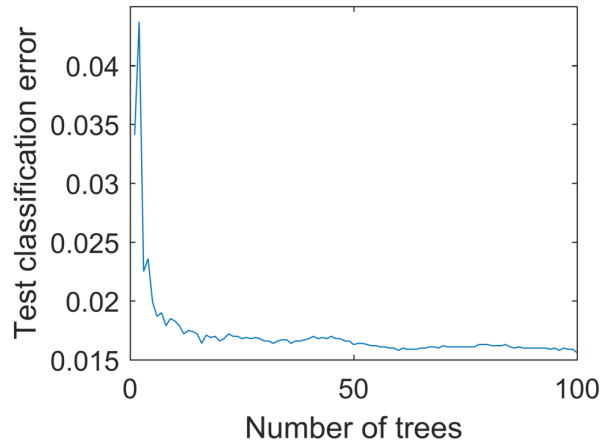


Fig. 3.3: Evaluation of number of classification trees to be grown.

Tab. 3.2: Statistical evaluation of machine learning classifiers for wood-leaf separation.

Features	Classifier	<i>E. fordii</i>			birch		
		Sensitivity	Specificity	Accuracy	Sensitivity	Specificity	Accuracy
5	SVM	0.94	1.00	0.97	0.88	0.93	0.93
	NB	0.91	0.99	0.95	0.90	0.90	0.90
	RF	0.96	1.00	0.98	0.93	0.94	0.94
	GMM	0.90	0.99	0.95	0.88	0.94	0.94
10	SVM	0.93	1.00	0.97	0.92	0.98	0.97
	NB	0.91	0.98	0.95	0.92	0.89	0.89
	RF	0.96	1.00	0.98	0.96	0.98	0.98
	GMM	0.91	0.99	0.95	0.87	0.97	0.97
15	SVM	0.93	1.00	0.97	0.94	0.97	0.97
	NB	0.91	0.97	0.94	0.93	0.86	0.86
	RF	0.95	1.00	0.98	0.96	0.98	0.98
	GMM	0.91	0.99	0.95	0.87	0.97	0.97
20	SVM	0.94	1.00	0.97	0.94	0.97	0.97
	NB	0.92	0.96	0.94	0.93	0.86	0.87
	RF	0.95	1.00	0.98	0.96	0.98	0.98
	GMM	0.91	0.99	0.95	0.87	0.97	0.97
26	SVM	0.94	1.00	0.97	0.94	0.97	0.97
	NB	0.93	0.95	0.94	0.93	0.86	0.87
	RF	0.97	1.00	0.98	0.95	0.98	0.98
	GMM	0.91	0.99	0.95	0.87	0.97	0.97
NDVI threshold					0.78	0.97	0.96

RF is a decision tree based ensemble learning method that was proposed by (Breiman, 2001). The learned model is a collection of weak models. Multiple decision trees are grown on random subsets of training data. The class determination is based on a majority votes fashion. RF has proven to be an accurate and robust classification and regression approach, even on noisy data (Geiß et al., 2015).

When employing RF, two necessary parameters need to be specified; the number of classification tree n_{trees} and the number of input features m_{ft} used at each node (Geiß et al., 2015). A higher number of n_{trees} increases model accuracy until convergence. We used our data with all features to train models. We observe that in our study, the model performance converges at the point of approximate 60 trees (Figure 3.3). However, since our data set is not large enough for us to consider a trade

off for computation time, we keep the number as 100. We set another parameter, $m_{ft} = \sqrt{p}$, where p denotes the number of input feature, as suggested by (Breiman, 2001).

Gaussian Mixture Model

GMM is a modeling technique that uses a probability distribution to estimate the likelihood of a given feature vector. The assumption is that classes obey a normally distributed density function. For a binary classification problem, the continuous probability density function can be approximated as a linear combination of two probability density functions (Ma et al., 2016),

$$p(x) = \sum_{k=1}^m w_k p(x|k) \quad (3.5)$$

where w_k is the weight for each probability density function. $p(x|k)$ is the conditional probability of a point x belonging to the k th density function. The probability that a point x_i lies within the a distribution with parameters μ and Σ is given by

$$N(\mu_k, \Sigma_k) = \frac{e^{-\frac{1}{2}(x_i - \mu_k)^T \Sigma^{-1} (x_i - \mu_k)}}{\sqrt{|2\pi\Sigma|}}. \quad (3.6)$$

In this study, manually delineated training points are used to train the GMM model. The *Expectation-Maximization algorithm (EM)* is used to estimate the μ and Σ of each class. Consequently, a point will be labeled as the class with the highest probability.

3.3.4 Evaluation

The performance of each classifier is evaluated based on three statistical indexes; sensitivity, specificity, and accuracy. Sensitivity measures the correctly classified positive samples (true positive rate, TP). In this study, it represents that the correct rate for wood points. Specificity gives the true negative rate (TN), thus it measures the correct rate for leaf points. Accuracy (ACC) gives the overall correctness by

$$ACC = \frac{TP + TN}{P + N}, \quad (3.7)$$

where P and N are the number of real positive (wood) and negative (leaf) samples.

3.4 Experiments and Results

We manually selected approximate 10% points from each tree as the training data for the machine learning classifiers. These training points are evenly distributed from the bottom to the top of each tree. Consequently, four machine learning classifiers were trained accordingly with different feature sets. The statistical performance indices are summarized in Table 3.2.

For both trees, RF model resulted in best performance invariably, while NB model gave least accuracy. The accuracy of four classifiers with various feature sets are demonstrated in Figures 3.4 and 3.5. Feature sets are selected based on the ranking lists resulted from the *Fisher* filter method (section 3.2). For the *Erytrophleum fordii* tree, all classifiers' performances remained similar, indicating little effects from the number of feature used. All four classifiers showed promising results with more than 94% accuracy, which are comparable to e.g., Ma et al., 2016. Although, it is noted that Ma et al., 2016 worked on a more complex and littery scene. For the silver birch tree, the accuracy of the SVM, RF, and GMM model became stable when number of features used reached 10. The NB model performed less well in this study, and its performance reduced with increased feature sets. A similar trend also can be observed from the study of the *Erytrophleum fordii* tree, although in this case the trend was weak. The reason may be that the assumption in NB that a particular feature is independent of the value of any other feature was violated when more features were involved. In such a case, the Bayesian Network model (Friedman et al., 1997) will be more suitable. In addition, NB is known to have difficulties when dealing with unbalanced data.

We observed that the high classification accuracy of the *Erytrophleum fordii* might be caused by the fact that the distributions of its stem and crown are essentially very well distinct. To assess the performances of machine learning classifiers in regions where leaf and wood components are heavily interacted, we selected a subset point cloud between 16 and 20 m above ground of the *Erytrophleum fordii* (Figure 3.6), and ran the experiments on this subset. The results are given in Table 3.3. The accuracy remained almost identical compared to those from the whole point cloud, indicating that machine learning algorithms can commendably separate leaf and wood components by providing proper training samples.

For the silver birch, calibrated spectral attributes exist. Therefore, leaf and wood can be separated from the spectral information of each point as well. This is based on the fact that different components of a tree feature discriminatory optical properties at the operating wavelengths of the laser scanning system (Tao et al., 2015a). In this study, the birch leaf and wood were separated with a hard normalized difference

vegetation index (NDVI) threshold value of 0.2. All points that have NDVI value less than 0.2 were labeled as wood components, and vice versa. The accuracy of the spectral method is included in Table 3.2. The sensitivity (i.e., accuracy for wood identification) is lower than those from machine learning algorithms, mainly because some higher parts of the stem were misclassified as leaves.

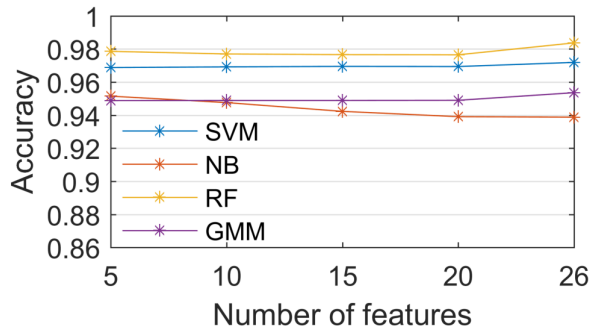


Fig. 3.4: Performance of four classifiers for the *Erytrophleum fordii* as a function of the different feature sets. Feature sets were determined based on the *Fisher* filter method described in section 3.2

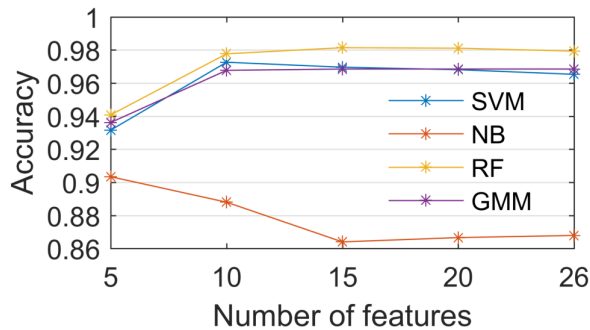


Fig. 3.5: Performance of four classifiers for the silver birch as a function of the different feature sets. Feature sets were determined based on the *Fisher* filter method described in section 3.2

3.5 Discussion

3.5.1 Classifier Performance

As summarized in the Tables 3.2 and 3.3, the performances of selected machine learning classifiers are comparable to and surpassing published studies (Ma et al.,



Fig. 3.6: A crown subset (i.e., 16 - 20 m) of the *Erytrophleum fordii*. Branches and leaves heavily interact.

Tab. 3.3: Statistical evaluation of machine learning classifiers for the crown subset of the *Erytrophleum fordii* with 5, 10, 15, 20, and 26 features.

Features	Classifier	Sensitivity	Specificity	Accuracy
5	SVM	0.93	0.97	0.95
	NB	0.95	0.95	0.95
	RF	0.95	0.98	0.96
	GMM	0.92	0.95	0.94
10	SVM	0.93	0.97	0.95
	NB	0.95	0.92	0.94
	RF	0.96	0.98	0.97
	GMM	0.91	0.96	0.94
15	SVM	0.94	0.98	0.96
	NB	0.96	0.90	0.93
	RF	0.96	0.98	0.97
	GMM	0.91	0.96	0.94
20	SVM	0.94	0.98	0.96
	NB	0.96	0.90	0.93
	RF	0.96	0.98	0.97
	GMM	0.91	0.96	0.94
26	SVM	0.94	0.98	0.96
	NB	0.96	0.90	0.93
	RF	0.96	0.98	0.97
	GMM	0.91	0.96	0.94

2016; Tao et al., 2015a). In our tests, RF model produced best results, proving that RF might be very well suitable for wood-leaf classification. This can also be justified by visualizations of the classification results in this study (Figure 3.7 and 3.8). The popular SVM model also gave promising results, however, its model training time were much longer than others'. NB model performed worse in this study and might not be suitable for leaf-wood separation, unlike its high efficiency in text classification (Kim et al., 2006). GMM model is typically used in unsupervised classification problems (Koo et al., 2014), although it was previously used in separating leaf, wood, and ground points (Ma et al., 2016). We briefly tested

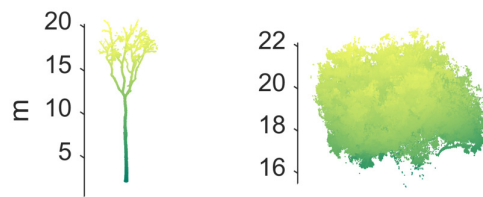


Fig. 3.7: Classification results of RF model for *Erytrophleum fordii*. Left part shows the wood components and right part shows the leaf points.

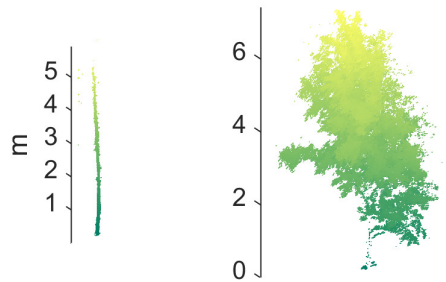


Fig. 3.8: Classification results of RF model for silver birch. Left part shows the wood components and right part shows the leaf points.

the performance of the GMM classifier without training data, so that the data were clustered into two groups in the feature space. We obtained an accuracy of 93% and 91% for the *Erytrophleum fordii* and silver birch, respectively, which are lower than that of the supervised GMM.

3.5.2 Feature Importance

In this study, features were ranked based the *Fisher* filter feature selection method (Table 3.1). Furthermore, feature sets with different sizes based on the rankings are tested. For both trees, point height and local density seem to be the most vital features, as they were both ranked as top 5. This indicates that local density characteristics might play a vital role in leaf-wood separation. However, both of them are bound to perform worse in a more complex scene. Commonly used

structure inferring features such as linearity and planarity turned out to be less important as they were ranked as non-significant (e.g., 50% in the case of the latter). This can also be justified from the performances of various feature sets. For both trees, the first 10 best features according to the ranking are enough to stabilize the model accuracy, meaning that features such as linearity and planarity are not necessary to be included in such a wood-leaf classification issue. However, we note that feature selection should consider the local tree structure characteristics, such as tree species. In addition, more feature selection approaches should be tested, possibly in connected with the chosen machine learning model. Such methods are known as *wrappers*.

3.5.3 Training Sample Delineation

In this study, training samples were manually and evenly selected from the bottom to the top of each tree. The selected training data take up around 10% of the whole point cloud. In order to assess the influences of training samples, we re-selected a different training sample set with 1m height intervals for the crown subset of the *Erytrophleum fordii* (Figure 3.6). The re-selected training sample only occupies ~1% of the whole data. The classification results are compared in Table 3.4. It is noted that the accuracy decreased when less and unevenly distributed training data were used. In particular, model sensitivities reduced drastically, meaning that some wood points were misclassified as leaf points. This implies that the local geometry properties of branch points are not well represented by a small set and vertically spaced training data.

In addition, we trained all classifiers with training data from both trees, meaning that half training data are from the *Erytrophleum fordii* and left are from the silver birch. The results for the *Erytrophleum fordii* remain identical compared to those classifiers trained with only *Erytrophleum fordii* data (Table 3.5 and Table 3.2). However, the results for the silver birch are worse, especially in terms of the sensitivities, except the RF model. This indicates that the wood parts of the silver birch are severely misclassified as leaf points when using the classifiers trained with a combined training set. RF is immune from this situation, again indicating its efficiency and capability for such as task.

3.6 Conclusion

In this study, we compared four machine learning algorithms, namely Support Vector Machine, Naïve Bayes, Random Forest, and Gaussian Mixture Model, for separating wood and leaf points from TLS data. In general, there is a lack of com-

Tab. 3.4: Comparison of performances with different training data on the crown subset. Sample f denotes the manually selected 10% training set. Sample s refers to a training set with 1m height intervals.

Classifier	Sample	Sensitivity	Specificity	Accuracy
SVM	f	0.94	0.98	0.96
	s	0.76	0.96	0.91
NB	f	0.96	0.90	0.93
	s	0.89	0.84	0.85
RF	f	0.96	0.98	0.99
	s	0.84	0.96	0.93
GMM	f	0.91	0.96	0.94
	s	0.68	0.97	0.89

Tab. 3.5: Performances of all classifiers trained with a combined training set from both trees.

Data set	Classifier	Sensitivity	Specificity	Accuracy
Birch	SVM	0.67	1.00	0.98
	NB	0.48	1.00	0.97
	RF	0.88	1.00	0.99
	GMM	0.53	1.00	0.97
<i>E. fordii</i>	SVM	0.90	0.90	0.95
	NB	0.94	0.90	0.92
	RF	0.95	1.00	0.97
	GMM	0.89	0.96	0.93

parative studies of machine learning algorithms for such problems. Our study highlighted the feasibility of the methodology. Specifically, two trees were tested, an *Erytrophleum fordii* and a silver birch. Twenty-six geometry-based features were extracted and individually ranked by a filter feature selection method. Various feature sets and training data were tested. Our results show that machine learning algorithms can efficiently separate wood and leaf point from TLS data with an accuracy of, in general, more than 95%. Evenly distributed training data are recommended, as sparse training data can reduce the classification accuracy especially for branches inside the tree crown. It is noted that our studies were performed on purer data sets. More tests on tree data from more complex natural conditions should be carried out in the future. In addition, more tree species should be tested.

Publication II: Separating Tree Photosynthetic and Non-Photosynthetic Components from Point Cloud Data Using Dynamic Segment Merging

” *This section is a reproduced version of: Wang, D., Brunner, J., Ma, Z., Lu, H., Hollaus, M., Pang, Y., & Pfeifer, N. (2018). Separating tree photosynthetic and non-photosynthetic components from point cloud data using dynamic segment merging. Forests, 9(5), 252.*

4.1 Introduction

Forest foliage profile affects the photosynthesis and evapotranspiration processes (Ma et al., 2016), species competition, wood production, and ecosystem and agro-ecosystem dynamics (Béland et al., 2014). Many biophysical forest properties such as wood volume (Levick et al., 2016) and leaf area index (LAI) (Zheng et al., 2013) require prior knowledge on either photosynthetic (e.g., leaf, grass, and flower) or non-photosynthetic (e.g., stem and branch wood) components. For example, understanding the spatial distribution of wood volume contributes to the monitoring of carbon stocks in forested ecosystems (Levick et al., 2016). Above ground biomass estimation typically requires wood-only parts (Calders et al., 2015). On the other hand, LAI (m^2/m^2), which is defined as one-half of the total green leaf area per unit ground surface area (Chen and Black, 1992), is a key descriptor of vegetation condition in numerous physiological and biogeochemical studies (Asner et al., 2003). For a better estimation of leaf area density (LAD) (m^2/m^3), which is defined as the total one-sided leaf area per unit volume, the wood and leaf parts of each tree should be separated (Li et al., 2017). Otherwise, the LAI/LAD will be

overestimated if woody components were not eliminated. Therefore, it is vital to quantitatively describe forest structures.

Laser scanning, also known as light detection and ranging (lidar), emerges as an innovative technique for nondestructive quantification of forest structures (Wang et al., 2016a; Liang et al., 2014a; Liang et al., 2016; Maas et al., 2008). From single tree level to plot level forest studies, terrestrial laser scanning (TLS) is often utilized, while airborne laser scanning (ALS) is usually applicable for region scale studies. TLS is a type of ground-based scanning strategy. It acquires three-dimensional (3D) coordinates in combination with radiometric information of objects. The acquired high-density point clouds enable detailed tree quantification in a nondestructive way (Wang et al., 2016a). TLS has widespread applications in estimating tree attributes, such as stem location (Liang et al., 2012), diameter at breast height (DBH) (You et al., 2016), basal area and volume (Chen et al., 2007), above ground biomass (Feliciano et al., 2014) and LAD (Li et al., 2017). Some efforts have been made to separate photosynthetic and non-photosynthetic components (Ma et al., 2016; Li et al., 2017; Tao et al., 2015a; Yun et al., 2016; Pfennigbauer and Ullrich, 2010; Béland et al., 2014). However, separating these components in TLS data is still challenging (Disney et al., 2018).

Overall, existing methods for separating photosynthetic and non-photosynthetic components from point cloud data can be categorized into two groups: intensity based and geometry based. A different third approach uses the combination of radiometric and geometric features (Zhu et al., 2018). Intensity-based methods (Pfennigbauer and Ullrich, 2010; Béland et al., 2014) use radiometric information of objects captured by a laser scanner. For forest analysis, the assumption is that wood and leaf components have different optical properties at the operating wavelength of the laser scanner (Tao et al., 2015a). However, these optical properties are influenced by the distance, partial hit, and laser incident angle (Kaasalainen et al., 2009). Therefore, a key challenge of using intensity values is that they have to go through instrument-specific radiometrical calibration before being included in further processing (Calders et al., 2017; Höfle and Pfeifer, 2007; Kaasalainen et al., 2011). Calderys et al. (Calderys et al., 2017) have shown that the radiometrical calibration carried out for a specific scanner cannot be transferred to another scanner, which greatly limits the applicability of using intensity information for downstream processing. Various authors have made attempts to construct and use multi-wavelength laser scanning to exploit different material reflectance at different wavelengths (Li et al., 2013; Hakala et al., 2012; Vauhkonen et al., 2013).

On the other hand, geometry-based methods only use the three-dimensional coordinates of the point cloud captured by a laser scanner, thus giving more potential and usability as point coordinates are the most fundamental information acquired

by a laser scanner (Tao et al., 2015a). For separating photosynthetic and non-photosynthetic components, supervised machine learning classification has shown promise and is potentially applicable to any tree point clouds (Disney et al., 2018). Geometrical features are extracted for each point. Machine learning classifiers such as Support Vector Machine (SVM) (Yun et al., 2016), Gaussian Mixture Model (GMM) (Ma et al., 2016; Belton et al., 2013), and Random Forest (RF) (Wang et al., 2017a) have been employed to classify wood and leaf points. A major drawback of supervised machine learning classification is the requirement of training data. First of all, manual delineation of various components from point cloud data can be extremely tedious. Rendering and manipulating the high density TLS data is also an intensive task for hardware. Furthermore, manual selection of training points is impractical for processing large numbers of trees (Disney et al., 2018). Second, the spatial distribution of training data greatly impacts the overall performance of machine learning methods. Points on main stems, small branches, leaves, bushes, and so on have to be carefully covered, which impedes the feasibility of manual manipulation. A group of other unsupervised geometry methods (Li et al., 2017; Tao et al., 2015a) look at specific geometric properties of certain components. For example, Li et al. (Li et al., 2017) separated magnolia leaves by assuming that those leaves were basically flat in surfaces. Tao et al. (Tao et al., 2015a) observed that tree trunk and branch boundaries appear as circles or circle-like shapes. However, these methods were only applied to single trees with multi-scan TLS data coverage. It is unclear if they can be adapted to nature forest scenes and to point cloud data acquired from strategies other than multi-scan TLS such as single-scan TLS and Simultaneous Localization and Mapping (SLAM).

The current study focuses on developing a fully unsupervised approach that is free of user intervention and manual training data, for separating tree photosynthetic and non-photosynthetic components from various point cloud data with varied acquisition sources. The core observation applied in our method is that non-photosynthetic components such as stems and branches appear to be linear at various scales. Therefore, we firstly propose a robust and dynamic point cloud segmentation routine, namely Dynamic Segment Merging (DSM), to partition a point cloud into homogeneous parts. Then, the linear segments are identified by examining segments' feature saliency (Ma et al., 2016). We test the effectiveness of the proposed DSM method using one single tree dataset, and four plot-level datasets. These datasets cover varied data acquisition strategies, scene complexities, and scanning instruments. One plot additionally features calibrated intensity information. We also compare our results to a supervised random forest model. Another incidental aim of our work is to efficiently process large amounts of points such as forest level data. We show examples of how point cloud structuring can accelerate the process.

In the following, our test data are described in Section 4.2. In Section 4.3, the proposed DSM method is explained in detail, together with a brief description of the compared RF method. We give visual and quantitative results in Section 4.4. In Section 4.5, we discuss the performances and potential improvements of our method. A general application extension example is also given. Finally, the major findings and conclusions of our work are summarized in Section 4.6.

4.2 Study Data

Five datasets consisting of one single tree set and four plot-level sets are used in this study. These datasets are intended to cover various data sources such as single-scan TLS, multi-scan TLS, and hand-held laser scanning; various tree species including both coniferous and deciduous trees; various terrain conditions such as urban roadside, flat terrains, and steep mountains. Terrain points were removed in advance using the method proposed in Zhang et al. (Zhang et al., 2016), which is also freely available as a plugin in the open-source software CloudCompare (CloudCompare 2.9.1, 2018). One of the plot-level datasets was also radiometrically calibrated, so that we can derive results from calibrated intensity information as well.

4.2.1 Single Tree Data—SD-1

The first dataset represents TLS data of an evergreen sub tropical tree, *Erythrophleum fordii*, which is provided by Hackenberg et al. (Hackenberg et al., 2015). The data were acquired in October 2013 from eight scan positions. For our single tree analysis purpose, the acquired point cloud was further manually cleaned, as the tree crown interacts with other trees. Therefore, points from adjacent trees' foliage need to be removed. The cleaned point cloud contains ~ 3.9 million points. In this study, we cut out of a section of crown in order to analyze in depth the capability of our method for separating photosynthetic and non-photosynthetic components inside the canopy (Figure 4.1a).

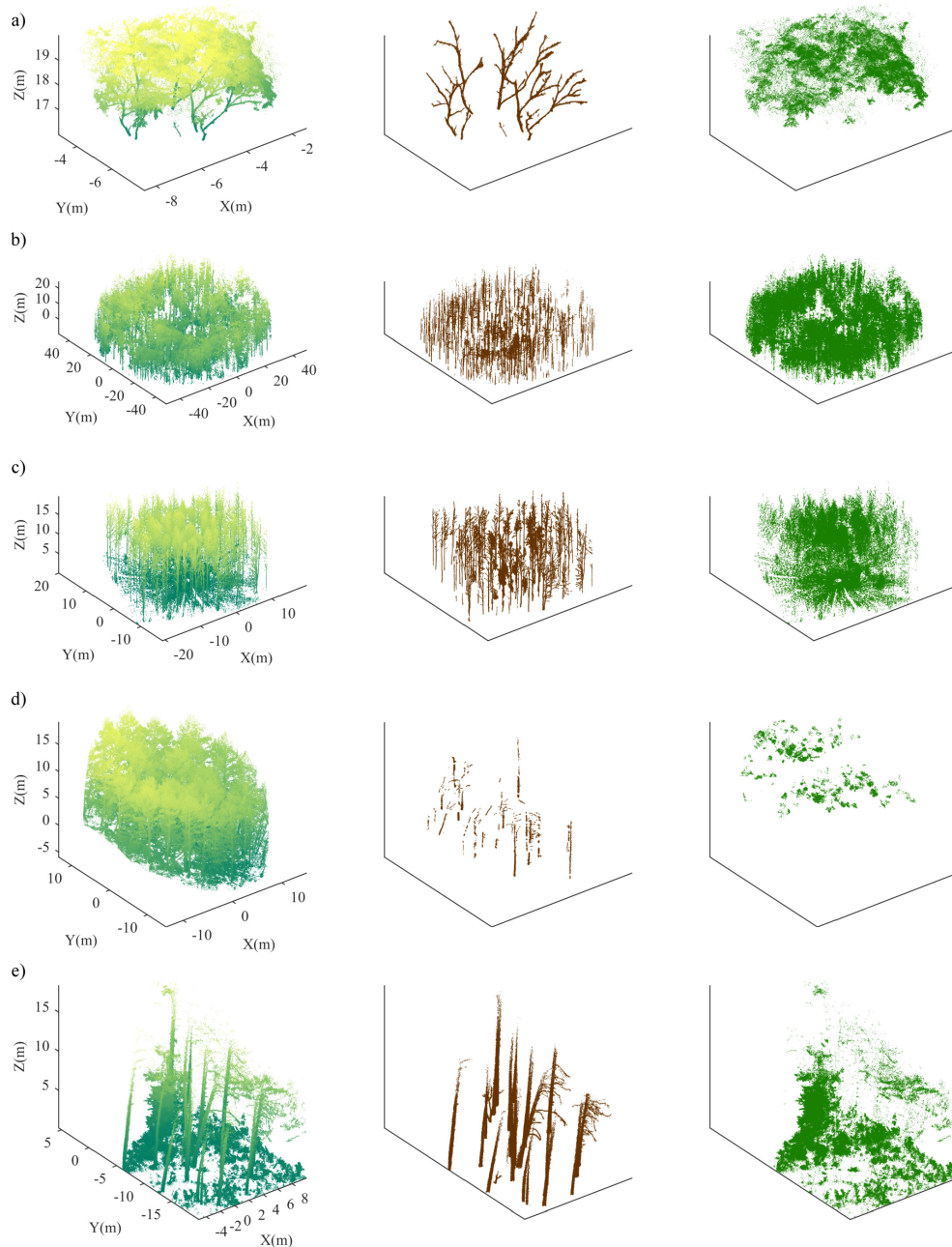


Fig. 4.1: Five datasets used in this study. (a) SD-1. (b) PD-1. (c) PD-2. (d) PD-3. (e) PD-4. The left column shows the original point clouds. Manually classified point clouds are shown in the middle column (non-photosynthetic components) and right column (photosynthetic components). These manually classified points served as validation sets in this study.

4.2.2 Plot-Level Data—PD-1

In May 2017, a plot with 50 m radius inside a forest in Großgöttfritz in the federal state of Lower Austria (Austria) was scanned with a TLS Riegl VZ-2000 scanner (RIEGL Laser Measurement Systems, Horn, Austria) (Figure 4.1b). The measure-

ment was carried from two scanning positions. These two measured point clouds were co-registered later using Riegl’s RiSCAN PRO software (RIEGL Laser Measurement Systems, Horn, Austria). The forest consists of mainly conifers (*Pinus sylvestris* L.) and a couple of silver birches (*Betula pendula*). A radiometric calibration was performed prior to the present study with a Spectralon of a known reflectivity of 99%. Twenty-five measurements were made with the lidar at distances ranging from 1 to 50 m in order to calibrate the intensity measured by the lidar (Kaasalainen et al., 2009). Approximately 600,000 wood and leaf points were manually selected in order to examine their corresponding intensity values. Consequently, the corrected intensity information is shown in Figure 4.2. By setting a threshold of 0.78, we separate photosynthetic and non-photosynthetic components for this dataset, besides using the proposed geometry method.

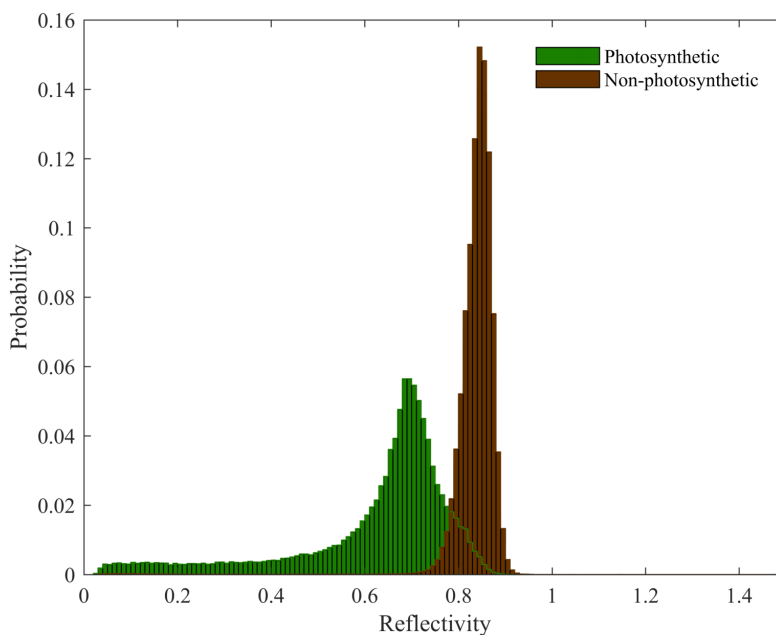


Fig. 4.2: Distribution of reflectances of photosynthetic and non-photosynthetic components after radiometrical calibration.

4.2.3 Plot-Level Data—PD-2

This plot is one of a large set of plots provided by the EuroSDR International TLS benchmark project: Benchmarking of Terrestrial Laser Scanning for Forestry Applications (*Project Benchmarking on Terrestrial Laser Scanning for Forestry Applications*). These plots were located in a southern Boreal forest in Finland, and were scanned by the Finnish Geodetic Institute (FGI) during the summer of 2014, with a Leica HDS6100 scanner (Leica Geosystems AG, Heerbrugg, Switzerland). Twenty-four sample plots were provided by this project. Each plot features two TLS datasets; a single-scan set from the plot center, and a multi-scan set from the center and four

corners. Each plot has a size of 32 m × 32 m. In this study, we randomly select one plot from the single-scan datasets (Figure 4.1c).

4.2.4 Plot-Level Data—PD-3

TLS data of a plot with 15 m radius were acquired by the Chinese Academy of Forestry (CAF) in April 2017. The plot is located in the Baihuashan National Natural Reserve (Beijing, China). The tree species consists of mainly Dahurian Larch (*Larix gmelinii*) and white birch (*Betula platyphylla*). The measurement was carried out with a Trimble TX8 scanner (Trimble Inc., Sunnyvale, CA, USA). Multi-scans were performed from five locations. The resulting point clouds were further co-registered by using the Trimble RealWorks software (Trimble Inc., Sunnyvale, CA, USA) (Figure 4.1d).

4.2.5 Plot-Level Data—PD-4

This plot is a section of a test dataset from a roadside forest in Wolfsgraben in the federal state of Lower Austria (Austria) (Figure 4.1e). The main tree species in this plot is European beech (*Fagus sylvatica*) with a coniferous tree and broad-leaved weeds. The dataset was acquired by a hand-held scanner GeoSlam Zeb-1 (GeoSLAM Ltd., Nottinghamshire, UK). Zeb-1 is a lightweight and hand-held laser scanner which records more than 40,000 measurement points per second. Due to the limitation of its measurement range, the canopy level was barely covered. The purpose of acquiring this dataset was to test the lightweight scanner in forest-related studies, such as location detection, wood-leaf separation, diameter estimation, and stem curve retrieval.

4.2.6 Validation Data

Validation data are needed to test the separation accuracy in this study. We manually classified whole point clouds (Figure 4.1) except the PD-3 dataset, due to its extremely complex subcanopy and understory structure. Validation data for the PD-3 set were spatially evenly distributed, and covered all class types such as leaf, small branch, main branch, and trunk (Figure 4.1d). Manual classification was carefully performed in the open-source software CloudCompare (CloudCompare 2.9.1, 2018). In addition, we downsampled the validation points to equal numbers for both non-photosynthetic and photosynthetic components, so that the separation accuracy will not be biased by the category that has more points than the other.

4.3 Methods

Our method builds upon the conventional region growing algorithm mentality (Adams and Bischof, 1994). We intend to semantically segment a point cloud into meaningful parts, so that each segment will only contain points belonging to a unique class. In this way, tree stems and branches are isolated from leaf points. Subsequently, all segments representing stem and branch can be identified by examining the linearity feature saliency of each segment. However, the challenge lies in the fact that forests have extremely complex structures. A segmentation routine has to be robust against irregular point cloud structures, varied point cloud densities, and indistinct boundaries between object classes. The conventional region growing method has difficulties on gradual change regions, which causes under-segmentation (Huang et al., 2014). This deficiency is also evident in our objective, because tree branches and leaves often will not have distinct boundaries in point clouds. To mitigate such a disadvantage, we develop an over-segmentation-based dynamic merging strategy to segment a tree point cloud semantically and robustly.

Our proposed DSM method initially segments the point cloud into small parts, resulting in over-segmentation. Each small part is defined as a *Segment*. If these small segments are represented by a single point individually, the resulting representative is also known as a collection of *Superpoints* (e.g., Landrieu and Simonovsky, 2017). The following merging process is a dynamic approach, which is similar to the region merging idea applied in the image process (e.g., Huang et al., 2014; Peng et al., 2011). We defined a similarity metric which was estimated for each segment and used it for merging similar neighboring segments step by step. Meanwhile, the similarities of neighboring segments are updated after each merging event occurs. Therefore, the merging procedure is dynamic, while the conventional region growing method uses static strategies to test and merge neighboring regions, thus not preserving global properties.

Our DSM algorithm was implemented in Matlab 2017a (The MathWorks, Inc., Natick, MA, USA).

4.3.1 Dynamic Segment Merging

In a point cloud region growing routine (e.g., Rabbani et al., 2006), a constraint or a combination of constraints has to be defined for deciding whether neighboring points can be merged with the current segment. Such constraints are typically on features such as normal vector variation (Rabbani et al., 2006), amplitude density

(Höfle, 2014), and coordinates of the origin’s normal projection on the best fitted plane (Lari et al., 2011). In this study, we use a simple constraint that is the deviation between the z-component of normal vectors. The z-component of normal vectors represents its spatial orientation relative to the vertical direction (i.e., verticality). In other words, it stands for the angular disparity between a normal vector and the z-axis. For example, the z-component of a normal vector will vary—in absolute value—from 0 for a point located on a vertical surface to 1 for a point on a horizontal surface. This simple criterion is useful to segment tree stem and branches, as they will grow in the similar orientation locally in space.

Normal Vector

Consistent with many other studies (e.g., Rabbani et al., 2006), our proposed DSM method heavily relies on point cloud normal vectors. In fact, estimation of surface normal vectors is one of the fundamental problems for point cloud analysis (Klasing et al., 2009). Challenges arise from outlier points, non-uniform distributions, and missing points (Liu et al., 2012). When estimating normal vectors, a group of neighboring points has to be defined. A point cloud can be defined as $P = \{x_i, y_i, z_i, \|i = 1..n\}$; $P \subset \mathbb{R}$, x_i, y_i, z_i are the coordinates of a point p_i in P . The covariance measures the variation of each dimension from the mean with respect to each other. The eigenvalues of the covariance matrix represent the variation along the direction of the eigenvectors (Garland, 1999). Therefore, the normal vector NV at a point $p_i \in P$ can be estimated as the eigenvector to the smallest eigenvalue EV_i of the covariance matrix (Bazazian et al., 2015) given by

$$Cov_{p_i} = \frac{\sum_{i=1}^K (p_i - \bar{p})(p_i - \bar{p})^T}{K}, \quad (4.1)$$

where \bar{p} is the barycenter of the K nearest neighbors of the point p_i . The z-component of the normal vector is denoted as N_z .

The selection of K neighborhoods is often determined by empirical or prior knowledge on the scene, and usually with a fixed size (Weinmann et al., 2014). However, many scenes contain structures with diverse sizes. For example, in forests, tree trunks and different levels of branches have varied structure scales. This indicates that multi-scale analysis or adaptive analysis can be useful in better sensing the scene (e.g., Chen et al., 2018; Xia et al., 2015; Brodu and Lague, 2012). To examine the effects raised from K , we test two strategies with a fixed K at 10 neighborhoods and an adaptive one. To select adaptive optimal neighborhoods, we follow the

approach proposed in Weinmann et al. (Weinmann et al., 2014). This approach minimizes an eigenentropy given by

$$E_{EV} = -\frac{EV_1}{\sum_{n=1}^3 EV} \ln\left(\frac{EV_1}{\sum_{n=1}^3 EV}\right) - \frac{EV_2}{\sum_{n=1}^3 EV} \ln\left(\frac{EV_2}{\sum_{n=1}^3 EV}\right) - \frac{EV_3}{\sum_{n=1}^3 EV} \ln\left(\frac{EV_3}{\sum_{n=1}^3 EV}\right) \quad (4.2)$$

across different scales ranging from 9 to 99 nearest neighbors with an increment of 9 to find the optimal neighborhood size.

Initial Segmentation

We firstly partition the point cloud into small segments. Each segment should satisfy the homogeneity requirement and be geometrically simple. Several methods were deployed to overly segment a point cloud, such as spectral clustering (Kaick et al., 2014) and global energy model (Landrieu and Simonovsky, 2017). There are several advantages of overly segmenting the point cloud into small simple and homogeneous segments. First, a segment that contains a group of points carries on more information in describing the geometric characteristics of objects than a single point (Peng et al., 2011; Vosselman et al., 2017). Second, the number of initial segments (e.g., *Superpoints*) is much fewer than the number of original points in a point cloud, thus accelerating the processing speed (Peng et al., 2011). Lastly, the initial segments help to identify isolated points. These isolated points are not grouped with other points, meaning that they are local outliers that cannot be merged with surrounding points. Therefore, they can be preliminarily removed as they will also participate in the dynamic similarity tests, which will greatly slow down the processing. However, they cannot be simply removed exhaustively, because locally isolated points may be grouped to a large structure. In this study, we simply re-allocated each isolated point to the final results by majority voting in a sphere neighborhood.

In this study, we develop a computationally efficient strategy to overly partition the point cloud into geometrically simple segments. For a single point, a sphere is created around the point. The radius of the sphere is relevant to the study data. It should be large enough to contain meaningful geometry properties, but retain computational efficiency as a point cloud can easily contain millions of points. The range query can be exhausted with a large search radius (Hackel et al., 2016). For forest scenes, we use a radius of 25 cm for all datasets in this study. The 25 cm radius is loosely defined, and other numbers should work equally as long as they reflect local geometry and retain the computation efficiency. For example, a sensitivity test with values ranging from 15 cm to 35 cm with an increment of 5 cm showed that the standard deviation of accuracy is only 1.2%. All neighboring

points within the sphere are ranked based on the distance to the center point in ascending order. The ranked points are tested orderly if the difference between its N_z and that of the center point is smaller than a threshold T (see Section 4.3.1). This procedure is terminated if the current tested point is unqualified. Consequently, all previously qualified points are merged with the center point, thus forming a small segment. All other points are returned to the point cloud. This process is repeated to a new ungrouped point, and continued until all points have a segment ID. The resulting segments are a group of cover sets (Figure 4.3), similar to that of Raumonon et al. (Raumonon et al., 2013). We further note that the outcome of the initial segmentation only serves as the underlying architecture of the DSM algorithm, and does not significantly affect the merging result. Different degrees of over-segmentation can be carried out depending on the dataset and available computation power.

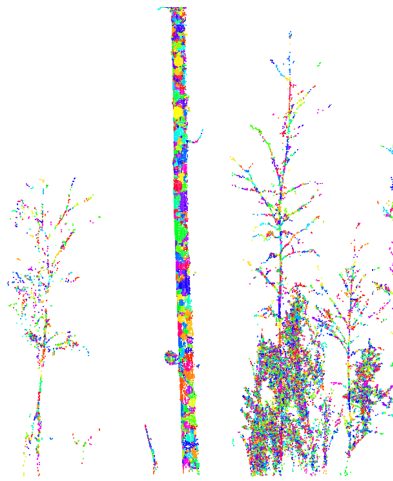


Fig. 4.3: Initial segments by over-segmentation. Each segment is randomly colored. The stem surface has large size segments because it is geometrically homogeneous, while bushes have smaller segments as they are more irregular in shape.

Dynamic Merging

The segment merging processing requires the knowledge of neighboring relations (Raumonon et al., 2013). In image processing, identifying neighbor pixels is more straightforward. Nevertheless, it can be cumbersome for a point cloud because a point cloud is unstructured. Usually, a search radius has to be defined to find adjacent points and segments (Pöchtrager et al., 2017; Filin and Pfeifer, 2005). In this study, we define the search radius as the 99th quantile of point spacing. Point spacing for a single point is defined as the distance to its nearest point. Consequently, the search radius is adapted to the point cloud itself, without the need of user setup.

For each segment, its adjacent segments can be identified (Figure 4.4). For efficient computation, we can build an adjacency matrix for all segments. The adjacency relationship of the target segment in Figure 4.4 is shown in Figure 4.5a. Initially, the adjacency graph is unweighted. Our DSM method finds the most similar adjacent segment and dynamically updates the adjacency relation with similarity metrics of adjacent regions if the target segment is changed. For this purpose, we define a similarity measure (SL) as

$$SL(s, s') = \begin{cases} 1 - D_{n_z} D_q D_d & \text{if } D_{n_z} \leq T \text{ and } std(N'_{z\{z=1, \dots, n'\}} \cup N_{z\{z=1, \dots, n\}}) \leq 0.8 * T \\ 0 & \text{else} \end{cases} \quad (4.3)$$

where s and s' are adjacent segments, and T is a threshold value. D_{n_z} , D_q , and D_d are three dissimilarity metrics. All three metrics are individually normalized to their max values, so that the similarity metric SL is within the range from 0 to 1. D_{n_z} stands for the N_z dissimilarity with $D_{n_z} = |\bar{N}'_z - \bar{N}_z|$. \bar{N}_z denotes the average value in the segment. D_q is the size dissimilarity. It is calculated as the difference in number of points between two segments. D_d represents the distance dissimilarity. To accelerate the computation, we calculate the D_d as the closest distance among distances between any points in an adjacent region s' to the center of the target region s (Equation (4.4)).

$$\operatorname{argmin}_i D(i) = \{i \mid D(i) = \sqrt{(x_{s'_i} - \bar{x}_s)^2 + (y_{s'_i} - \bar{y}_s)^2 + (z_{s'_i} - \bar{z}_s)^2}\}, \quad (4.4)$$

where \bar{x} , \bar{y} , and \bar{z} stand for the mean values. As described in Section 4.3.1, the constraint of merging used in this study is the D_{n_z} . Therefore, we define the threshold T as 0.1 for dataset PD-1, PD-2, and PD-3, as TLS has higher range accuracy. For dataset SD-1 and PD-4, we set the T as 0.2 to tolerate the noisy data inside the canopy and data generated from the hand-held scanner.

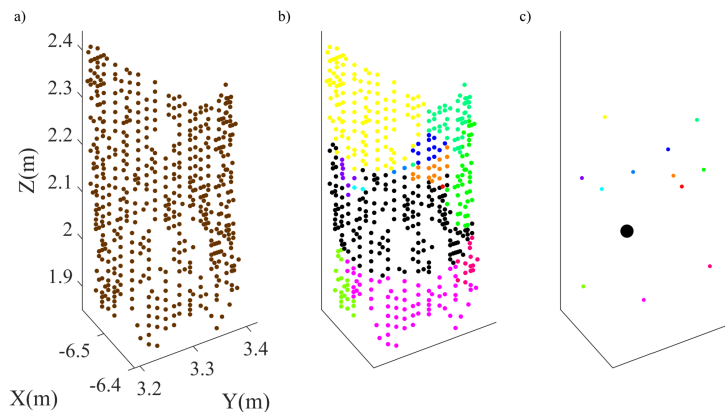


Fig. 4.4: Identifying adjacency relations. (a) Original point cloud. (b) Overly partitioned segments. The middle segment with black color is the target segment. Its adjacent segments are founded by the adaptive search radius, and are randomly colored. (c) Superpoints representation of (b).

We start with the initial segment with the largest size (target segment). Its adjacent segments are identified and ranked by their SL metrics in ascending order by the above-mentioned strategy. If there is at least one adjacent segment with a SL value unequal to 0, meaning that at least one segment is qualified, the adjacent segment with the largest SL is merged with the target segment. Afterwards, the adjacency relation has to be updated since the target segment is grown. The adjacent segments of the original target segment of the merged segment are combined. The similarity metrics SL are re-calculated and ranked against the new enlarged target segment. Furthermore, we constrain that the standard deviation of N_z within a segment cannot exceed 80% of the threshold T (Equation (4.3)). The 80% is set empirically. In this way, we ensure the global geometrical homogeneity of each segment. If no adjacent segments can be merged, the procedure is terminated and the segment with the largest size among the rest of the segments again serves as the target segment. The process is traversed over all segments. As a consequence, our proposed DSM method tries to merge the most similar qualified adjacent segment, and adjusts the testing during the whole procedure.

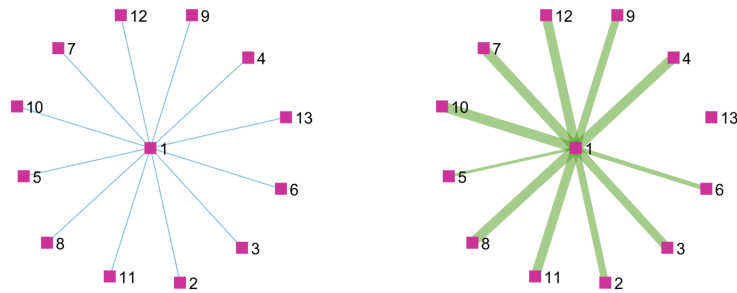


Fig. 4.5: Adjacency graph of segments in Figure 4.4. The identified graph is initially unweighted (**left**), while it is further weighted by SL values defined in Equation (4.3) (**right**). Segment 13 is unqualified as in Equation (4.3), thus it has 0 weight to the target segment 1. For this example, segment 10 has the largest weight, meaning that it is the most similar qualified segment. Therefore, it will merge with the target segment 1 in this step.

4.3.2 Post Processing

In this study, we use the absolute deviation of N_z as a unique constraint for merging the segments of a point cloud. In some cases, several branches can grow closely and with the same vertical orientation (Figure 4.6a). As a consequence, they will be grouped as a single segment. Although the segment only contains most points from stems and branches, the linearity of the segment will be impeded as multiple branches are merged as one segment. To mitigate such a situation, we further develop a top-shift algorithm to separate multiple branches into individual ones. The top-shift method works similarly to the mean-shift algorithm (Comanicu and Meer, 2002). Instead of iteratively projecting points to their local mean, we project

points to their local highest points. The search radius (bandwidth) is the same as the one used in the DSM method, which is the 99th quantile of point spacing. This simple idea will separate points from various branches, because they grow into different directions at some point following the branch structures (Figure 4.6b). Meanwhile, this top-shift processing also helps to identify wrongly merged points from the DSM procedure (Figure 4.6b), as they will converge to the local highest, while branch points converge to the top of each branch, respectively.

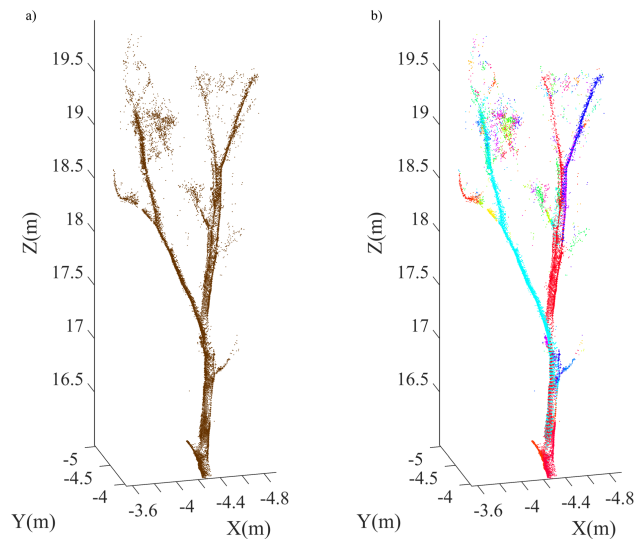


Fig. 4.6: An example of tree branches grouped into one segment with the Dynamic Segment Merging (DSM) method (a) and then separated with the top-shift procedure (b).

4.3.3 Segment Feature

The DSM method robustly partitions the point cloud into meaningful segments. For each segment, we estimate its linearity feature saliency to examine if the segment is part of tree stems or branches. Unlike point-wise features (e.g., Wang et al., 2017a), segment features are calculated based on all points of the segment. Linearity is defined as $(EV_1 - EV_2)/EV_1$. EV_1 , EV_2 , and EV_3 are three eigenvalues from the covariance matrix (Equation (5.1)), and are sorted in descending order. For segment features, the covariance matrix is formed by all points in a segment. In this study, we recognize segments with linearity values above a threshold TH_l and number of points more than TH_n as tree stems and branches (non-photosynthetic components of trees). The thresholds TH_l and TH_n are determined by trial-and-error (Figure 4.7).

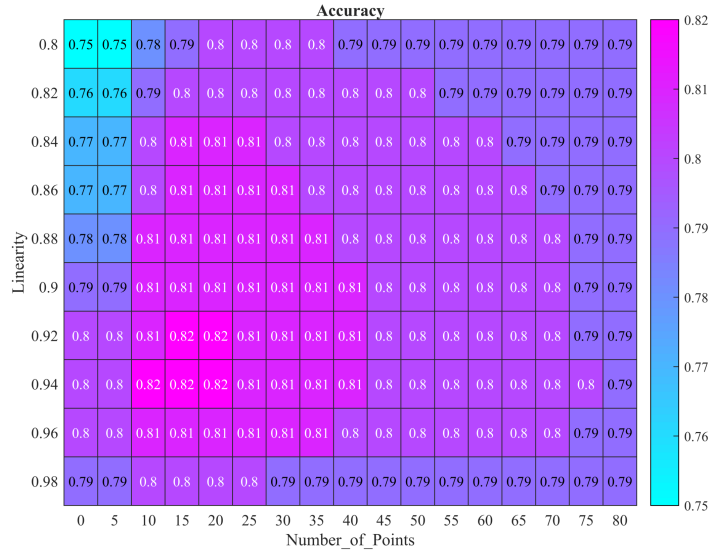


Fig. 4.7: An example of a Heat map of acquired accuracy for the PD-2 dataset to locate proper TH_l and TH_n values.

4.3.4 Tile Processing

Point cloud manipulation can be computationally intensive. Data measured from TLS can contain millions to billions of points (Liang et al., 2016), thus efficient manipulation is important. As used in other software and studies (Pfeifer et al., 2014; Vosselman, 2013), we partition the whole point cloud into tiles, and process each tile individually and in parallel. We develop three routines to partition a point cloud; uniform voxels, octree, and 2D tiles (Figure 4.8). Point cloud voxelization is a commonly used approach to partition a point cloud into local spaces (e.g., Papon et al., 2013). It is fast to generate, and works with satisfaction for a point cloud with homogeneous density distribution. For a point cloud with varied point density, such as data from single-scan TLS measurement, Octree is better at balancing the needed computational resources in each tile. Two-dimensional tiles (Figure 4.8c) are often deployed for large-scale datasets, such as ALS data (Pfeifer et al., 2014). By tiling the point cloud, the processing can be run in parallel, and the memory consumption is distributed to each computer worker, avoiding memory overcommitment for a single worker. In each tile, a $k-d$ tree structure is constructed to enable fast neighborhood and range searching. Besides, individually processed tiles are further merged afterwards (Vosselman, 2013). Figure 4.9 shows an example of point cloud processing on tiles and merging afterwards. The tile processing greatly facilitates and accelerates point cloud manipulation.

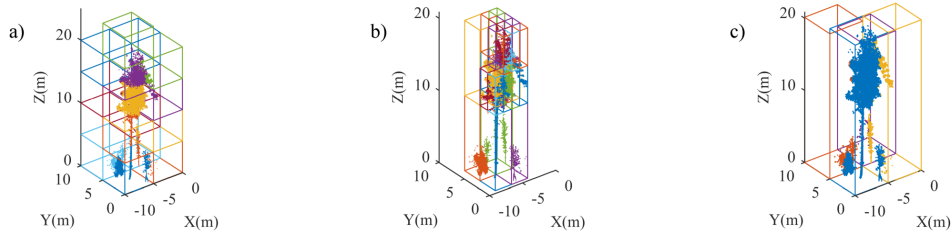


Fig. 4.8: Point cloud tiling. (a) Uniform voxels. (b) Octree partition. (c) 2D tiles on XY plane.

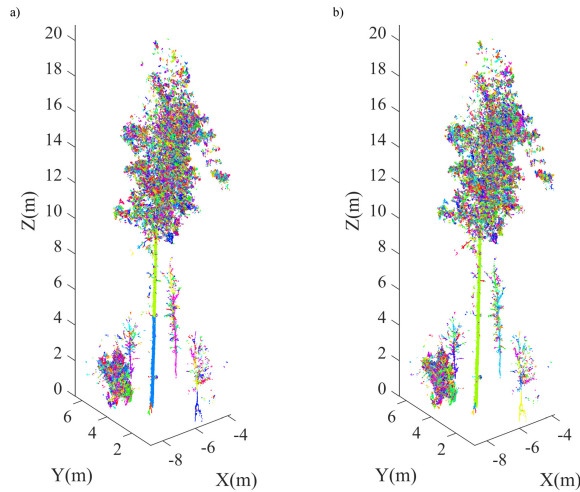


Fig. 4.9: Point cloud tile processing and merging. (a) DSM results on tiles. (b) Results after tile merging.

4.3.5 Random Forest Classification

In this study, we additionally apply supervised machine learning classification as a method comparison (Yun et al., 2016; Ma et al., 2016). Only point-wise geometric features are used, and the random forest (RF) classifier is explored (Breiman, 2001). Previous studies showed that the RF model is particularly effective for separating tree photosynthetic and non-photosynthetic components from point cloud data (Wang et al., 2017a; Zhu et al., 2018). RF is a decision tree-based ensemble learning method that was proposed by Breiman et al. (Breiman, 2001). The learned model is a collection of weak models. Multiple decision trees are grown on random subsets of training data. The class determination is based on a majority votes approach. Two necessary foundational parameters need to be specified for the RF model; the number of classification trees n_{trees} and the number of features m_{ft} used at each node. We set the number of trees n_{trees} as 100 (Wang et al., 2017a). Another parameter m_{ft} is determined as \sqrt{p} , where p denotes the number of input features, as suggested by Breiman, 2001. Thirty-two 3D and 2D geometrical features are calculated for each point (Table 4.1). Two-dimensional features are calculated from projected grids on the XY plane. Many of these features are defined and used in

other point cloud classification studies (Weinmann et al., 2015). Training data are manually selected for each dataset. The spatial distribution of training data follows a strategy used in Ma et al. (Ma et al., 2016). Points that belong to different classes at the 25%, 50%, and 75% height of the bounding box of the forest plot are manually identified in the open source software CloudCompare (CloudCompare 2.9.1, 2018). Training points near the ground are additionally selected if low vegetation is present in the dataset. The RF classification was performed using the Statistics and Machine Learning Toolbox in Matlab 2017a (The MathWorks, Inc., Natick, Massachusetts, United States).

Tab. 4.1: Thirty-two features extracted from the point cloud. EV denotes the eigenvalue and NV is the normal vector. Three EV s are sorted in descending order. EV_1 defines the first eigenvalue, and so on.

No.	Feature	Description
1	linearity _{3D}	linear saliency $(EV_1 - EV_2)/EV_1$.
2	planarity _{3D}	planar saliency $(EV_2 - EV_3)/EV_1$.
3	scattering _{3D}	volumetric saliency EV_3/EV_1 .
4	omnivariance _{3D}	volume of the neighborhood $(EV_1 * EV_2 * EV_3)/3$.
5	anisotropy _{3D}	$(EV_1 - EV_3)/EV_1$.
6	eigenentropy _{3D}	$-\sum_{n=1}^3 EV_n * \log(EV_n)$
7	sum_EV _{3D}	$\sum_{n=1}^3 EV_n$.
8	surface_variation _{3D}	change of curvature $EV_{min}/(\sum EV)$.
9	X value X _{3D}	X coordinate of the point.
10	Y value Y _{3D}	Y coordinate of the point.
11	Z value Z _{3D}	height of the point.
12	density _{3D}	local point density.
13	verticality _{3D}	$1 - NV_z$.
14	ΔZ_{knn_3D}	height difference of local neighborhood.
15	σZ_{knn_3D}	standard deviation of heights of local neighborhood.
16	N_{z3D}	z-component of the normal vector NV .
17	radius _{2D}	radius of local neighborhood.
18	density _{2D}	local point density.
19	sum_EV _{2D}	$\sum_{n=1}^2 EV_n$.
20	EV_ratio _{2D}	EV_2/EV_1 .
21	cell_density _{2D}	density of projected 2D cells.
22	skewness _{2D}	skewness of point heights in each cell.
23	kurtosis _{2D}	kurtosis of point heights in each cell.
24	Max_z _{2D}	maximum of heights of points in each cell.
25	Min_z _{2D}	minimum of heights of points in each cell.
26	Mean_z _{2D}	average height of points in each cell.
27	Median_z _{2D}	median height of points in each cell.
28	EV_1 _{3D}	first eigenvalue of 3D covariance matrix.
29	EV_2 _{3D}	second eigenvalue of 3D covariance matrix.
30	EV_3 _{3D}	third eigenvalue of 3D covariance matrix.
31	EV_1 _{2D}	first eigenvalue of 2D covariance matrix.
32	EV_2 _{2D}	second eigenvalue of 2D covariance matrix.

We note that our aim is not to achieve the best performance from the supervised machine learning method. Some optimization strategies such as feature selection, hyper-parameters fine-tuning, and model pruning may further improve the classification performance. However, the deployed RF classifier, in combination with our crafted features, has shown promising results in a machine learning benchmark study for wood-leaf separation (Wang et al., 2017a).

4.3.6 Evaluation

The performance of our DSM method and the supervised RF method is evaluated based on three statistical indexes; sensitivity, specificity, and accuracy. Sensitivity measures the correctly classified positive samples (true positive rate, TPR). In this study, it represents the correct rate for non-photosynthetic components such as wood and other points. Specificity gives the true negative rate (TNR), thus it measures the correct rate for photosynthetic components (i.e., leaf points). Accuracy (ACC) gives the overall correctness by

$$\text{Sensitivity} = \frac{TP}{TP + FN} \quad (4.5)$$

$$\text{Specificity} = \frac{TN}{TN + FP} \quad (4.6)$$

$$\text{Accuracy} = \frac{TP + TN}{P + N}, \quad (4.7)$$

where P and N are the number of real positive (non-photosynthetic components) and negative (photosynthetic components) samples. TP and TN are the correctly identified positive and negative samples, respectively.

4.4 Results

4.4.1 Single Tree Data

A visual inspection of the separation result from the proposed DSM method for the SD-1 dataset is shown in Figure 4.10a. We observe that some small branch sections at the bottom were misclassified as leaf points. Some leaf points on the canopy surface were also wrongly labeled as wood points. Nevertheless, the branches inside the canopy were generally separated from leaves successfully. Quantitatively, the overall classification accuracy of our DSM method reached 86.9% with fixed neighborhood sizes, and 88.5% when using adaptive neighborhood sizes, which were higher than that of 82.1% and 83.9% from the supervised RF method (Table 4.2). The achieved sensitivity from the DSM method were higher than the RF

method, while the specificity was of the same class. This indicates that our method is particularly confident in detecting non-photosynthetic components.

Tab. 4.2: Results summary of various methods on all datasets. Bold numbers are the best results among methods. (F) denotes the results acquired with fixed neighborhood sizes, and (A) stands for adaptive neighborhood sizes. * Training and validation points have an equal split of photosynthetic and non-photosynthetic components.

Evaluation	Method	Dataset				
		SD-1	PD-1	PD-2	PD-3	PD-4
Number of points		553,556	16,259,081	2,013,331	3,901,367	1,269,318
Number of RF training points *		86,618	117,534	53,872	59,114	31,776
Number of validation points *		279,580	15,492,926	1,648,514	77,462	945,262
Sensitivity (%)	DSM(F)	94.7	97.9	92.2	97.5	95.5
	DSM(A)	93.7	96.4	90.5	96.7	95.2
	RF(F)	81.5	73.1	88.4	86.2	95.7
	RF(A)	86.6	84.7	92.5	91.8	95.9
	Intensity	–	92.1	–	–	–
Specificity (%)	DSM(F)	79.1	74.5	64.8	81.5	76.1
	DSM(A)	83.3	81.1	73.0	87.4	79.4
	RF(F)	82.7	92.9	77.2	97.1	70.3
	RF(A)	81.1	87.9	74.0	95.8	73.5
	Intensity	–	83.1	–	–	–
Overall accuracy (%)	DSM(F)	86.9	86.2	78.5	89.5	85.8
	DSM(A)	88.5	88.7	81.8	92.0	87.3
	RF(F)	82.1	83.0	82.8	91.7	83.0
	RF(A)	83.9	86.3	83.2	93.8	84.7
	Intensity	–	87.6	–	–	–

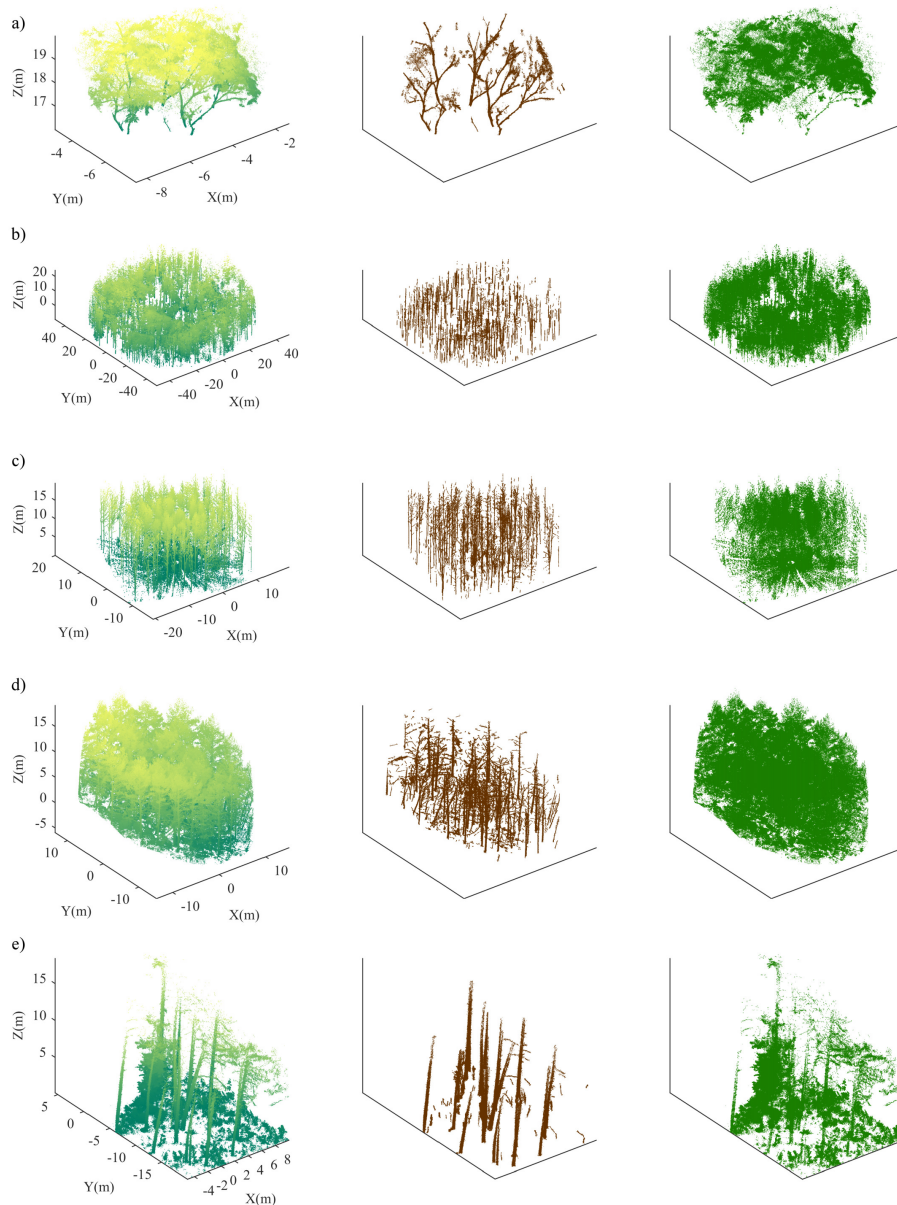


Fig. 4.10: Separation results with adaptive neighborhoods from the DSM method for (a) SD-1, (b) PD-1, (c) PD-2, (d) PD-3, and (e) PD-4. Photosynthetic and non-photosynthetic components are colored by green and brown, respectively.

4.4.2 Plot-Level Data

Figure 4.10b–e gives an overview of the separation results for our four plot-level datasets from PD-1 to PD-4. We observe that most non-photosynthetic components were resoundingly separated from photosynthetic components, regardless of their spatial orientations. The overall accuracy for the four plot-level datasets ranged from 78.5% to 89.5% in our DSM method with fixed neighborhood sizes, and from 81.8% to 92.0% with adaptive neighborhood sizes (Table 4.2). The PD-2 dataset had

the worst overall accuracy. Its associated specificity was only 64.8%/73.0%, meaning that many non-photosynthetic components were mislabeled as photosynthetic points. This deduction can also be observed in Figure 4.10c, in which some high stem points were mislabeled as leaf points, potentially due to the low point density on the top and severe occlusions in the single-scan TLS data. Our DSM method had a sensitivity from 92.2% to 97.9% with fixed neighborhood sizes, and from 90.5% to 96.7% with adaptive ones, which were overall higher than the RF method. However, the supervised RF had significantly higher specificity than the DSM method, except the PD-4 dataset. The average overall accuracy for the DSM and RF method was 85.0% (87.5% with adaptive neighbors) and 85.1% (87.0% with adaptive neighbors), respectively.

The PD-1 dataset contains useful intensity information after radiometrical calibration. The intensity calibration and separation thresholding is described in Section 4.2.2. As a result, the intensity method achieved an overall accuracy of 87.6%, with a sensitivity of 92.1% and a specificity of 83.1% (Table 4.2). The performance of the intensity method was similar to our DSM method.

4.5 Discussion

In this study, tree photosynthetic and non-photosynthetic components are automatically separated by the proposed dynamic segment merging method. The proposed method is fully unsupervised, thus not requiring any training data and user interventions. The core concept of the DSM method is a robust point cloud segmentation routine. We have shown in this study that the DSM method has been successfully used in separating tree photosynthetic and non-photosynthetic components from point cloud data. To some extent, we solve an ongoing challenge in an unsupervised manner, and overcome the bottlenecks in other methods such as calibrating laser intensities or manually selecting training data Disney et al., 2018. In the following subsections, we discuss some vital inputs of our algorithm, its performance, and future applications. At the same time, we address several challenges about the separation of tree photosynthetic and non-photosynthetic components from point cloud data.

4.5.1 Calculation of Normal Vectors

Calculation of normal vectors is crucial in this study. Figure 4.11 gives an example of normal vectors calculated by the adaptive method, compared to those with fixed neighborhoods for the PD-4 dataset. This dataset was acquired with a hand-held scanner, with a lower position accuracy compared to TLS. Points on the

stem surfaces are not smooth due to low accuracy, thus giving a good example of the performance of normal vector estimation. Visually, the normal vectors are more homogeneous on the stems after using the optimal neighborhood selection method.

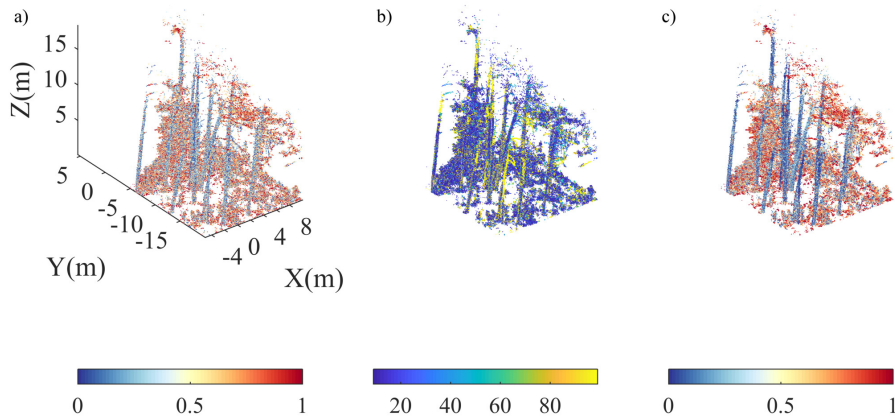


Fig. 4.11: Normal vector estimation. (a) Normal vectors estimated with fixed neighborhoods, and colored by N_z . (b) Optimal neighborhood size for each point. (c) Normal vectors estimated with optimal neighborhoods, and colored by N_z .

The accuracy for the PD-4 dataset was improved from 85.8% to 87.3%, proving the positive effects in estimating normal vectors (Figure 4.11). A similar trend was also found for other datasets and for the performances of the supervised RF method. The average overall accuracy for all datasets was improved from 85.0% to 87.5% for the DSM method, and from 85.1% to 87.0% for the RF model. The improvements are more significant for our DSM method. Theoretically, this is expected as our DSM method is a kind of segmentation approach which heavily relies on the quality of normal vectors. The selection of optimal neighborhoods is inherently a multi-scale analysis. The local irregularity is smoothed in a large scale, resulting in more homogeneous normal vectors. Consequently, these branches can be identified, and the specificity was broadly improved. The supervised RF method is a machine learning classification technique that relies more on the feature distinguishability and the classifier mechanism.

However, robust and efficient estimation of normal vectors from complex scenes is still a challenging task. Although methods with adaptive neighborhood searching can be effective in quality, they are computationally intensive. The computation time and memory consumption are significantly higher for large datasets. For example, the computation time is about six times longer for the adaptive neighborhood than the fixed neighborhood in our SD-1 dataset, when using seven CPU threads. This is still a bottleneck for most applications (Liu et al., 2012). A possible solution is to explore GPU processing using a parallel implementation (Liu et al., 2012).

4.5.2 Algorithm Performance

The DSM method achieved generally constant performances across different datasets. The standard deviation of accuracy was 4.1% with fixed neighborhood sizes and 3.7% with adaptive sizes. The accuracy was low for the PD-2 dataset (Table 4.2), mostly because it was acquired with single-scan TLS, which resulted in severe occlusions and shadows in the point cloud, and low point density at distances away from the scanner. Consequently, the branches were not well represented as linear segments in the point cloud, and our DSM method relies on segmenting and detecting linear objects. In addition, we observed that our proposed DSM method achieved higher sensitivity than specificity (Table 4.2) across all datasets. This indicates a systematic tendency of our method for having confidence in detecting non-photosynthetic components over photosynthetic components. In this study, a low specificity means that many wood points were mislabeled as leaf points, while in general high sensitivity states our method is good at detecting wood points robustly. We note that this can be an effect of the irregularity of branch structures. If a section of a branch is severely deformed in terms of growing orientation, it will not be grouped as one segment as its normal vectors are corrupted. This challenge was partly mitigated when using normal vectors with optimal neighborhoods. The specificity ranged from 73.0% to 87.4%, compared to those with fixed neighborhoods which ranged from 64.8% to 81.5%.

In this study, we also deployed the supervised machine learning method RF as a comparison of our DSM method to the state-of-the-art methods. Overall, the RF method achieved similar accuracy compared to the DSM method. However, it required tedious works to delineate training points. These training points must be representative, as they will greatly influence the outcomes of machine learning methods. For example, if we exclude training points on the bushes for the dataset PD-2, the RF results dropped dramatically. In contrast to our method, the RF achieved better model specificity than sensitivity. Ma et al. (Ma et al., 2016) used a supervised GMM model to separate photosynthetic and non-photosynthetic components from TLS data. Their overall accuracy for single tree data was 82.6%, and further improved to 99.6% after applying a series of post filters. Yun et al. (Yun et al., 2016) deployed a SVM model for four single trees. The overall accuracy was from 89.1% to 93.5%. The result from our DSM method on the single tree dataset SD-1 was 88.5%. The RF method had an accuracy of 83.9%. For plot-level datasets, Ma et al. (Ma et al., 2016) reached a preliminary accuracy ranging from 65.8% to 75.2%, which was further improved to a range from 84.3% to 97.8%. Our DSM results for plot-level datasets were in the same standard (81.8% to 92.0%) compared to the improved results from Ma et al. (Ma et al., 2016). We note that our implemented RF achieved higher accuracy than the GMM model in Ma et al. (Ma

et al., 2016). A potential explanation is that we crafted more features, and the RF model may be more efficient than GMM for such a task (Wang et al., 2017a).

The proposed DSM method effectively partitions forest point cloud into photosynthetic and non-photosynthetic components. It dynamically adjusts the merging process, while the conventional region growing method uses a static strategy. For complex scenes such as forests, the conventional region growing method has difficulties in distinguishing gradual changing regions. Therefore, it under-segmented trees, as illustrated in Figure 4.12b. For a fair comparison, we used the same normal vectors and searching radius to compare our DSM method. Figure 4.12a demonstrates that our DSM method can effectively separate leaf and wood points, where conventional region growing failed. We further show a detailed inspection of PD-3 in a magnified view (Figure 4.13). We chose to show fine-detail information of the PD-3 plot because its complexity in tree structures is instrumental in testing the performance of our DSM method. In addition, we used a simple constraint in this study—the deviation of z-component of normal vectors (verticality)—to group tree trunks and branches. We have shown that it is effective for irregular branches (Figure 4.13). It is further noted that the constraint in our DSM method only serves a role to check if an adjacent segment is qualified, while the merging is determined by the similarity ranking (Equation (4.3)). In a nutshell, our DSM method is less sensitive to the selected constraints, which is one other distinction compared to conventional region growing routines.

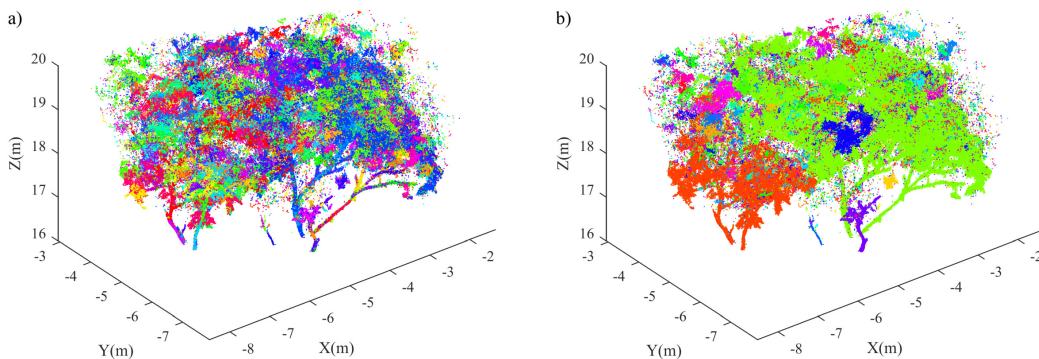


Fig. 4.12: Comparison of segmentation for the SD-1 dataset. Each segment is randomly colored. (a) Segmentation from the proposed DSM method. (b) Segmentation from the conventional region growing method.



Fig. 4.13: A close inspection of results for the PD-3 dataset.

4.5.3 Challenges in Components Separation

Apart from the methodology shortage, there are still many challenges in separating tree photosynthetic and non-photosynthetic components from a point cloud. Forest structures are multifarious in nature. The acquired point cloud will be affected by severe occlusions. This results in data shallows and non-uniform density distributions. For intensity-based methods (Pfennigbauer and Ullrich, 2010; Béland et al., 2014), this effect is less significant. However, geometry-based methods will suffer from these challenges. For machine learning-based methods, the crafted features should cope with non-uniform density, and be robust and distinctive to guide the model. However, this is still challenging for complex scenes. Recently developed deep networks on point clouds may further help to extract higher level features (Qi et al., 2017; Li et al., 2018). Nevertheless, these models are still in the very early development stage, and hardly work with high-density TLS data.

Another bottleneck of TLS data processing is to deal with the large amount of data. With millions and billions of data (Liang et al., 2016), point cloud manipulation can be intensive. Efficient point cloud management and processing are mainly targeted at ALS data (Pfeifer et al., 2014). In this study, we briefly implemented tile processing together with the $k-d$ tree structure to accelerate TLS processing. Future optimization is still imperative.

4.5.4 Future Applications of the DSM Method

In this study, we developed an efficient method applied to a wood-leaf separation task. This processing is a crucial step in reducing uncertainties in TLS-derived estimates of above ground biomass (Disney et al., 2018). Our method can greatly

facilitate the automation in this processing. For example, Figure 4.14 gives an example on how our method was applied to the reconstruction and parameter retrieval of the entire *Erythrophleum fordii* tree (SD-1). Leaf points were detected and removed automatically by using our DSM method (Figure 4.14b). Subsequently, the entire tree was reconstructed by the Quantitative Structure Model (QSM) (Raumonen et al., 2013). Some vital parameters can then be extracted from the QSM, such as total volume (581.6L), trunk volume (436.6L), and branch length (84.4m). On the other hand, our algorithm can be easily deployed for other applications. For example, the presented pipeline in this study can be adapted to detect tree stems by simply filtering linear segments based on their spatial orientations and sizes. Based on the detected tree stems, downstream processing such as diameter estimation (Wang et al., 2017b) and stem curve (Wang et al., 2016a) retrieval can be realized.

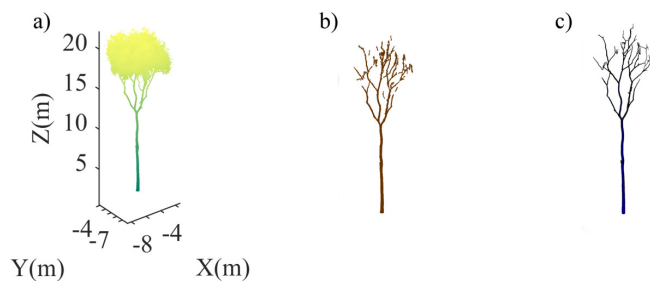


Fig. 4.14: An example of our DSM method applied to detect wood points of the entire *Erythrophleum fordii* tree (a). Detected wood components are shown in (b), and the corresponding Quantitative Structure Model (QSM) is given in (c).

4.6 Conclusions

In this study, we present a fully automatic and unsupervised approach to separate tree photosynthetic and non-photosynthetic components from point cloud data. This geometry-based method is free of user interventions and dispenses with manual delineation of training data, which is a tedious prerequisite for the supervised machine learning algorithms. Our method is based on a robust dynamic point cloud segmentation routine. The point cloud is firstly partitioned into meaningful segments by using the proposed DSM method. Non-photosynthetic segments such as stems and branches are then identified by estimating their linear feature saliency. The approach is tested for a single tree dataset and four plot-level datasets. These datasets cover single-scan TLS, multi-scan TLS, hand-held laser scanning, varied terrain conditions, and various tree species. The achieved accuracy reached 88.5% for the single tree dataset, and ranged from 81.8% to 92.0% for plot-level datasets. We also compared our results to a supervised machine learning method. In addition, we show that point cloud structuring enables efficient point cloud manipulation even for large datasets. Furthermore, we have discussed the performances and

some challenges of separating photosynthetic and non-photosynthetic components in nature forests.

The extensive experiments on various datasets suggest that the proposed DSM method is efficient, and can be equally as effective as supervised machine learning methods. Nevertheless, the distinct advantage of our method lies in that it is unsupervised and fully automatic. Our work highlights the potential of unsupervised separation of wood and leaf points even in plot-level analysis.

Publication III: Automatic and Self-Adaptive Stem Reconstruction in Landslide-Affected Forests

” *This section is a reproduced version of: Wang, D., Hollaus, M., Puttonen, E., & Pfeifer, N. (2016). Automatic and self-adaptive stem reconstruction in landslide-affected forests. Remote Sensing, 8(12), 974.*

5.1 Introduction

Forest attributes, such as stem location, diameter at breast height (DBH), height, basal area, stem curve and volume, are critical to timber industry management (e.g., Kankare et al., 2014), assessing the potential of wild fire hazard (e.g., Fernandes, 2009) and natural biodiversity conservation (e.g., Kim et al., 2009; Hollaus et al., 2009; Mücke et al., 2013). Among them, the stem curve, which describes the diameter at any height along the stem, is of great importance Burkhart and Tomé, 2012. Studying the stem curve is crucial not only for forest management and biometrics, but also for research on the geomorphological environment. In particular, understanding the role of trees and forests is increasingly important in high mountain areas, as sloping regions are often characterized by shallow and very slow moving landslides (Kalvoda and Rosenfeld, 2012). The so-called “drunken trees”, which means that tree stems are displaced from their vertical alignments, are caused by such soil movements (Alexandrowicz and Margielewski, 2010). In recent decades, there has been an increased occurrence of soil erosion in many alpine regions (citeAlewell2014). Climate change adaption and natural disasters in these regions are receiving considerable attention (Forbes and Broadhead, 2013). For example, recently-developed dynamic slope stability models (e.g., Steger et al., 2015; Kuriakose et al., 2009) studied the interdependencies of different processes,

including deforestation or afforestation. Detailed stem volume and biomass information at single tree level can greatly benefit and facilitate such studies (Schmaltz et al., 2016). Moreover, the stem curve can be used to quantify the tree growth anomaly in landslide forests (e.g., Razak et al., 2013). Some vital attributes can be derived, such as taper (Thies et al., 2004) and inclination angle (Razak et al., 2013).

The interest of studying the stem curve, or stem form, or taper dates back long before the 1950s (Gray, 1956). There are a number of ways to measure the stem curve. Conventional forest inventory approaches for stem curve measurement are labor intensive and sometimes harmful to trees. Trees are often felled and then measured from the stump to the top level. In addition, mathematical models also are developed to predict stem curves (Lappi, 2006). These methods use only fixed measurements, usually DBH, total height and several measurements on the stem. The stem curve is then interpolated by mathematical functions (e.g., Lee et al., 2003). The relation of different components of trees is often estimated by allometric functions (e.g., Repola, 2008; Repola, 2009; Raumonon et al., 2013; Hackenberg et al., 2014) based on DBH, tree height or other parameters of interest. However, these functions are not always valid, because they were developed from specific local morphological or climate conditions and do not provide the position at any height along the tree stem. Precise stem models would help to improve the accuracy of such estimations (Chiba, 1990).

Terrestrial laser scanning (TLS) has been widely used in forest-related studies (e.g., Liang et al., 2016; Eysn et al., 2013; Olofsson et al., 2014; Pfeifer and Winterhalder, 2004; Sun et al., 2015; Thies et al., 2004). A laser scanner acquires a high density point cloud, which enables the stem form reconstructions in a nondestructive way. Tree attributes, such as stem location, DBH, basal area and volume, can be effectively retrieved from the TLS point cloud using some automatic algorithms (e.g., Eysn et al., 2013; Olofsson et al., 2014; Pfeifer and Winterhalder, 2004; Sun et al., 2015; Kankare et al., 2013; Liang et al., 2012; Moskal and Zheng, 2011). Previous studies mostly focused on retrieving DBH or tree height, whereas a limited number of publications explored the applicability of modeling the stem curve (e.g., Brolly and Kiraly, 2009; Maas et al., 2008). Circle fitting (e.g., Watt and Donoghue, 2005) and cylinder fitting (e.g., Hopkinson et al., 2004; Wezyk et al., 2007) are the primary strategies often mentioned in the literature. A robust stem curve retrieval method based on cylinder fitting was described by the authors in Liang et al., 2014a, but their method focused on a forest in a flat environment. Nonetheless, most of the previous works focused on forests in flat environments or planned forests. To our best knowledge, similar approaches have not yet been applied to high mountain natural forests or shallow landslide-affected forests. Such forests are often characterized by steep terrain with a multi-layered canopy structure, including dense understory, mixed tree species and deformed stem shapes. The stem formation is often influenced by

factors, such as the site fertility, spacing and light conditions, wind and landslide events (Koizumi and Hirai, 2006). Therefore, the stems are often growing in a manner deviating from the vertical direction and have irregular forms (Figure 5.1). Special methods have to be developed to adapt to these challenges.

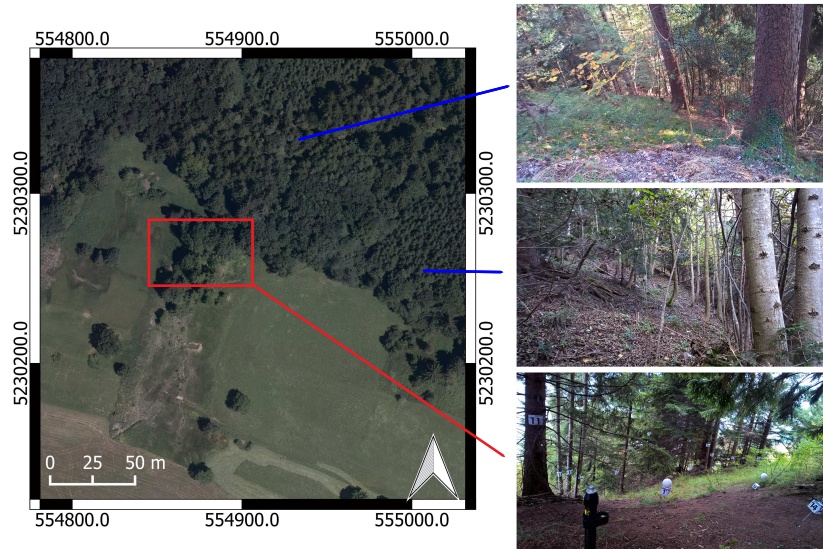


Fig. 5.1: Landslide-affected forest in the Austrian Alps. Trees are inclined after shallow landslide caused soil movements. The red rectangle covers the area in this study. Coordinates in WGS84 UTM Zone 32N.

The current study focuses on using TLS for automatic stem curve modeling in landslide-affected forests. The objective of this study is to expand the stem curve investigation to landslide-affected forests and to discuss the concomitant challenges. Finally, we present a novel algorithm for stem modeling in mountain forest environments.

5.2 Study Data

The study site is located in the federal state of Vorarlberg, Austria (47.224°N, 9.725°E). The Vorarlberg Alps features widespread translational landslides Depenthal and Schmitt, 1996. Our specific study site covers a plot of approximately 31 m × 16 m, inside a small forest located near the rupture surface of a shallow landslide. The site is characterized by steep terrain (>30°) with a multi-layered canopy structure, including dense understory, mixed forests and dead tree branches (Figure 5.1). Tree stems are overall anfractuous due to the effects of soil movement. The dominant tree species is Norway spruce (*Picea abies* (L.) H. Karst.). The study site consists of 27 trees with a DBH larger than 5 cm, whereas other small trees are neglected in this study. The density of trees is approximately 544 stems/ha. The

DBH was manually measured in the field using a measuring tape. The DBH value in this study site ranges from ~ 9.4 cm– ~ 61.2 cm, with a mean value of 32.8 cm and a standard deviation of 14.3 cm.

The TLS measurement was carried out in October 2015, using a Riegl VZ-2000 scanner (RIEGL Laser Measurement Systems, Horn, Austria). The scanner has a vertical view angle of 100° ($+60^\circ/-40^\circ$) and a full 360° horizontal view angle, with an effective measurement rate up to 400,000 points per second. Table 5.1 summarizes the detailed specifications of the scanner. Seven scans were done according to the terrain accessibility in order to achieve a good laser scanning coverage (i.e., the percentage of a stem cross-section that is covered by the TLS point cloud) of all tree stems from different directions (Figure 5.2). Each tree was visible from the perspective of several scans depending on occlusions. The average TLS coverage rate for a single tree was 77.7% (Figure 5.2). The full coverage is defined as the complete stem (i.e., full cross-section) being scanned. Figure 5.2 displays the coverage rate for each tree. Reflectors were placed on the tree stems for the purpose of registration. The placements of reflectors ensured that one scanning position can be integrated with other scans. Afterwards, the seven scans were registered using Riegl’s RiSCAN PRO software (RIEGL Laser Measurement Systems, Horn, Austria). The overall registration accuracy is ± 7.5 mm. Consequently, seven scans were merged, and no processing was applied to the data (e.g., removal of undergrowth, manual identification of trees), meaning that all branch and outlier points near a stem were retained.

Tab. 5.1: Specifications of the Riegl VZ-2000 scanner.

Specifications	Riegl VZ-2000
Max. vertical field of view ($^\circ$)	100
Max. horizontal field of view ($^\circ$)	360
Accuracy (mm) at 150 m range	8
Points per second (max)	396,000
Beam divergence (mrad)	0.3
Max. resolution ($^\circ$)	0.0015

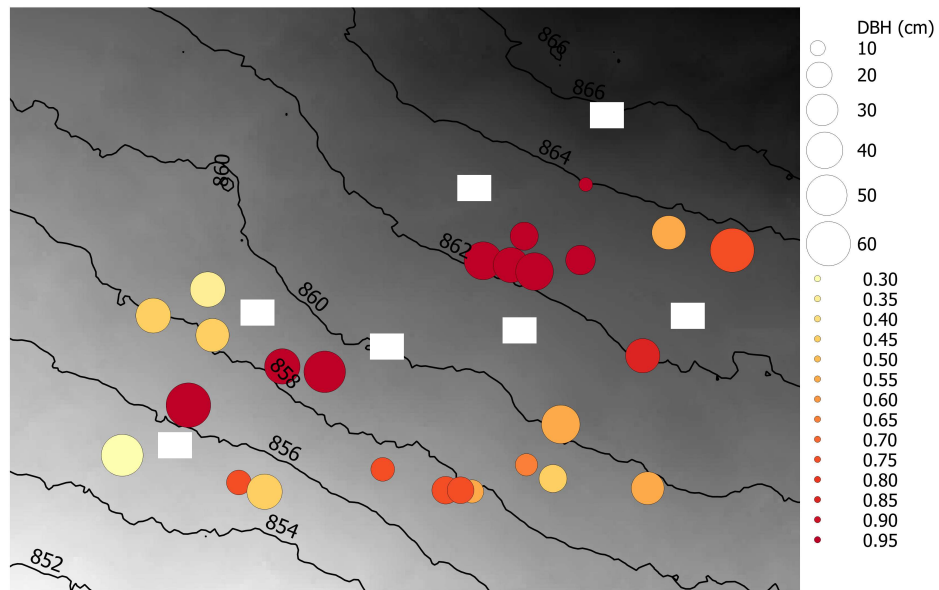


Fig. 5.2: The area of the study site approximately equals $31\text{ m} \times 16\text{ m}$. Seven scan locations are marked by white rectangles. Tree positions are marked by solid circles. The size is scaled by the DBH, and color is scaled by the percentage of TLS coverage (i.e., 0–1 (100%)). Contours are derived from the DTM.

In addition to TLS and DBH field measurements, stem curves were manually measured from the acquired point cloud using the CloudCompare software (CloudCompare 2.6.2, 2016). The diameter and the location of the stem center at the height of 0.65 m above ground were measured. The following measurement height was at 1.3 m (i.e., the height of DBH), then every one meter above until reaching the top of the stem or where no points can be identified as part of a stem. The diameter was determined by averaging the values from two directions (W-E, N-S), and the location of the stem center was the intersection.

5.3 Methods

The proposed approach automatically models tree stems from the point cloud. The anticipated workflow contains four procedures. First, the original point cloud is down sampled by a leveled histogram sampling method (Puttonen et al., 2013). Second, the terrain points are identified and removed by a hierarchical approach (Kraus and Pfeifer, 1998), so that trees are assigned with normalized heights above the ground. Third, stem locations are recognized from the spatial distribution of stem points and labeled as individual groups. Finally, the stems are modeled by fitting a series of cylinders, based on a 2D-3D robust cylinder fitting strategy. In this step, the stem parameters, such as the DBH, diameter and location at various

5.3.2 Terrain Model Derivation

The determination of the digital terrain model (DTM) was done by a hierarchical approach (Pfeifer and Mandlbürger, 2008). Starting from a thinned point cloud, the lowest points within $4\text{ m} \times 4\text{ m}$ raster cells were used for robust moving planes' interpolation. For filling the gaps in the derived model, a triangulated model was used, which was derived from the lowest points within the $4\text{ m} \times 4\text{ m}$ raster cells. The determined elevation model is used for normalizing the elevations of the point cloud.

The robust filtering approach was originally developed for DTM extraction from airborne laser scanning data (e.g., Kraus and Pfeifer, 1998). One main assumption is that terrain points are located at the lowest. Thus, starting with a rough surface model, it can be assumed that it is more likely that a point below the "rough surface model" belongs to a terrain point than points above the "rough surface model". Based on this assumption, a weight function can be defined (details can be found in Kraus and Pfeifer, 1998). This procedure is done in an iterative way starting with a coarse raster and ending with a fine one. Therefore, we started first with a cell size of $4\text{ m} \times 4\text{ m}$ and did the refinement with $2\text{ m} \times 2\text{ m}$, $1\text{ m} \times 1\text{ m}$ and, finally, 0.2 m . The entire workflow is implemented as a batch script using the software Orientation and Processing of Airborne Laser Scanning data (OPALS) developed at the Vienna University of Technology (Pfeifer et al., 2014) and does not need any user interactions.

5.3.3 Stem Location Detection

There are a number of methods to delineate single tree stems in the TLS point cloud from forest plots. Hough transform and circle searching were explored in Olofsson et al., 2014; points between 1 and 2 m above ground were selected to find tree positions. The authors in Sun et al., 2015 used the spatial clustering method for points lower than 4 m above the ground. Points were projected to the horizontal plane and grouped by their spatial distances. The work in Forsman and Halme, 2005 searched trees in the TLS range images. Salient features and the normal vector method were also used as an operative approach to identify points from different tree components based on their spatial distribution patterns (Liang et al., 2012; Ma et al., 2016).

In this study, we propose a two-layer projection approach to determine the location of each tree, instead of directly delineating stem points, due to the difficulty or specific challenges in identifying stem points in landslide-affected forests. The severe occlusion causes trouble for the circle searching and range image methods.

Local foliage aggregations may resemble the stems, and the tree stem shapes are irregular (e.g., Figure 5.1 and 5.4); thus, spatial pattern recognition with normal vectors becomes often impractical. Hence, we define the first layer as a full layer, in which all points from the laser scans after terrain removal are retained. The second layer is a sub-layer, which only includes points between 2 m and 4 m above the ground. Such a height range is useful to diminish the disturbance from dense undergrowth and tree crowns. Points in the sub-layer were down sampled by grid boxes with a 2-cm side length in order to make the point density uniform for all trees, which is crucial for calculating the density map and normal vectors. Points within each grid box were merged by averaging their locations.

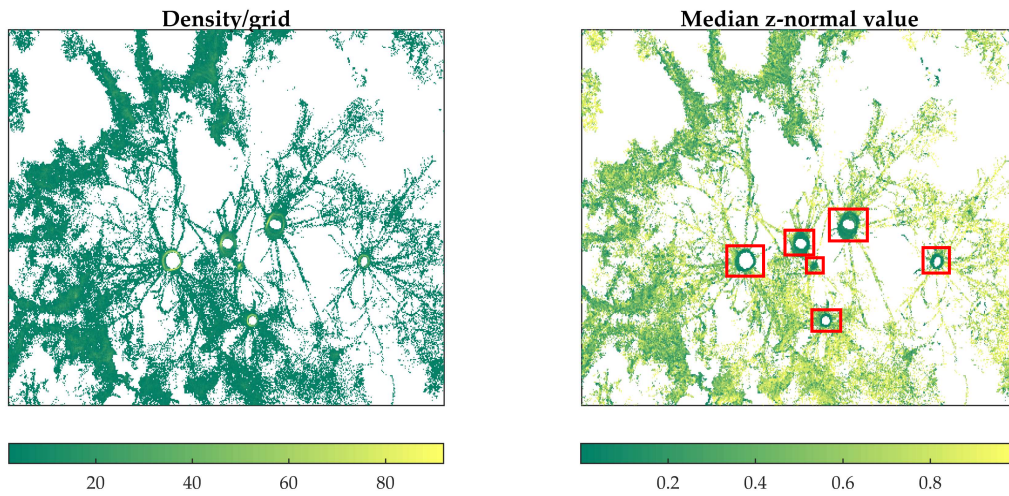


Fig. 5.4: (a) An example of the projection density map of a point cloud subsection, which contains six trees. The map is generated by 2 cm \times 2 cm grids. (b) Corresponding map of the average z-normal vectors. Red rectangles show six trees identified by our method.

One can define a point cloud as $P = \{x_i, y_i, z_i, \|i = 1..n\}$; $P \subset \mathbb{R}$, x_i, y_i, z_i are the coordinates of a point p_i in P . The normal vector n at a point $p_i \in P$ can be estimated as the eigenvector to the smallest eigenvalue λ_i of the covariance matrix given by:

$$Cov_p = \frac{\sum_{i=1}^K (p_i - \bar{p})(p_i - \bar{p})^T}{K}, \quad (5.1)$$

where \bar{p} is the barycenter of the K points. A low value of the z-component of n (n_z) (z-normal) means that a point is approximately on a vertical structure (Liang et al., 2012). In this study, the normal vectors are calculated for the sub-layer. The z-normal is estimated from the covariance matrix. A point then can be represented by $p_i(x_i, y_i, z_i, n_{z_i})$. The sub-layer is then projected onto a horizontal plane of 2 cm \times 2 cm cells. The size of the cell is determined to separate stems. For each cell, the number of corresponding points N (i.e., the density map) and the median value of z-normals (i.e., the z-normal map) for all points in this cell are determined. We

use the median value so that the impacts from some outliers and poorly calculated normal vectors can be minimized. For a cell belonging to a stem, a high value of N together with a low value of the average z-normal mean that this represents a vertical planar surface. Nonetheless, in mountain forests, locally aggregative dense foliage could also result in garbled characters with stems (Figure 5.4). Therefore, it is difficult to separate stem points with foliage points merely from projection density or normal vectors. Moreover, the determination of the the thresholds for density and normal vectors (or fatness) is unclear, because they depend on the overall laser point density and local field conditions. The authors in Liang et al., 2012 and Sun et al., 2015 did not mention how they selected their thresholds. In light of that, we further develop a quantitative method to combine the density map and the z-normal map and determine their thresholds for identifying tree locations.

Figure 5.5 shows the relation between the density and z-normal for points in Figure 5.4. In general, such a relation curve will have an “L” shape, because the cells represent foliage that will normally have lower densities with high z-normal values. Therefore, the curve drops quickly in the beginning. When the density increases, the z-normal value will eventually become small enough until reaching a stable state, where the density is high enough so that the cells are dominated by stems. Such a curve can be well approximated by the Gaussian curve (bell-shape). A second order Gaussian curve:

$$f(x) = a_1 e^{-\frac{(x - b_1)^2}{2c_1^2}} + a_2 e^{-\frac{(x - b_2)^2}{2c_2^2}} \quad (5.2)$$

is accurate enough. The thresholds are the values where the curve becomes flat (i.e, the maximum curvature). Consequently, the density and z-normal thresholds can be determined, and all cells having a larger density and a smaller z-normal value will be identified as stems.

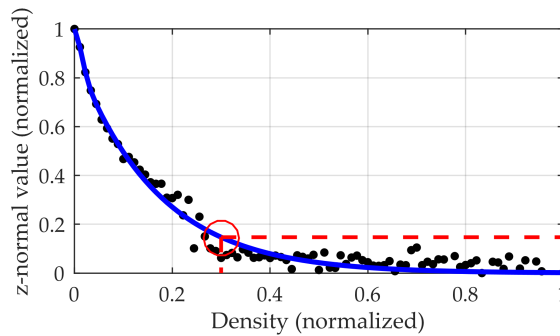


Fig. 5.5: The relation between the density and z-normal for all cells. The thresholds are determined by finding the maximum curvature, at which the curve becomes flat. The cells framed by the red dotted line rectangle are identified as stems.

The corresponding points are further grouped by the density-based spatial clustering of applications with noise (DBSCAN) algorithm (Ester et al., 1996) on x - y coordinates. This algorithm finds all connected points from arbitrary shapes within 2 cm (radius of the neighborhood) and clusters them as groups. It does not require the number of clusters as an input, different from other methods (e.g., the k -means algorithm). Further, the natural occlusions may separate the points belonging to the same stem to different groups. Thus, the groups that are distributed closer than 40 cm are merged as one.

Notably, in theory, the aforementioned DBSCAN detection method only works well for vertical stems or trees with similar inclination angles; while in complex forests where some trees are vertical and some are not, such an assumption sometimes holds wrong. Our method assumes that at least part of the stem points are recognized and grouped (i.e., the parts with similar inclination angles). The x - y extent of every group is enlarged by a certain factor (e.g., a factor of 1.5 in this study) for every group, so that the surrounding points from the full layer can be retained if only parts of the stem are detected. Moreover, the group enlargement is important as a significant portion of trees in landslide-affected forests is typically inclined. This is also the reason we only estimate the location of every stem, instead of delineating stem points directly from the TLS point cloud. The range extension will probably also incorporate points from branches, foliage and even the understory. Nonetheless, the proposed stem modeling technique is able to mitigate such effects in a subsequent processing step.

5.3.4 Stem Reconstruction

A tree stem can be modeled by fitting a series of cylinders (e.g., Liang et al., 2014a) or circles at various heights (e.g., Olofsson et al., 2014). The latter seems problematic in mountain forests because the severe occlusions could block the laser from reaching the stem at many heights. For the cylinder fitting approach, the challenges arise from the dense understory and foliage and irregular stem shapes in our study. Here, we propose a 2D-3D robust cylinder fitting and self-adaptive growing strategy to reconstruct the whole stems. A circular cylinder can be parameterized as:

$$\|(P - Q) \times a\| - r = 0, \quad (5.3)$$

where $P = (x_i, y_i, z_i)$ is a point fulfilling this equation; thus, it is on the cylinder surface. $Q = (x_a, y_a, z_a)^T$ is a point on the cylinder axis, and r is the radius. a denotes the direction of the cylinder axis and has a unit length. The infinite cylinder can be defined by 5 parameters, radius r and 4 more to define the axis.

The solution of the nonlinear problem is to minimize the residual $\sum_{i=1}^n v_i^2$ where $v_i = \|(P - Q) \times a\| - r$. It can be solved by the Gauss–Newton or Levenberg–Marquardt schemes. However, the performance of iterative algorithms heavily depends on the choice of the initial guess. Besides, there is always a chance that they would be trapped in a local minimum (Al-Sharadqah and Chernov, 2009). Further, standard least square, however, is not able to eliminate the outliers originating from branches, leaves and wind. The authors in Liang et al., 2014a used a robust method with Tukey’s estimator. We solve this problem by introducing a 2D-3D approach. Outliers are preliminarily first removed by a 2D region growing method on the density map. Robust estimation of the initial guess values of a cylinder is also determined on 2D by a random sample consensus (RANSAC)-based (Fischler and Bolles, 1981) circle inscribing approach. Finally, the cylinder is fitted and extended in 3D.

Starting Cylinder

For each tree, we start from a 20-cm section between 2 m and 4 m above the ground, which is consistent with the stem location detection procedure. A section is selected if it contains more points than other sections. The section with the most points is more plausible to achieve a good fitting, as possible occlusion may present between 2 m and 4 m above the ground. The critical issue is then how to eliminate the effects of outliers. Moreover, the determination of the initial guess for the cylinder axis position and radius is of great importance for solving the nonlinear least square fitting. Robust estimation should be developed at this stage.

A region growing algorithm is firstly applied to remove some conspicuous outliers for each tree (Figure 5.6) on the density map. We only consider the cells that have valid densities. The cell that has the largest density is defined as the starting seed. The starting seed is assigned with a group. A neighbor cell is added to the same group if its density is larger than 20% of the seed. After all qualified neighbor cells are added to the seed group, a new seed is selected (i.e., the cell that has the largest density of the rest of the cells). The procedure is continued until all cells are visited. The resultant group that contains the most points is regarded as the dominant structure, thus kept as the stem or at least part of the stem. Figure 5.6 shows an example of two traversed groups for a stem section.

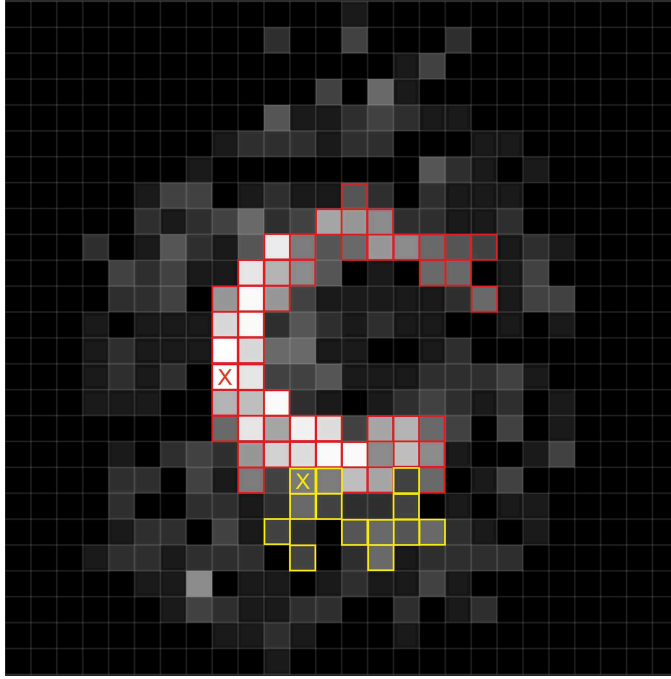


Fig. 5.6: Example of the region growing method used in this study. Two groups are generated. The “X” denotes the starting seeds for each group.

Some branches may also comprise a large amount of points and have similar density with stems; thus, they cannot be eliminated from the aforementioned region growing method. We further introduce a RANSAC-based approach to achieve a robust estimation of an initial guess for the cylinder axis position and its radius. The approach is done in 2D by inscribing a circle to the stem cross-section and then transform the circle to 3D.

The RANSAC algorithm iteratively estimates the parameters of a mathematical model by randomly sampling the data. Its effective iteration time M is defined by:

$$M = \frac{\log(1 - p)}{\log(1 - (1 - \lambda)^m)} \quad (5.4)$$

where p is the probability to achieve a good model; m is the minimum amount of data required for determining the model. For circle determination, m equals 3; λ denotes the estimated percentage of error in the data, which is determined to be 40% in this study because of the complex field conditions. For each iteration S , a circle is determined by three randomly-selected points. Next, the distances d from all other points to the circle are computed by:

$$d_i = \sqrt{(x_i - x_0)^2 + (y_i - y_0)^2} - R \quad (5.5)$$

where x_0 and y_0 are the center location and R is the circle radius. We define asymmetric distance thresholds to identify the inliers and outliers (Figure 5.7). The

asymmetric thresholds work equally for an circle inscribing technique. A point is considered as an inlier if $-1 \text{ cm} \leq d_i \leq +2 \text{ cm}$. The number of inliers is marked with N_i . Further, we constrain that $\frac{N_i}{N_w} < 0.2$, where N_w denotes the amount of points with $d_i < -1 \text{ cm}$, as laser pulses are not able to penetrate into stems; thus, no points should be spread inside the cylinder. However, this assumption holds wrong under certain circumstances, such as due to co-registration error, texture of the tree bark, long ranges or wind effect. Therefore, we allow 20% tolerance. This restriction is important for stems that are only partially covered by TLS, as the example given in Figure 5.7. We would like to stress that the circle inscribing is only used to estimate the starting values for solving the nonlinear cylinder fitting problem. After M iterations, the consensus set S_i , which contains the largest N_i , is selected, and the circle associated with S_i is considered as the solution. One can think that a circle is exactly the projection of a vertical circular cylinder. Therefore, the determined circle can be easily transformed to a cylinder by introducing a height along the z -axis. Consequently, a robust initial guess for the following cylinder fitting is generated.

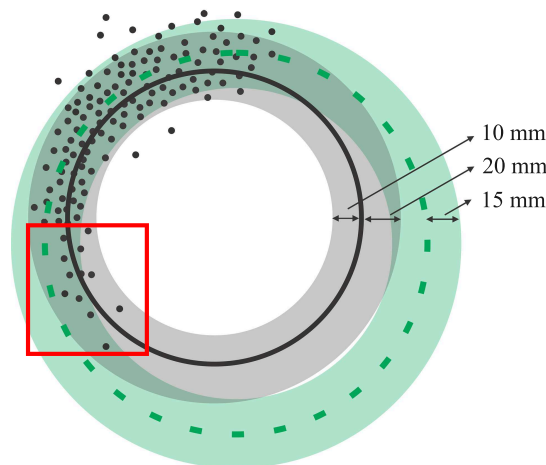


Fig. 5.7: The asymmetric thresholds for circle fitting. The black circle is the one determined by our algorithm. The dotted green circle is over fitted and determined by symmetric thresholds. When using symmetric thresholds, the points in the red rectangle have weak effects; thus, the fitted circle is biased by the unbalanced weights introduced by the point distribution.

Cylinder fitting features the same strategy as the circle fitting, except that it is performed in 3D. Thereby, we simply apply the RANSAC again on top of the standard least square solution. The work in Beder and Förstner, 2006 proved that seven is the minimum amount of points to achieve a unique solution of cylinder fitting. Therefore, a consensus set of seven points is randomly selected and fitted with a cylinder.

Cylinder Growing

The fitted starting cylinder is the basis for tracking the whole stem. The position of the next cylinder can be found by adjusting the starting cylinder upwards or downwards. We here take upwards growing as an example (Figure 5.8). The cylinder is shifted by a length of L . Here, L is 20 cm to give enough flexibility to accommodate the curvature of the stem. The axis of the shifted cylinder is then rotated to the vertical direction in order to simplify the subsequent processing by:

$$v_t = R \times v_a, \quad (5.6)$$

where $v_t = [0, 0, 1]^T$ is the unit vertical vector. v_a denotes the unit vector representing the axis of shifted cylinder. R is the rotation matrix. All points are rotated by R , as well. Consequently, a new coordinate system is introduced. The new axis is tilted vertically by a gradually increased angle from 0 – α , with 20% of α for every step. α is determined proportionally to the height of the cylinder. The largest α is assigned to the lowest cylinder with 20° , because the stem tends to grow in a more straight direction on the upper part. The vertically tilted axis is then rotated on the horizontal plane clockwise (or anticlockwise) by a successive step angle of β (30°) until a full turn. The coordinate of the upper vertex of the axis is then:

$$\begin{aligned} x_u &= x + L \sin \alpha \cos \beta \\ y_u &= y + L \sin \alpha \sin \beta \\ z_u &= z + L \cos \alpha \end{aligned} \quad (5.7)$$

where x , y and z are the coordinates of the upper vertex of the directly shifted cylinder, which is determined from the previous cylinder. Furthermore, the radius r of the shifted cylinder is also adjusted by downscaling the value by 20%, gradually by steps of 4%, by assuming that the stem will become thinner at the upper parts, and vice versa. The shifted cylinder is tilted, rotated and scaled by testing all combinations of values of α , β and r . The goodness of fitting is determined by identifying the amount of qualified points with the same asymmetric criteria of the circle inscribing step. Consequently, the position of the next cylinder can be resolved by evaluating the goodness of each fitting. Finally, the determined cylinder is transformed back to the original coordinate system.

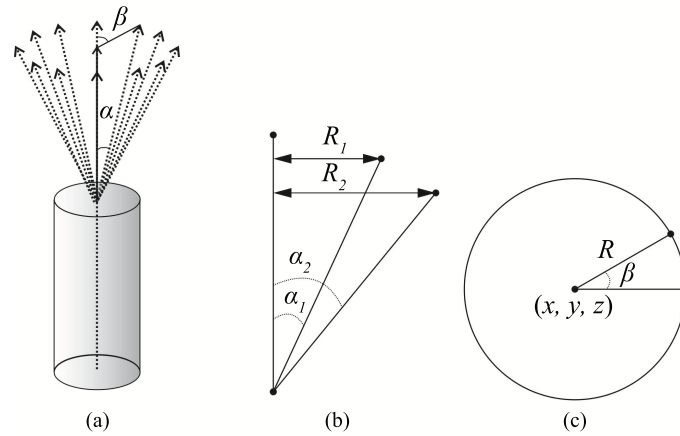


Fig. 5.8: Cylinder growing strategy. The cylinder is shifted (a); vertically tilted (b); and horizontally rotated (c).

This elongation is continued upwards until there are not enough points to form a cylinder. For example, in the canopy, there are no sufficient points that are conforming the tested cylinder. The downwards elongation follows the same strategy until reaching the ground.

5.3.5 Post Processing

The cylinder fitting and growing allow the reconstruction of each tree stem with cylinders in every 20-cm section. We further apply a moving window approach to smooth the connection parts of successive cylinders for each stem. As shown in Figure 5.9, a moving window with a 20-cm height is placed on the connection part of two cylinders, which contains part of the data from Section 5.1 and part from Section 5.2. All contained data are tested against Cylinder 1 and Cylinder 2, respectively. The radius of one of the two cylinders that better fits all contained data will be selected. Consequently, each stem section at a specific height can be described by the radius and the center location. A truncated cone is then generated to represent each section, instead of a circular cylinder.

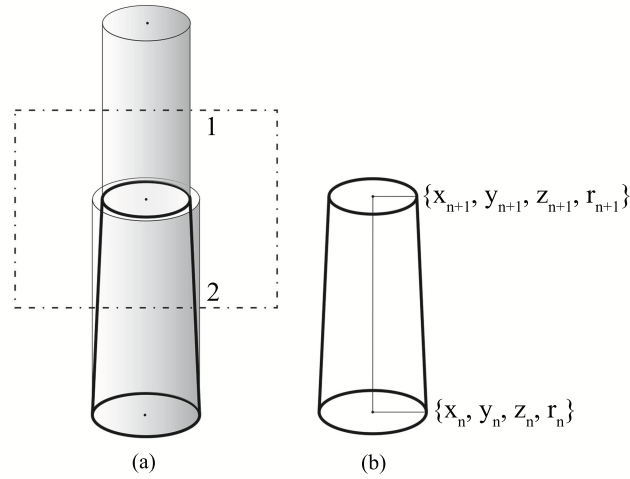


Fig. 5.9: (a) A moving window technique to smooth the connection part of two consecutive cylinders; (b) after smoothing, a truncated cone is generated.

5.3.6 Evaluation

The automatically-reconstructed stems are compared with the reference measurements. The accuracy of DBH, location and diameter at various heights and the stem volume is evaluated. The stem volume is determined by:

$$V = \sum_{i=1}^m v_i = \sum_{i=1}^m \frac{\pi h}{3} (r_1^2 + r_2^2 + r_1 r_2) \quad (5.8)$$

where h denotes the section height, r_1 and r_2 are the top and bottom radii and m is the number of sections.

The estimation accuracy will be evaluated by the bias and root mean square error (RMSE):

$$\text{Bias} = \frac{1}{k} \sum_{i=1}^k (y_i - \hat{y}_i), \quad (5.9)$$

$$\text{RMSE} = \sqrt{\frac{1}{k} \sum_{i=1}^k (y_i - \hat{y}_i)^2}, \quad (5.10)$$

$$\text{RMSE}(\%) = 100 \times \frac{y}{\bar{y}}, \quad (5.11)$$

where k is the number of observation data, \hat{y}_i denotes the reference value and \bar{y} is the mean value of the variable.

5.4 Results

The results of the automatic stem location estimation are given in Table 5.2. “Completeness” refers to the percentage of trees that are detected and reconstructed out of 27 trees, respectively. The results of stem reconstruction are summarized in Table 5.3. All trees were successfully recognized. We constrain a bias of DBH worse than ± 5 cm as reconstruction failure. Thereby, 25 out of 27 stems are successfully reconstructed. The estimated DBH shows a mean bias of 0.03 cm and an RMSE of 1.80 cm (5.50%) compared to the reference values. Figure 5.10 shows a high correlation between field-measured DBH and automatically modeled DBH values from TLS. The R^2 value is 0.99.

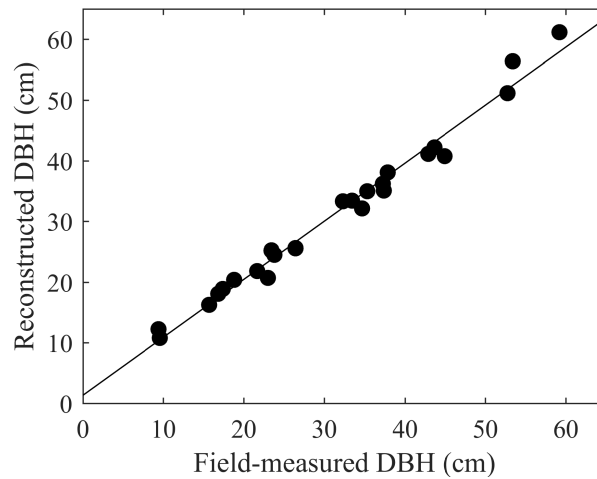


Fig. 5.10: Scatter plot of DBH automatically estimated from TLS and reference measurements in the field. The R^2 is 0.99.

Tab. 5.2: Results of the stem detection rate and reconstruction rate.

	Stem Detection	Stem Reconstruction
True positive	27	25
False positive	0	0
False negative	0	2
Completeness	100%	92.6%

Tab. 5.3: Bias and RMSE of automatically estimated DBH, diameter, location and volume.
 * Results are evaluated from all heights along all stems.

	Bias	RMSE	RMSE (%)
DBH (cm)	0.03	1.80	5.50
DBH (TLS coverage >80%, cm)	0.05	1.50	4.58
Diameter (cm) *	0.13	2.45	8.94
Location (cm) *	1.60	2.09	-
Volume (cm ³)	84.88	451.38	7.07

The stem curve is evaluated from two variables, the stem diameters and the locations of stem centers. TLS often cannot cover the stem on the upper part of a tree, especially inside the canopy, because of the occlusions in the forest. Therefore, the accuracy of the stem curve is compared based on the fact that both manual measurement and automatic modeling are performed as high up the stem as possible. What is worth mentioning, the uppermost model from TLS may even reach higher heights than manual measurements, because our self-adaptive method is able to identify a group of points that in fact belong to a stem, but are not necessarily clustered in a cylinder or at least a portion in space. Nonetheless, the average relative heights of stem top between TLS modeling and field measurement is 98% in this study, showing a good agreement. The mean bias of stem diameters from all trees is 0.13 cm and the RMSE is 2.45 cm (8.94%). The accuracy of the center of the stem has a mean bias of 1.60 cm and an RMSE of 2.09 cm. The box plots of these two variables are given in Figure 5.11 and 5.12, respectively.

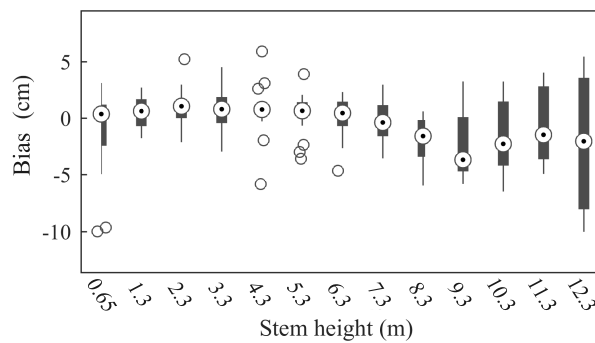


Fig. 5.11: Bias of diameter estimation and its distribution with height. Results are evaluated from all trees.

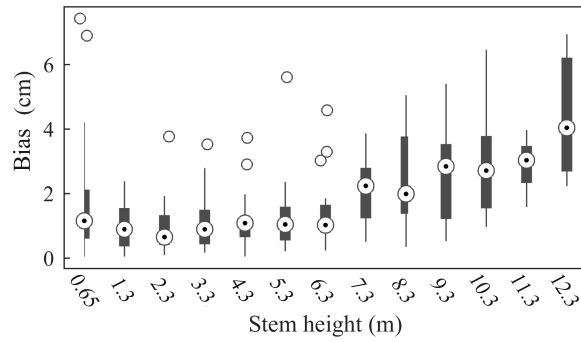


Fig. 5.12: Bias of stem location estimation and its distribution with height. Results are evaluated from all trees.

Stem volume is calculated from the stem curve using Equation (6.6). The result of the volume comparison also shows a good accuracy, with a relative RMSE of 7.07%.

5.5 Discussion

In this study, tree stems are automatically detected and modeled by a robust cylinder fitting scheme. Figure 5.13 shows an overall representation of our results. In the following subsections, the parameters used in the algorithms and possible error sources that could affect the results of the presented algorithms are discussed. At the same time, we address several challenges about the application of TLS in a landslide region, which potentially also apply to other high mountain heterogeneous forests.

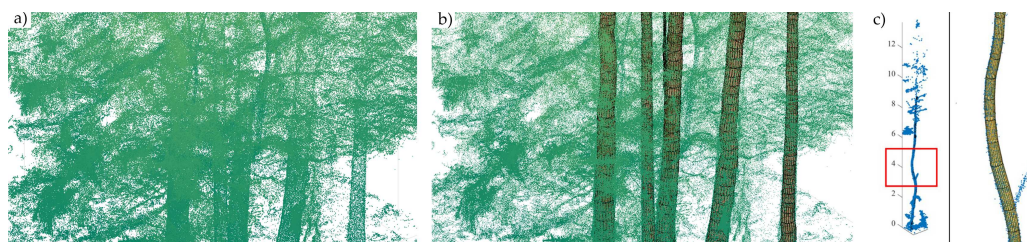


Fig. 5.13: (a) Point cloud of a proportion of the forest; (b) a visualization of the corresponding reconstructed stems in (a); (c) an example tree shows that our method is able to handle the curvature of the deformed stem.

5.5.1 Parameters

In the stem detection and modeling steps, various parameter were determined. Parameters used for stem detection include the search radius of the DBSCAN

algorithm and the stem group extent enlargement factor. Stem modeling-related parameters include cell size, circle inscribing parameters, cylinder growing step length L and cylinder shifting and rotating parameters α and β . However, none of these parameters is sensitive to the methodology. Furthermore, they can be determined according to the datasets and field conditions.

The search radius of the DBSCAN algorithm depends on the point density (Tao et al., 2015b). The criterion is that it should be able to connect adjacent stem points. The stem group extent enlargement factor is used to retain points from the upper part of the stem in case the stem is inclined. We chose a factor of 1.5 because the trees in our study region are not heavily inclined. It can be increased for heavily curved trees or those with more irregular stem forms, such as deciduous trees.

Smaller value of cell size should be chosen if trees are grown close to each other. Besides, we used the -1 cm and $+2$ cm thresholds for inscribing the circle in 2D. They are chosen based on the fact that the mean bark thickness is ~ 18 mm in our study region according to empirical functions (see Section 5.5.2). The step length L should be determined according to the stem shapes. For forests where trees are in general vertical (e.g., managed forests), L can be longer to simplify the modeling; while a smaller value should be used for complex stem shapes in order to represent the curvature of stems. The cylinder shifting and rotating parameters are also related to stem shapes. They can be explicitly refined if smaller shifting and rotating intervals for cylinder tests are required. However, this will increase the computation time accordingly.

5.5.2 Error Analysis

Terrain model estimation is a prerequisite to determine the normalized height of a tree. The accuracy of DTM, theoretically, could introduce a bias of DBH and stem curve, because of the false estimation of stem heights. However, we do not anticipate that the stem diameter would change sharply within a short distance. In addition, the field measurements also contain uncertainties arising from the human-determined absolute height of the tree (Huang, 1994). Practical tests show that a change of terrain height by ± 5 cm will only introduce a small change of the results of DBH determination by 0.2%–0.6%; thus, this does not affect the results significantly.

Further, one of the main challenges in high mountain forest is the terrain accessibility. Therefore, the scan locations are often disjointed. Point coverage and density for every individual tree vary according to the scanning visibility, as well as the occlusions. To account for the effects of such coverage inconsistency, we plot the

results of DBH against the TLS coverage percentage for every tree, as demonstrated in Figure 5.14. In general, the higher TLS coverage results in smaller absolute bias. The RMSE of DBH estimation decreases from 1.80 cm down to 1.50 cm for trees with TLS coverage larger than 80%, comparing with the results from all trees (Table 5.3). Nonetheless, the improvements are not significant, because our algorithm models the partially covered stems with a robust approach. In fact, the largest RMSE is smaller than 4 cm, demonstrating the capability of our approach for suppressing the deficiency of disjointed TLS scans.

We have shown in Figure 5.7 that the asymmetric thresholds are critical when fitting the circle or cylinder to points that cover only an arc. The fitted primitive could be heavily biased by the unbalanced weights introduced by the point distribution, if symmetric thresholds are given. To evaluate the effect of the asymmetric thresholds, we fit a circle to a stem whose cross-section is fully covered (i.e., full TLS coverage), by applying asymmetric and symmetric thresholds, respectively. We obtained an underestimation of ~ 15 mm of diameter for the asymmetric thresholds. However, such a disparity is on the same scale with natural ambiguities, like tree bark roughness or stem texture. The asymmetric thresholds enforce the fitted primitive inside the stem points (i.e., inscribing), which is a plausible assumption in practice as laser pulses cannot penetrate into stems. However, the bark or surface texture does introduce a certain thickness of laser points around the stem (i.e., effectively forming a toroid). In other words, the inside primitive determines the diameter of the stem without bark. On the other hand, field-measured DBH was based on the peripheral surface of the bark, thus leading to an underestimated result compared to our algorithm. We calculated the bark thicknesses in our study site according to Equation (4) in Stangle et al., 2015. The mean bark thickness is ~ 18 mm, which is similar to the underestimation of 15 mm in our study. Therefore, the determined diameter is simply compensated by +15 mm in this study.

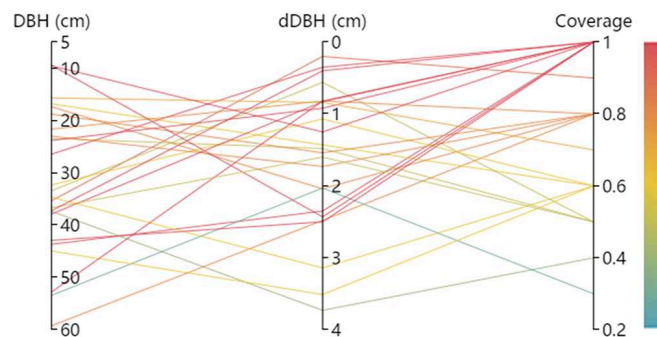


Fig. 5.14: The results of DBH plotted against TLS coverage. The DBH in the left axis denotes the field-measured DBH. dDBH refers the absolute bias. Color is scaled by the TLS coverage.

Asymmetric thresholds could result in significant underestimation of the stem diameter under one circumstance. For example, Figure 5.15 shows the cross-section at the height of DBH of the tree that is marked as reconstruction failure in our study site. The irregular shape significantly differs from a circle. Thereby, the fitted circle (or cylinder) from our algorithms will have a much smaller diameter. In the landslide region, such a phenomenon often exists, because of the disturbance from soil movements, which change the wood formation mechanism (Plomion et al., 2001).

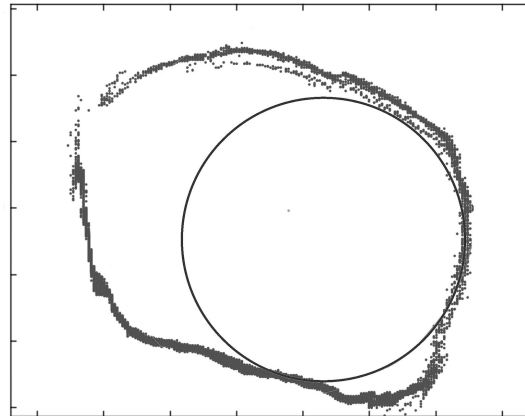


Fig. 5.15: The cross-section of a tree at 1.3 m above the ground. The severe irregularity leads to an underestimation of the diameter using our algorithm.

In addition, the stem shape becomes more anomalous on the parts close to the root (e.g., similar to Figure 5.15). Lower segments feature more complex stem shapes, especially when the root systems are partially exposed. Figure 5.11 and 5.12 show that the biases of estimated diameter and location at the height of 0.65 m are usually larger than, for example, 1 m–2 m. Advanced curve fitting strategy should be developed for future studies, such as Pfeifer and Winterhalder, 2004; You et al., 2016, to resolve such issues. Figure 5.11 and 5.12 also indicate that the results' accuracy drops along with the height starting from approximately 6 m above the ground. This addresses another challenge of using TLS in the forest. In particular, the multi-layered canopy structure in mountain regions blocks the laser pulse from reaching the top of the tree. A previous study also shows that there is a significant disparity of tree height estimation using TLS in urban heterogeneous forests (e.g., Moskal and Zheng, 2011). This issue can be possibly improved by combing data from other sources, such as unmanned aerial vehicle (UAV) laser scanning (e.g., Wieser et al., 2016). Nevertheless, our self-adaptive cylinder growing strategy aims to model the stem up to the tree top if point data are available. The highest fitted cylinder reaches 12.3 m, which is consistent with the manual delineation.

5.5.3 Algorithm

Our algorithm is designed to meet the aforementioned challenges of processing TLS data from high mountain heterogeneous forests. The tree stem recognition method combines the z-normal value and projection density. The stem curve is retrieved by a robust cylinder fitting and self-adaptive growing scheme. The performance of our method is similar to those on a flat environment (e.g., Hopkinson et al., 2004; Maas et al., 2008; Watt and Donoghue, 2005), demonstrating the effectiveness of precise stem modeling in mountain and landslide regions.

The unique capability of our method is that it is noise free. Many previous publications require fine estimation of stem points and then estimate or model the DBH (e.g., Maas et al., 2008; Watt and Donoghue, 2005). Yet, our RANSAC-based stem reconstruction method does not require a fine delineation of stem points and is robust with points from branches, leaves and other outliers. Figure 5.16 gives an example of one stem section with branches and outliers. Our method achieves a robust and accurate stem fit even when a significant number of disturbing points persist. This enables us to estimate tree stem locations instead of direct stem point delineation, which can be difficult due to the complex field conditions.

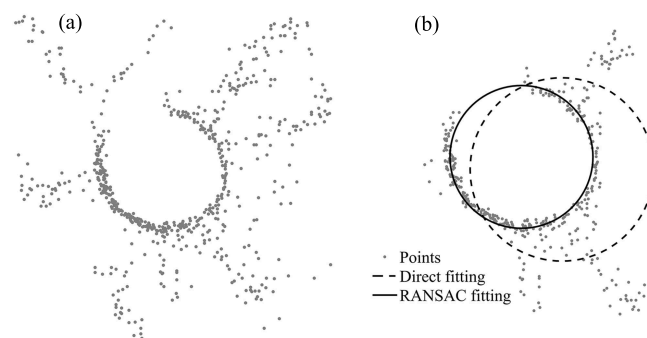


Fig. 5.16: An example of the effectiveness of RASANC algorithm in circle fitting. The outliers in original points (a) are first filtered by the region growing method (b).

The presented cylinder growing strategy handles the challenge of occlusion. The growing cylinder always takes advantage of previous robustly fitted cylinder. In other words, the rough location of the next cylinder is confident. Therefore, the shifted cylinder connects points that belong to the stem even if they are partially occluded. Moreover, the cylinder length growth step can be adapted to cover the zone on the stem where the tree is occluded. For example, the step length can be elongated to 1 m or even longer, if necessary, although we fix it as 20 cm in this study.

The employed method in this study utilizes a 2D to 3D robust circle and cylinder fitting scheme. Most of the previous studies on using TLS focused on retrieving tree parameters, such as location, DBH and tree height (e.g., Olofsson et al., 2014; Sun et al., 2015; Maas et al., 2008; Litkey et al., 2008). Some of them fit a circle to a slice of stem points (e.g., Maas et al., 2008; Watt and Donoghue, 2005). Errors may arise from the projection of points to 2D, because tree stems are not always strictly vertical in space, and the project points will form an ellipse if the stem is tilted. Thereby, the circle fitting becomes implausible. In our method, the purpose of circle inscribing in 2D is to provide a good initial guess for 3D cylinder fitting. The final model is performed in 3D by cylinder fitting; thus, it is not subject to a specific case if the stem is strictly vertical or tilted. For previous cylinder fitting approaches (e.g., Hopkinson et al., 2004; Wezyk et al., 2007), errors could originate from branches and outliers if the standard least square is directly applied. Moreover, the solution of the nonlinear problem will be heavily affected by the initial guess, whereas in our method, it is determined by an RANSAC scheme. Table 6.9 gives a comparison of the performance of our work with previous studies. It is worth mentioning that Table 6.9 is not a comprehensive overview of TLS applications in forests, but it rather shows how different methods were applied to various forests and their corresponding performances. From the comparison, we can see that our method performed equally well or even better when compared to previous works that focused on flat regions or planned forests.

In addition, our method is also applicable for other tree species, such as deciduous trees, and the point cloud acquired from other approaches, such as UAV laser scanning. Figure 5.17 shows an example of our method applied to point clouds of a deciduous tree acquired from TLS and UAV laser scanning, respectively.

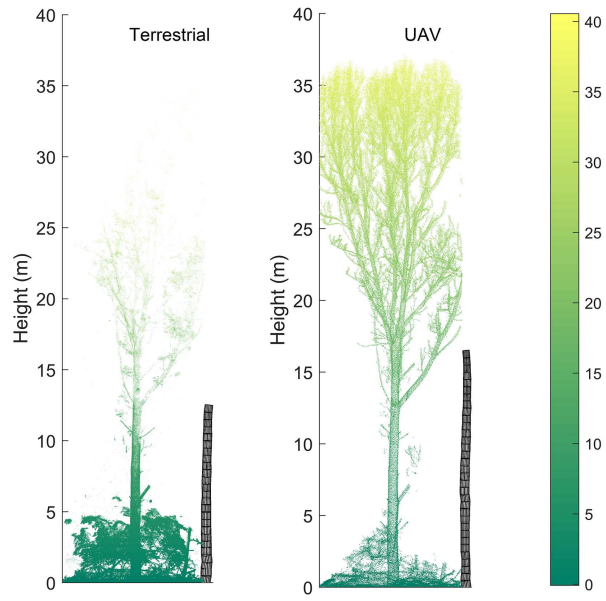


Fig. 5.17: An example of our method applied to a deciduous tree. The point cloud was acquired from TLS and UAV laser scanning, respectively.

Tab. 5.4: Summary of several selected studies on automatic stem detection and modeling from TLS data. Only the first authors are shown to save space. Some of the contents and values are visually inspected or calculated from corresponding publications. S and M in scan mode stand for single scan and multiscan, respectively. M(p) means that multiscan is only performed partially.

Study	Environment	Sample Size	Density (Stem/ha)	Scan Mode	Method	Completeness	Level of Automation	DBH Result (RMSE (cm) or R^2)
Thies and Spiecker, 2004	steep	50	556	S, M	Circle fitting	22% (S) 52% (M)	full	3.48 (S) 3.22 (M)
Hopkinson et al., 2004	flat	138	661	M	Circle fitting 1.25 m-1.75 m	93%	semi	$R^2 = 0.85$
Watt and Donoghue, 2005	flat planned	12	600	M(p)	Circle fitting	100%	semi	$R^2 = 0.92$
Wezyk et al., 2007	flat	-	-	M	Cylinder fitting 1.28 m-1.32 m	63%-90%	semi	$R^2 > 0.946$
Maas et al., 2008	flat	14-29	212-410	S, M	Circle fitting	87%-100%	full	1.48-3.25
Yao et al., 2011	flat	-	1017-3281	S	Angular width	-	full	7.0-8.0
Calders et al., 2015	flat	65	317-347	M	Circle fitting	-	semi	2.39
Olofsson et al., 2014	-	-	358-1042	S	Circle fitting RANSAC	87% on average	full	2.0-9.6 14%
Moskal and Zheng, 2011	heterogeneous	25	-	S	Cylinder fitting voxel modeling	-	full	9.2 $R^2 = 0.91$
Liang et al., 2014a	flat	28	-	M	Cylinder fitting robust	-	full	0.82 4.2%
Brolly and Kiraly, 2009	flat	213	852	S	Circle fitting cylinder fitting	81%	full	4.2-7.0
Our work	steep landslide	27	554	M(p)	Cylinder fitting RANSAC	93%	full	1.8 (5.5%) $R^2 = 0.99$

5.5.4 Applicability of TLS in Landslide-Affected Forest

In this paper, “landslide-affected forests” not only refers to the regions where intense landslides occurred. In fact, a wide range of high mountain forests share similar features. Soil movement is a common threat in many mountainous areas, such as the Alpine mountain range. Trees in these regions are interacting with soil as the tree roots try to cling to the soil. On the other hand, the moving soil drags the tree. Therefore, tree growth is disturbed, and stems typically have different shapes compared with flat areas.

Our self-adaptive cylinder growing strategy enables the modeling of the whole stem. Stem parameters are then calculated from the fitted models. This opens up the opportunity for precisely deriving more valuable forest variables, such as taper, stem volume and other information related to tree morphology. In particular, stem shape is of special value in high mountain landslide regions. Biomass estimation on the single tree level can be integrated into physical models to improve the understanding of tree-soil interaction (e.g., Steger et al., 2015). Different biomass components are also of great interest, for example, in estimating the stem, branches and leaf/needle biomass (e.g., Ma et al., 2016) and to quantify the leaf area index. Stem volume provides the basis for single tree biomass determination (e.g., Kankare et al., 2013).

5.6 Conclusions

In this study, we present a full automatic tree stem detection and modeling method. The approach is tested for 27 trees in a landslide-affected forest in the Austrian Alps. A robust cylinder fitting scheme is exploited to reconstruct the whole stem. Stem curves are compared at various heights for the diameter and center location. Results showed good accuracies when compared to manually-measured reference data. Furthermore, we have discussed some challenges of TLS applications in landslide-affected forests. In general, the lack of application of TLS in high mountain forests calls for a specific point cloud processing approach, and our study highlighted the potential of the methodology. In the form demonstrated here, a limitation of our method is the handling of irregular stem cross-sections, which significantly deviate from a circle. The possible solution is to fit free-form curves. Our method can also be exploited for branch modeling. However, a higher point density is needed, especially for the upper parts of the tree. The combination of TLS with other data sources, such as airborne laser scanning, UAV laser scanning, optical images and hyperspectral images, is assumed to advance the research of forest

management and other ecosystems research activities. In future studies, we will test our algorithm for other tree species and study areas.

Publication IV: Reconstructing Stem Cross Section Shapes from Terrestrial Laser Scanning

” *This section is a reproduced version of: Wang, D., Kankare, V., Puttonen, E., Hollaus, M., & Pfeifer, N. (2017). Reconstructing stem cross section shapes from terrestrial laser scanning. IEEE Geoscience and Remote Sensing Letters, 14(2), 272-276.*

6.1 Introduction

Tree stem cross section shapes are of particular interest to forest managements and the timber industry because some vital attributes can be derived from them, such as the minimum, maximum, and average diameters (Matérn, 1956), taper (Thies et al., 2004), ovality (Pfeifer and Winterhalder, 2004), and bending moment (Koizumi and Hirai, 2006). Conventional measurements are collected in field observations, a process that is time- and labor-consuming, and often requires felling the trees. Terrestrial laser scanning (TLS), on the other hand, has shown a clear potential in estimating stem attributes in an automatic manner (e.g., Åkerblom et al., 2015).

The common methods of forest measurement assume that the cross sections of tree stems can be approximated by circular shapes (e.g., Maas et al., 2008). However, such an assumption is rarely true in practice, especially in unmanaged forests, in which the tree growth conditions are complex and unpredictable. The wood formation mechanism is often influenced by such factors as the site fertility, spacing and light conditions, wind, and landslide events (Plomion et al., 2001). Thus, the shapes of the stem cross sections differ significantly from a circle (e.g., Koizumi and Hirai, 2006).

Previous studies (e.g., Pfeifer and Winterhalder, 2004) have modeled the cross section of a stem or branch by using closed B-spline or other parameterizable curves. The shape of the stem cross section can be tracked; thus, the average diameter and other attributes can be inferred. However, the number of outlier and branch points is not determined, which affects the fitting quality. Moreover, the closed B-spline performs best on cross sections with full TLS coverage (i.e., the whole cross section is scanned by TLS). This is rarely the case in many mountain forests because of the difficult terrain accessibility. Therefore, more tests and approaches should be explored for data sets with different features, such as single-scan TLS data. In general, there is a lack of methods for determining the accurate cross section curve.

This study aims to develop a robust and effective approach to precisely reconstruct stem cross sections from TLS data. The average stem diameter (DBH) is used to evaluate the results. The approach is designed to work with data from various conditions. To test the proposed approach, two data sets collected from different forest types and under different TLS acquisition modes are analyzed. The analysis is carried out by using an advanced curve fitting strategy in comparison to a conventional circle fitting technique.

6.2 Study Area and Data

6.2.1 Study Site I

The first study site is located in the federal state of Vorarlberg, Austria (43.22°N, 9.73°E; Fig. 6.1). The dominant tree species in the site is Norway spruce (*Picea abies* (L.) H. Karst.). The stem density is approximately 544 stems/ha. The TLS measurement was done with a RIEGL VZ-2000 laser scanner (RIEGL Laser Measurement Systems, Horn, Austria) in October 2015 and covered 26 trees near the corrupted surface of a translational landslide. The scanned trees showed irregular stem shapes because of the soil movement and the shapes of their cross sections differed significantly from a circle. Seven scans were carried out from different directions according to the terrain accessibility. The average TLS coverage rate for a single tree was 77.7%. DBH was manually obtained in the field by using a measuring tape. These manual measurements served as reference data. The average DBH in the study site was 32.8 cm, with a standard deviation of 14.3 cm.

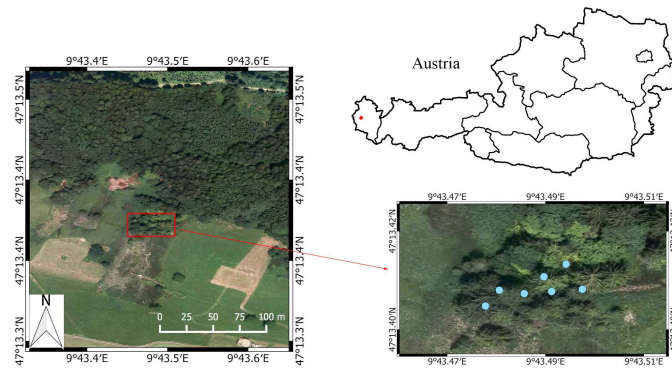


Fig. 6.1: Study site I: the red rectangle covers a small transection roughly equal to an area of 31 m × 19 m. The blue dots indicate the locations of seven TLS scans.

6.2.2 Study Site II

The second study site is located in Evo, Finland (61.19°N, 25.11°E). The TLS data were collected from a single sample plot in 2010. The plot is a mature Scots pine (*Pinus sylvestris* L.) forest with sparse understory vegetation (Fig. 6.2). The stem density is 424 stems/ha, with an average DBH of 21.3 cm and a standard deviation of 3.2 cm. The TLS data were collected with a Leica HDS6100 TLS system (Leica Geosystems AG, Heerbrugg, Switzerland) in single-scan mode. Reference measurements for 23 trees were obtained manually from the full-density TLS point cloud by using the 3D environment of TerraScan (Terrasolid Ltd, Helsinki, Finland). The DBH for each tree within the sample plot was manually measured by averaging the diameters from two directions (W-E, N-S) from the point cloud with the use of distance measurement tools in TerraScan.

6.3 Method

6.3.1 Stem Mapping

Tree stems were manually identified from the point cloud data. Although there are various methods of automatic stem mapping (e.g., Liang et al., 2012), this study focuses on reconstructing cross section shapes and does not incorporate automatic stem delineation algorithms in order to ensure that all stems are identified. The stems were identified from their spatial locations and grouped into a circular region with a 40-cm radius. Manual cleaning was omitted, meaning that all branch and outlier points near a stem were retained. A digital terrain model (DTM) was generated based on the TLS data, and the 3D points were normalized by subtracting the DTM heights from each z-value. A slice between 1.25 m and 1.35 m above

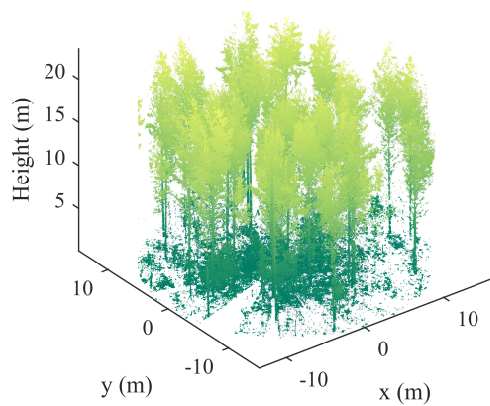


Fig. 6.2: Study site II: a mature Scots pine forest scanned with TLS in single-scan mode.

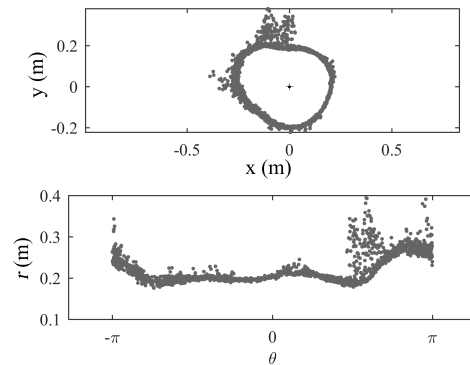


Fig. 6.3: Transformation of coordinates from Cartesian (x, y) to polar (r, θ) . The angular domain in the polar frame is $[-\pi, \pi]$.

ground from each stem was selected and projected onto a horizontal plane for DBH estimation.

6.3.2 DBH Estimation

DBH is usually estimated by determining the diameter of a fitted circle or cylinder. Nevertheless, it can also be estimated by measuring the perimeter of the corresponding cross section. The latter requires tracking the stem outline at the cross section. Accurate fitting becomes more difficult when branch points or possible measurement errors are present.

For the curve fitting we move from Cartesian to polar coordinates (Fig. 6.3). With the polar coordinates, the closed curve fitting becomes a more general case of a wave-like curve fitting. The period of the wave-like curve is limited to 2π because it corresponds to a closed curve in Cartesian coordinates. To transform the points to

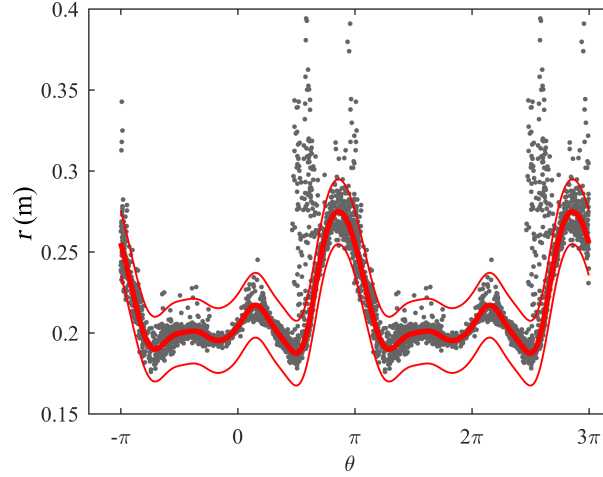


Fig. 6.4: Fourier approximation of points (full coverage) on the angular domain. The actual domain is $[-\pi, \pi]$, which is duplicated to $[-\pi, 3\pi]$ to show the periodicity. The thick red line indicates the final approximated curve, and the thin red lines denote the threshold boundaries of 2 cm. The points outside the boundaries are iteratively excluded.

polar coordinates, an initial origin inside the cross section needs to be defined. Here, we apply a Random Sample Consensus (RANSAC)-based (Fischler and Bolles, 1981) circle fitting routine with asymmetric distance thresholds to inscribe a circle inside the cross section. In this way, a circle is determined to lie within the cross section. Consequently, all points are centered with respect to the initial circle origin and further transformed to polar coordinates by $\theta = \tan^{-1} \left(\frac{y}{x} \right)$ and $r = \sqrt{x^2 + y^2}$, where θ denotes the angular coordinate, and r is the radial coordinate. The angular domain is $[-\pi, \pi]$. A periodic wave-like curve can be approximated accurately with Fourier series,

$$r(\theta) = a_0 + \sum_{i=1}^n \left(a_i \cos \left(\frac{2\pi}{T} i\theta \right) + b_i \sin \left(\frac{2\pi}{T} i\theta \right) \right), \quad (6.1)$$

where a_0 , a_i , and b_i are the Fourier coefficients, n is the number of harmonics, and T is the period length. Here, T is set to 2π . The curve is a combination of simple oscillating waves. The degree of Fourier series n is determined according to the complexity of the cross section shape and the point density. A high degree for sparse points or incomplete cross sections will cause unnecessary oscillation. In general, practical tests are advisable. We selected orders 8 and 3 for study sites I and II, respectively.

Another advantage of using Fourier approximation is that it is easy to constrain the periodicity, which is equivalent to a closed form in the Cartesian coordinates. With T equal to 2π , the solution of Eq. (6.1) becomes an ordinary linear least square problem. Considering an overdetermined system $r = X\beta$ (i.e., the matrix form of

Eq. (6.1)), where $\beta_{1,2,..,m}$ refers to m unknown coefficients, and $m = 2n + 1$ with k observations, the expansion is shown as

$$\begin{bmatrix} r_1 \\ \vdots \\ r_k \end{bmatrix} = \begin{pmatrix} 1 & \cos(\theta_1) & .. & \cos(n\theta_1) & \sin(n\theta_1) \\ \vdots & \vdots & \vdots & \vdots & \vdots \\ 1 & \cos(\theta_k) & .. & \cos(n\theta_k) & \sin(n\theta_k) \end{pmatrix} \times \begin{pmatrix} a_0 \\ a_1 \\ \vdots \\ a_n \\ b_n \end{pmatrix}, \quad (6.2)$$

where $a_0, a_1, .., a_n, b_n$ are the elements of β . The solution (e.g., Watson, 1967) is then given as

$$\hat{\beta} = (X^T X)^{-1} X^T r. \quad (6.3)$$

As shown in Fig. 6.3, the cross section may contain points from tree branches and noise that should be omitted from the curve fit. A simple method that can be applied is to detect and remove outlier points iteratively by introducing a distance threshold. First, Fourier approximation is done on all points. Then, if a point's residual from the curve is larger than 2 cm, it is identified as an outlier and excluded from further iterations. This procedure is continued until all points are located within the 2-cm distance threshold (Fig. 6.4).

The perimeter of a cross section in polar coordinates is the arc length of a Fourier curve fit in the domain of $[-\pi, \pi]$. Subsequently, the diameter can be determined. The arc length with angular coordinates is computed as

$$L = \int_{\theta_1}^{\theta_2} \sqrt{r^2 + \left(\frac{dr}{d\theta}\right)^2} d\theta. \quad (6.4)$$

In case of full TLS coverage, the perimeter calculation is straight-forward. Problems arise when the cross section is not completely covered by TLS. In particular, a single scan covers only a small fraction of the cross section, which means that fitting a curve in the domain lacking points is impossible. Furthermore, the covered continuous fraction of the cross section is likely to be disconnected by the axes of polar coordinates. Therefore, we define an effective domain when the cross section is not fully covered.

The effective domain range d_s is determined by clustering the connected points in polar coordinates (Fig. 6.5). The domain is duplicated to $[-\pi, 3\pi]$, and the

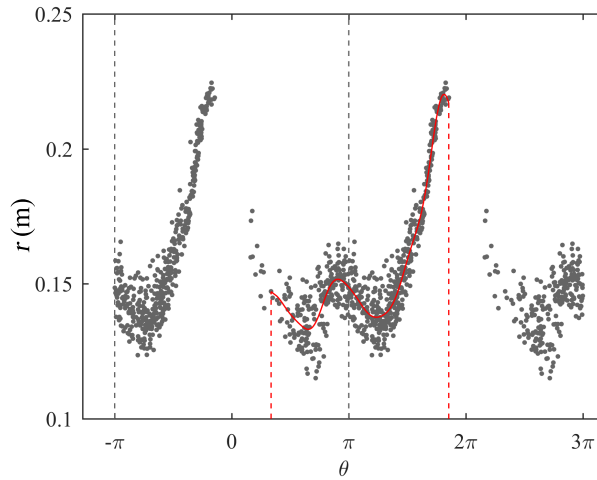


Fig. 6.5: The effective domain clamped by the dotted red lines is determined by clustering connected points. On the domain of $[-\pi, \pi]$, the points are disconnected by the $-\pi/\pi'$ axis. The presented example is from a stem with 60% TLS coverage.

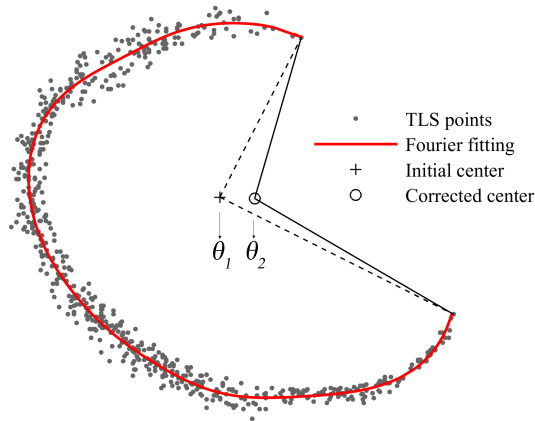


Fig. 6.6: The proportion of the effective domain to 2π is determined by the corrected center location. The new center location is identified by a circle fitting on filtered points.

disconnected points can be rejoined. The spatial distance between two points with polar coordinates is calculated by:

$$l = \sqrt{(r_1^2 + r_2^2 + 2r_1r_2 \cos(\theta_1 - \theta_2))}. \quad (6.5)$$

All points forming the largest connected component are identified by the Density-Based Spatial Clustering of Applications with Noise (DBSCAN) algorithm (Ester et al., 1996). Here, a distance threshold of 2 cm was used. Figure 6.5 shows the effective domain of the rejoined points within which curve fitting is possible.

We define and compare three routines for computing the DBH:

Extrapolated Fourier fit

The arc length L_{d_s} of the effective domain range d_s can be extrapolated to $[-\pi, \pi]$, and then the DBH can be estimated as

$$\text{DBH}^1 = \frac{L_{d_s} 2\pi}{d_s \pi} = \frac{2L_{d_s}}{d_s}. \quad (6.6)$$

Nonetheless, the proportion of the effective domain to 2π has to be determined precisely; otherwise, the resultant DBH will be biased. Therefore, a corrected center is obtained by fitting a new circle to filtered points (Fig. 6.6). The corrected circle is determined by applying an algebraic fitting approach (Taubin, 1991), which is a compromise between simplicity and realistic effectiveness. The DBH is then estimated with the corrected effective domain.

Combination of Fourier and circle fitting

The vacant part on 2π that is not included in the effective domain can also be complemented by a fraction of the corrected circle. However, the combined curve will be disconnected because the ends of the fitted circle are not required to meet the ends of the Fourier arc. DBH is computed as

$$\text{DBH}^2 = \frac{L_{d_s}}{\pi} + \left(1 - \frac{d_s}{2\pi}\right) p_c, \quad (6.7)$$

where p_c is the diameter of the corrected circle.

Direct circle fitting

For comparison, the simplest DBH proxy is to directly use the diameter of the corrected circle p_c .

6.3.3 Evaluation

The obtained DBH values are compared with the reference measurements. The residuals δ_i are calculated by $|\text{DBH}_i - \widehat{\text{DBH}}_i|$, where $\widehat{\text{DBH}}_i$ is the reference value. We report the bias as the average δ_i , and the accuracy as the root mean square error (RMSE) of δ_i and its relative value (%) to the $\overline{\text{DBH}}$ (i.e., the mean reference DBH).

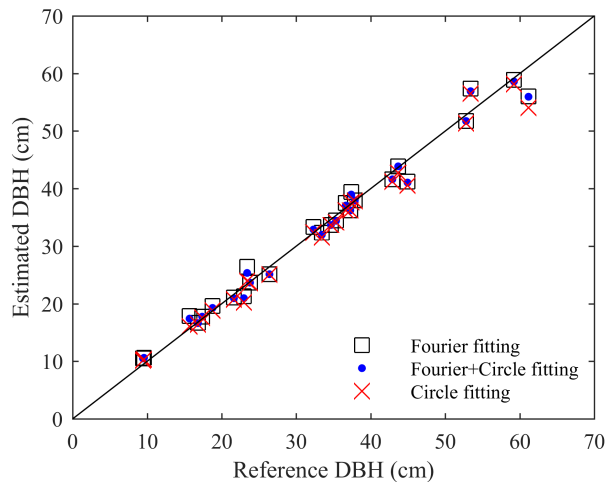


Fig. 6.7: Scatter plot of the DBH estimated from TLS by using three approaches and the reference values for the stems in study site I.

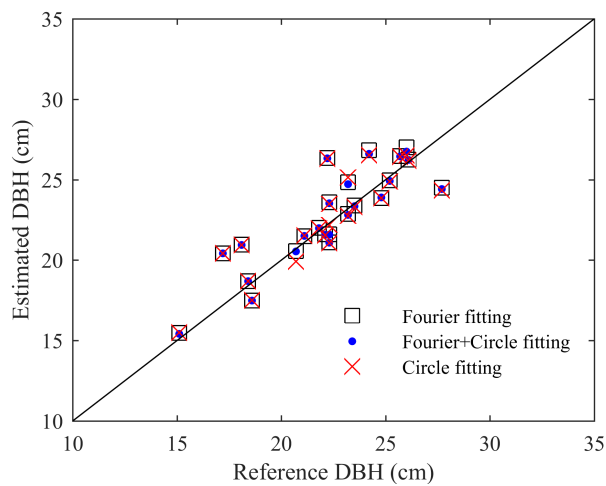


Fig. 6.8: Scatter plot of the DBH estimated from TLS by using three approaches and the reference values for the stems in study site II.

6.4 Results

Table 6.1 shows the bias and RMSE values. In study site I, we obtained an RMSE of 2.02 cm (6.2%) for circle fitting. This result is within the same range as in previous studies (e.g., Maas et al., 2008). The RMSE improved to 1.87 cm and 1.77 cm with the extrapolated Fourier fit and the combined Fourier and circle fitting, respectively. Compared with conventional circle fitting, the RMSE improved by 12.4% with the combination of Fourier and circle fitting. Moreover, we manually selected stems that were completely covered by multiple TLS scans, which further lowered the RMSE value from 12.4% to 24.7% for combined Fourier and circle fitting compared with direct circle fitting. In study site II, all three approaches showed similar accuracies. The resultant RMSE for circle fitting was 1.66 cm (11%). This improved marginally

Tab. 6.1: Bias and RMSE of the estimated DBH

Study site	Bias (cm)	RMSE (cm)	RMSE (%)	Method
I	0.11	1.87	5.7	Fourier
	0.30	1.77	5.4	Fourier+Circle
	0.84	2.02	6.2	Circle
II	0.46	1.67	11.0	Fourier
	0.41	1.64	10.9	Fourier+Circle
	0.40	1.66	11.0	Circle

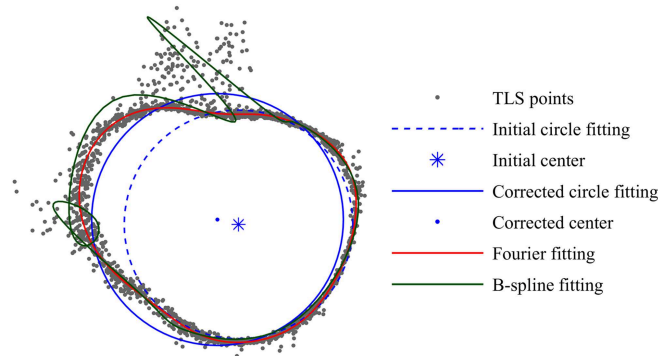


Fig. 6.9: Comparison of various fitting routines. The dashed blue circle indicates the initial circle estimation used to determine the center location within the cross section. The B-spline is troubled by outliers. Fourier series fitting creates an accurate perimeter estimate.

to 1.64 cm with the combination of Fourier and circle fitting. The relative RMSE was worse than that obtained in study site I. Figure 6.7 and 6.8 both show a high correlation between the reference DBH and the DBH estimated from TLS. The difference between the three proposed DBH estimates are minimal.

6.5 Discussion and Conclusion

In this study, stem cross sections are reconstructed by applying an advanced curve fitting strategy that uses coordinate transformation in polar coordinates and Fourier series fitting. The approach provides more realistic presentation of the cross section instead of the conventional circle approximation. The estimation of DBH is used as an indicator to compare our method and circle fitting with reference measurements made manually from the point clouds. The adoption of advanced curve fitting produced similar DBH accuracy compared with conventional circle fitting. In both study sites, the combination of Fourier and circle fitting produced the lowest RMSE.

In study site I, the tree stems have been exposed to long-term soil movements. As a result, some of their cross section shapes differed significantly from a circle (e.g., as shown in Fig. 6.9). Therefore, the advanced curve fitting approach performed better than circle fitting. The outcome indicates that the estimation of the DBH can be potentially improved by using an advanced curve fitting approach, especially for trees with irregular cross section caused by, e.g., mountain slopes.

Study site II featured data acquired in single-scan mode, with more regular tree stem shapes. Both Fourier series fitting and its combination with circle fitting resulted in similar accuracy compared with simple circle fitting. In this regard, a circle approximation was sufficient for the cross section estimate. Nonetheless, the Fourier series fit did not disserve the results, indicating that the suggested curve fitting approach is also applicable for tree species with circular stem cross sections.

Our Fourier fitting method iteratively detects and excludes gross errors, whereas conventional closed curve fitting methods (e.g., B-splines) present difficulties with outlier points and become problematic when the cross section is not fully covered by laser scans. Figure 6.9 shows the comparison between B-spline, circle, and Fourier fitting. The final circle fit also exploits the iterative noise removal used in Fourier series fitting.

We conclude that stem cross section shapes can be accurately reconstructed from TLS data by using an advanced curve fitting routine. The Fourier series fitting provides a more detailed cross section presentation while giving equally accurate DBH estimates as circle fitting. The proposed method is valuable for certain studies, such as in urban and mountain environments where tree forms are more complex. Our method provides a basis for quantitative studies, such as for determining the ovality and bending moment on tree cross sections in an automatic manner, and is thereby recommended for future studies.

General Conclusions

In this dissertation, 3D point cloud data acquired by laser scanning systems (mainly TLS) are used to quantify single-tree level structure in mountain forests. The main contributions are on the development of several novel algorithms that can mitigate the high degree of structure complexity associated to mountain forests. These contributions fill the research gap that most existing methods developed for forest inventory can hardly be directly applied in mountain forests. Moreover, some efforts are made to utilize smart point cloud structuring approaches to assist the processing of large volume of data. The outcomes of this dissertation promote the usage of laser scanning techniques for quantifying mountain structures at fine details with a large degree of automation and accuracy. The quantitatively described structure information can help to better understanding and managing the role of mountain forests in ecosystem service. To a large extent, these information are urgently needed in many regions worldwide to guide sustainable mountain forest management strategies.

Specifically, this dissection provides solutions to several important steps in processing TLS point cloud data that are needed towards a reliable estimation of single-tree attributes.

- **Separation of tree wood and leaf components** is firstly analyzed by testing the feasibility of four popular supervised machine learning methods and the impact of feature calculation. Random Forest classifier is suggested for its effectiveness and simplicity. Density based features prove to be effective. Meanwhile, the deficiency of supervised machine learning method is revealed on its harsh requirement of the quality of training data, which impedes the applicability to a large number of trees. To address this issue, a novel approach that is fully automatic and unsupervised is introduced. The proposed method can successfully separate wood and leaf components without the need of any user intervention. Experiments confirm its strength in dealing with plot-level mountain forests. The achieved accuracy is in line with the supervised machine learning methods, which ranges from 81.8% to 92.0%. The work shows that large region wood and leaf extraction using point cloud data can be broadly automated. Moreover, point cloud structuring is tested and recommended in future studies to accelerate the computation.

- **Tree stem detection and modeling in mountain landslide-affected forests** in this dissertation is among the very first attempts that extract and model tree stems in high mountain natural forests or shallow landslide-affected forests. The TLS acquisition in Austrian alps indicates that multi-scan setup can be difficult to perform due to the steep terrain, implying that advanced methods need to be developed to handle stems with only partial point cloud coverages. The proposed methodology is fully automatic and involves a routine for stem detection in rich understory environments and a robust stem reconstruction method that can model stems with irregular vertical orientations. The outcomes show that stems can be detected with a completeness of 93%, and stem curve can be successfully extracted with a high accuracy reaching a root mean square error of 2.45 cm.

However, a barrier lies in the efficient acquisition of TLS data in mountain forests. Future efforts should be made to investigate a more efficient approach to acquire laser scanning data in mountain forests that can fulfill the requirements of single-tree level quantification. A promising solution is to use ULS as a prime strategy to acquire high density point cloud from above trees, while deploy MLS or PLS to compensate the data coverage in lower stems, if needed.

- **Reconstruction of stem cross-sections** breaks down the assumption that the cross-section of tree stems is circular. A new method is developed to model the actual shape of stem cross-sections. Experiments demonstrate that the benefits of this work are twofold. First, the accuracy of diameter estimation is improved by 12.4% compared to that of using simple circle fitting. Second, the reconstructed cross-section shapes contain information about the growth anomaly of trees in specific morphological sites. This information is of importance value in monitoring the growth situation, thus also benefits the assessment of wood products such as timber managements. In addition, the developed method is robust against outliers, and remains very simple and easy to use. Therefore, it can be readily used for other datasets. It is noted that, multi-scan TLS is recommended to have a complete representation of the cross-sections, although experiments show that it works equally well for single-scan data in diameter estimation.
- **Point cloud structuring assisted data processing** is investigated in this dissertation, which is among the very first attempts that explore point cloud spatial structuring for forest applications. The potential of using proper spatial partition routines is confirmed in this dissertation from various application examples. Special benefits are achieved on the reduction of processing time

and generation of a continuum (i.e., regular structure). Therefore, certain point cloud structuring strategies are recommended in future studies.

The novel methods developed and knowledge gained in this dissertation provide practical examples and guidelines for understanding mountain forest structures at the single-tree level. A future focus should be integrating these single-tree level information with region level data to upscale the derived information to a broader scale. This untapped potential can surely contribute to a more intelligent and sustainable mountain forest management. In addition, new 3D measurement techniques or systems should be investigated to overcome the limitation of TLS brought by the steep terrain and occlusions in mountain forests.

Bibliography

- Adams, Rolf and Leanne Bischof (1994). „Seeded region growing“. In: *IEEE Transactions on pattern analysis and machine intelligence* 16.6, pp. 641–647.
- Åkerblom, Markku, Pasi Raunonen, Mikko Kaasalainen, and Eric Casella (2015). „Analysis of geometric primitives in quantitative structure models of tree stems“. In: *Remote Sensing* 7.4, pp. 4581–4603.
- Al-Sharadqah, Ali and Nikolai Chernov (2009). „Error analysis for circle fitting algorithms“. In: *Electronic Journal of Statistics* 3, pp. 886–911.
- Aldred, A. H and G. M Bonnor (1985). *Applications of airborne lasers to forest surveys*. Tech. rep. Petawawa National Forestry Institute, Canadian Forestry Service, Canada.
- Alewell, Katrin Meusburger; Christine (2014). *Soil Erosion in the Alps. Experience gained from case studies (2006–2013)*. Report. Federal office for the Environment, Environmental Studies: Bern, Switzerland.
- Alexandrowicz, Zofia and Włodzimierz Margielewski (2010). „Impact of mass movements on geo-and biodiversity in the Polish Outer (Flysch) Carpathians“. In: *Geomorphology* 123.3, pp. 290–304.
- Ali, Jawad and Tor A Benjaminsen (2004). „Fuelwood, timber and deforestation in the Himalayas: the case of Basho Valley, Baltistan region, Pakistan“. In: *Mountain Research and Development* 24.4, pp. 312–318.
- Asner, Gregory P, Jonathan MO Scurlock, and Jeffrey A Hicke (2003). „Global synthesis of leaf area index observations: implications for ecological and remote sensing studies“. In: *Global Ecology and Biogeography* 12.3, pp. 191–205.
- Bazazian, Dena, Josep R Casas, and Javier Ruiz-Hidalgo (2015). „Fast and robust edge extraction in unorganized point clouds“. In: *2015 International Conference on Digital Image Computing: Techniques and Applications (DICTA)*. IEEE, pp. 1–8.
- Beder, Christian and Wolfgang Förstner (2006). „Direct solutions for computing cylinders from minimal sets of 3d points“. In: *Computer Vision ECCV 2006*. Springer, pp. 135–146.
- Béland, Martin, Dennis D Baldocchi, Jean-Luc Widlowski, Richard A Fournier, and Michel M Verstraete (2014). „On seeing the wood from the leaves and the role of voxel size in determining leaf area distribution of forests with terrestrial LiDAR“. In: *Agricultural and Forest Meteorology* 184, pp. 82–97.

- Belton, David, Simon Moncrieff, and Jane Chapman (2013). „Processing tree point clouds using Gaussian mixture models“. In: *Proceedings of the ISPRS annals of the photogrammetry, remote sensing and spatial information sciences, Antalya, Turkey*, pp. 11–13.
- Blattert, Clemens, Renato Lemm, Oliver Thees, Manfred J Lexer, and Marc Hanewinkel (2017). „Management of ecosystem services in mountain forests: review of indicators and value functions for model based multi-criteria decision analysis“. In: *Ecological Indicators* 79, pp. 391–409.
- Breiman, Leo (2001). „Random forests“. In: *Machine learning* 45.1, pp. 5–32.
- Bribiesca, Ernesto (2008). „An easy measure of compactness for 2D and 3D shapes“. In: *Pattern Recognition* 41.2, pp. 543–554.
- Brodu, Nicolas and Dimitri Lague (2012). „3D terrestrial lidar data classification of complex natural scenes using a multi-scale dimensionality criterion: Applications in geomorphology“. In: *ISPRS Journal of Photogrammetry and Remote Sensing* 68, pp. 121–134.
- Brolly, Gabor and Geza Kiraly (2009). „Algorithms for stem mapping by means of terrestrial laser scanning“. In: *Acta Silvatica et Lignaria Hungarica* 5, pp. 119–130.
- Burkhardt, Harold E. and Margarida Tomé (2012). „Tree Form and Stem Taper“. In: *Modeling Forest Trees and Stands*. Dordrecht: Springer Netherlands, pp. 9–41.
- Calders, Kim, Glenn Newnham, Andrew Burt, et al. (2015). „Nondestructive estimates of above-ground biomass using terrestrial laser scanning“. In: *Methods in Ecology and Evolution* 6.2, pp. 198–208.
- Calders, Kim, Mathias I Disney, John Armston, et al. (2017). „Evaluation of the Range Accuracy and the Radiometric Calibration of Multiple Terrestrial Laser Scanning Instruments for Data Interoperability“. In: *IEEE Transactions on Geoscience and Remote Sensing* 55.5, pp. 2716–2724.
- Canadell, Josep G and Michael R Raupach (2008). „Managing forests for climate change mitigation“. In: *science* 320.5882, pp. 1456–1457.
- Chen, Jing M and TA Black (1992). „Defining leaf area index for non-flat leaves“. In: *Plant, Cell & Environment* 15.4, pp. 421–429.
- Chen, M., Y. Wan, M. Wang, and J. Xu (2018). „Automatic Stem Detection in Terrestrial Laser Scanning Data With Distance-Adaptive Search Radius“. In: *IEEE Transactions on Geoscience and Remote Sensing* 56.5, pp. 2968–2979.
- Chen, Qi, Peng Gong, Dennis Baldocchi, and Yong Q Tian (2007). „Estimating basal area and stem volume for individual trees from lidar data“. In: *Photogrammetric Engineering & Remote Sensing* 73.12, pp. 1355–1365.
- Chiba, Yukihiko (1990). „A quantitative analysis of stem form and crown structure: the S-curve and its application“. In: *Tree Physiology* 7.1-2-3-4, pp. 169–182.
- Comaniciu, Dorin and Peter Meer (2002). „Mean shift: A robust approach toward feature space analysis“. In: *IEEE Transactions on pattern analysis and machine intelligence* 24.5, pp. 603–619.
- Conto, Tiago de, Kenneth Olofsson, Eric Bastos Görgens, Luiz Carlos Estraviz Rodriguez, and Gustavo Almeida (2017). „Performance of stem denoising and stem modelling algorithms on single tree point clouds from terrestrial laser scanning“. In: *Computers and Electronics in Agriculture* 143, pp. 165–176.

- Dalponte, Michele, Liviu Theodor Ene, Terje Gobakken, Erik Næsset, and Damiano Gianelle (2018). „Predicting Selected Forest Stand Characteristics with Multispectral ALS Data“. In: *Remote Sensing* 10.4, p. 586.
- Depenthal, Claudia and Günter Schmitt (1996). „Monitoring of a landslide in Vorarlberg/Austria“. In: *Proc. Int. FIG Symp. on Deformation Measurements, 11th, Santorini (Thera) Island, Greece*, pp. 25–28.
- Disney, M. I., M. Boni Vicari, A. Burt, et al. (2018). „Weighing trees with lasers: advances, challenges and opportunities“. In: *Interface Focus* 8.
- Drusch, M, U Del Bello, S Carlier, et al. (2012). „Sentinel-2: ESA’s optical high-resolution mission for GMES operational services“. In: *Remote sensing of Environment* 120, pp. 25–36.
- Elseberg, Jan, Dorit Borrmann, and Andreas Nüchter (2011). „Efficient processing of large 3d point clouds“. In: *Information, Communication and Automation Technologies (ICAT), 2011 XXIII International Symposium on*. IEEE, pp. 1–7.
- (2013). „One billion points in the cloud - an octree for efficient processing of 3D laser scans“. In: *ISPRS Journal of Photogrammetry and Remote Sensing* 76, pp. 76–88.
- Ester, Martin, Hans-Peter Kriegel, Jörg Sander, and Xiaowei Xu (1996). „A density-based algorithm for discovering clusters in large spatial databases with noise.“ In: *Proc. 2nd Int. Conf. Knowledge Discovery and Data Mining (KDD)*. Vol. 96. 34, pp. 226–231.
- Evans, Douglas (2012). „Building the European Union’s Natura 2000 network“. In: *Nature conservation* 1, p. 11.
- Eysn, Lothar, Norbert Pfeifer, Camillo Ressel, et al. (2013). „A practical approach for extracting tree models in forest environments based on equirectangular projections of terrestrial laser scans“. In: *Remote Sensing* 5.11, pp. 5424–5448.
- Feliciano, Emanuelle A, Shimon Wdowinski, and Matthew D Potts (2014). „Assessing mangrove above-ground biomass and structure using terrestrial laser scanning: a case study in the Everglades National Park“. In: *Wetlands* 34.5, pp. 955–968.
- Fernandes, Paulo M (2009). „Combining forest structure data and fuel modelling to classify fire hazard in Portugal“. In: *Annals of Forest Science* 66.4, pp. 1–9.
- Filin, Sagi and Norbert Pfeifer (2005). „Neighborhood systems for airborne laser data“. In: *Photogrammetric Engineering & Remote Sensing* 71.6, pp. 743–755.
- Fischler, Martin A and Robert C Bolles (1981). „Random sample consensus: a paradigm for model fitting with applications to image analysis and automated cartography“. In: *Communications of the ACM* 24.6, pp. 381–395.
- Forbes, Keith and Jeremy Broadhead (2013). *Forests and landslides: the role of trees and forests in the prevention of landslides and rehabilitation of landslide-affected areas in Asia*. Food and Agriculture Organization (FAO) of the United Nations: Bangkok, Thailand.
- Forsman, Pekka and Aarne Halme (2005). „3-D mapping of natural environments with trees by means of mobile perception“. In: *IEEE Transactions on Robotics* 21.3, pp. 482–490.
- Friedman, Nir, Dan Geiger, and Moises Goldszmidt (1997). „Bayesian network classifiers“. In: *Machine learning* 29.2-3, pp. 131–163.
- Garland, Michael (1999). *Quadric-based polygonal surface simplification*. Tech. rep. School of Computer Science, Carnegie Mellon University, USA.

- Geiß, Christian, Patrick Aravena Pelizari, Mattia Marconcini, et al. (2015). „Estimation of seismic building structural types using multi-sensor remote sensing and machine learning techniques“. In: *ISPRS Journal of Photogrammetry and Remote Sensing* 104, pp. 175–188.
- Gorte, Ben and Daniel Winterhalder (2004). „Reconstruction of laser-scanned trees using filter operations in the 3D raster domain“. In: *International Archives of Photogrammetry, Remote Sensing and Spatial Information Sciences* 36.Part 8, W2.
- Gray, Hugh Richard (1956). *The form and taper of forest-tree stems*. Imperial Forestry Institute, University of Oxford, UK.
- Gu, Quanquan, Zhenhui Li, and Jiawei Han (2012). „Generalized fisher score for feature selection“. In: *arXiv preprint arXiv:1202.3725*.
- Guyon, Isabelle, Steve Gunn, Masoud Nikravesh, and Lofti A Zadeh (2008). *Feature extraction: foundations and applications*. Vol. 207. Springer: Heidelberg, Germany.
- Hackel, T., J. D. Wegner, and K. Schindler (2016). „Fast semantic segmentation of 3D point clouds with strongly varying density“. In: *ISPRS Annals of Photogrammetry, Remote Sensing and Spatial Information Sciences* III-3, pp. 177–184.
- Hackenberg, Jan, Christopher Morhart, Jonathan Sheppard, Heinrich Spiecker, and Mathias Disney (2014). „Highly accurate tree models derived from terrestrial laser scan data: a method description“. In: *Forests* 5.5, pp. 1069–1105.
- Hackenberg, Jan, Marc Wassenberg, Heinrich Spiecker, and Dongjing Sun (2015). „Non destructive method for biomass prediction combining TLS derived tree volume and wood density“. In: *Forests* 6.4, pp. 1274–1300.
- Hakala, Teemu, Juha Suomalainen, Sanna Kaasalainen, and Yuwei Chen (2012). „Full waveform hyperspectral LiDAR for terrestrial laser scanning“. In: *Optics express* 20.7, pp. 7119–7127.
- Höfle, Bernhard (2014). „Radiometric correction of terrestrial LiDAR point cloud data for individual maize plant detection“. In: *IEEE Geoscience and Remote Sensing Letters* 11.1, pp. 94–98.
- Höfle, Bernhard and Norbert Pfeifer (2007). „Correction of laser scanning intensity data: Data and model-driven approaches“. In: *ISPRS journal of photogrammetry and remote sensing* 62.6, pp. 415–433.
- Hollaus, M, W Wagner, K Schadauer, B Maier, and K Gabler (2009). „Growing stock estimation for alpine forests in Austria: a robust lidar-based approach“. In: *Canadian Journal of Forest Research* 39.7, pp. 1387–1400.
- Hollaus, Markus, Lothar Eysn, and Frédéric Berger (2015). „Alpine Forest Biomass Localization based on LiDAR Data: Results of the NEWFOR Project“. In: *Proceedings. talk: 23rd European Biomass Conference & Exhibition (EUBCE 2015), Vienna; 2015-06-01 – 2015-06-04*.
- Hopkinson, Chris, Laura Chasmer, Colin Young-Pow, and Paul Treitz (2004). „Assessing forest metrics with a ground-based scanning lidar“. In: *Canadian Journal of Forest Research* 34.3, pp. 573–583.
- Huang, Barney K (1994). *Computer simulation analysis of biological and agricultural systems*. CRC Press: Boca Raton, FL, USA.

- Huang, Zhijian, Jinfang Zhang, Xiang Li, and Hui Zhang (2014). „Remote sensing image segmentation based on dynamic statistical region merging“. In: *Optik-International Journal for Light and Electron Optics* 125.2, pp. 870–875.
- Hyypä, Juha and Xinlian Liang. *Project Benchmarking on Terrestrial Laser Scanning for Forestry Applications*. www.eurosdrr.net/research/project/project-benchmarking-terrestrial-laser-scanning-forestry-applications. Accessed: 2018-02-18.
- Kaasalainen, Sanna, Anssi Krooks, Antero Kukko, and Harri Kaartinen (2009). „Radiometric calibration of terrestrial laser scanners with external reference targets“. In: *Remote Sensing* 1.3, pp. 144–158.
- Kaasalainen, Sanna, Anttoni Jaakkola, Mikko Kaasalainen, Anssi Krooks, and Antero Kukko (2011). „Analysis of incidence angle and distance effects on terrestrial laser scanner intensity: Search for correction methods“. In: *Remote Sensing* 3.10, pp. 2207–2221.
- Kaick, Oliver Van, Noa Fish, Yanir Kleiman, Shmuel Asafi, and Daniel Cohen-Or (2014). „Shape segmentation by approximate convexity analysis“. In: *ACM Transactions on Graphics (TOG)* 34.1, p. 4.
- Kalvoda, Jan and Charles L Rosenfeld (2012). *Geomorphological hazards in high mountain areas*. Vol. 46. Springer: Dordrecht, The Netherlands.
- Kankare, Ville, Markus Holopainen, Mikko Vastaranta, et al. (2013). „Individual tree biomass estimation using terrestrial laser scanning“. In: *ISPRS Journal of Photogrammetry and Remote Sensing* 75, pp. 64–75.
- Kankare, Ville, Marianna Joensuu, Jari Vauhkonen, et al. (2014). „Estimation of the timber quality of Scots pine with terrestrial laser scanning“. In: *Forests* 5.8, pp. 1879–1895.
- Kankare, Ville, Eetu Puttonen, Markus Holopainen, and Juha Hyypä (2016). „The effect of TLS point cloud sampling on tree detection and diameter measurement accuracy“. In: *Remote Sensing Letters* 7.5, pp. 495–502.
- Kerr, Jeremy T and Marsha Ostrovsky (2003). „From space to species: ecological applications for remote sensing“. In: *Trends in ecology & evolution* 18.6, pp. 299–305.
- Kim, Sang-Bum, Kyoung-Soo Han, Hae-Chang Rim, and Sung Hyon Myaeng (2006). „Some effective techniques for naive bayes text classification“. In: *IEEE transactions on knowledge and data engineering* 18.11, pp. 1457–1466.
- Kim, Yunsuk, Zhiqiang Yang, Warren B Cohen, et al. (2009). „Distinguishing between live and dead standing tree biomass on the North Rim of Grand Canyon National Park, USA using small-footprint lidar data“. In: *Remote Sensing of Environment* 113.11, pp. 2499–2510.
- Klasing, Klaas, Daniel Althoff, Dirk Wollherr, and Martin Buss (2009). „Comparison of surface normal estimation methods for range sensing applications“. In: *Robotics and Automation, 2009. ICRA'09. IEEE International Conference on*. IEEE, pp. 3206–3211.
- Koizumi, Akio and Takuro Hirai (2006). „Evaluation of the section modulus for tree-stem cross sections of irregular shape“. In: *Journal of Wood Science* 52.3, pp. 213–219.
- Koo, Seongyong, Dongheui Lee, and Dong-Soo Kwon (2014). „Unsupervised object individuation from RGB-D image sequences“. In: *Intelligent Robots and Systems (IROS 2014), 2014 IEEE/RSJ International Conference on*. IEEE, pp. 4450–4457.
- Körner, Christian (2004). „Mountain biodiversity, its causes and function“. In: *Ambio* 13, pp. 11–17.

- Kraus, Karl and Norbert Pfeifer (1998). „Determination of terrain models in wooded areas with airborne laser scanner data“. In: *ISPRS Journal of Photogrammetry and Remote Sensing* 53.4, pp. 193–203.
- Kuriakose, Sekhar L, LPH Van Beek, and CJ Van Westen (2009). „Parameterizing a physically based shallow landslide model in a data poor region“. In: *Earth Surface Processes and Landforms* 34.6, pp. 867–881.
- Landrieu, Loic and Martin Simonovsky (2017). „Large-scale point cloud semantic segmentation with superpoint graphs“. In: *arXiv preprint arXiv:1711.09869*.
- Lappi, Juha (2006). „A multivariate, nonparametric stem-curve prediction method“. In: *Canadian Journal of Forest Research* 36.4, pp. 1017–1027.
- Lari, Z, A Habib, and E Kwak (2011). „An adaptive approach for segmentation of 3D laser point cloud“. In: *ISPRS Workshop laser scanning*, pp. 29–31.
- Lee, Woo-Kyun, Jeong-Ho Seo, Young-Mo Son, Kyeong-Hak Lee, and Klaus Von Gadow (2003). „Modeling stem profiles for *Pinus densiflora* in Korea“. In: *Forest Ecology and Management* 172.1, pp. 69–77.
- Lefsky, Michael A, Warren B Cohen, Geoffrey G Parker, and David J Harding (2002). „Lidar remote sensing for ecosystem studies: Lidar, an emerging remote sensing technology that directly measures the three-dimensional distribution of plant canopies, can accurately estimate vegetation structural attributes and should be of particular interest to forest, landscape, and global ecologists“. In: *AIBS Bulletin* 52.1, pp. 19–30.
- Levick, Shaun R, Dominik Hessenmöller, and E-Detlef Schulze (2016). „Scaling wood volume estimates from inventory plots to landscapes with airborne LiDAR in temperate deciduous forest“. In: *Carbon Balance and Management* 11.1, pp. 7.1–7.14.
- Li, Shihua, Leiyu Dai, Hongshu Wang, et al. (2017). „Estimating leaf area density of individual trees using the point cloud segmentation of terrestrial LiDAR data and a voxel-based model“. In: *Remote Sensing* 9.11, p. 1202.
- Li, Wenkai, Qinghua Guo, Marek K Jakubowski, and Maggi Kelly (2012). „A new method for segmenting individual trees from the lidar point cloud“. In: *Photogrammetric Engineering & Remote Sensing* 78.1, pp. 75–84.
- Li, Yangyan, Rui Bu, Mingchao Sun, and Baoquan Chen (2018). „PointCNN“. In: *arXiv preprint arXiv:1801.07791*.
- Li, Zhan, Ewan Douglas, Alan Strahler, et al. (2013). „Separating leaves from trunks and branches with dual-wavelength terrestrial LiDAR scanning“. In: *Geoscience and Remote Sensing Symposium (IGARSS), 2013 IEEE International*. IEEE, pp. 3383–3386.
- Liang, Xinlian, Paula Litkey, Juha Hyypä, et al. (2012). „Automatic stem mapping using single-scan terrestrial laser scanning“. In: *IEEE Transactions on Geoscience and Remote Sensing* 50.2, pp. 661–670.
- Liang, Xinlian, Ville Kankare, Xiaowei Yu, Juha Hyypä, and Markus Holopainen (2014a). „Automated stem curve measurement using terrestrial laser scanning“. In: *IEEE Transactions on Geoscience and Remote Sensing* 52.3, pp. 1739–1748.
- Liang, Xinlian, Antero Kukko, Harri Kaartinen, et al. (2014b). „Possibilities of a personal laser scanning system for forest mapping and ecosystem services“. In: *Sensors* 14.1, pp. 1228–1248.

- Liang, Xinlian, Juha Hyyppä, Antero Kukko, et al. (2014c). „The use of a mobile laser scanning system for mapping large forest plots“. In: *IEEE Geoscience and Remote Sensing Letters* 11.9, pp. 1504–1508.
- Liang, Xinlian, Ville Kankare, Juha Hyyppä, et al. (2016). „Terrestrial laser scanning in forest inventories“. In: *ISPRS Journal of Photogrammetry and Remote Sensing* 115, pp. 63–77.
- Lim, Kevin, Paul Treitz, Michael Wulder, Benoît St-Onge, and Martin Flood (2003). „LiDAR remote sensing of forest structure“. In: *Progress in physical geography* 27.1, pp. 88–106.
- Litkey, P, X Liang, H Kaartinen, et al. (2008). „Single-scan TLS methods for forest parameter retrieval“. In: *Proceedings of SilviLaser 2008*, 8th.
- Liu, Ming, François Pomerleau, Francis Colas, and Roland Siegwart (2012). „Normal estimation for pointcloud using GPU based sparse tensor voting“. In: *Robotics and Biomimetics (ROBIO), 2012 IEEE International Conference on*. IEEE, pp. 91–96.
- Lovell, JL, D LB Jupp, DS Culvenor, and NC Coops (2003). „Using airborne and ground-based ranging lidar to measure canopy structure in Australian forests“. In: *Canadian Journal of Remote Sensing* 29.5, pp. 607–622.
- Ma, Lixia, Guang Zheng, Jan UH Eitel, et al. (2016). „Improved salient feature-based approach for automatically separating photosynthetic and nonphotosynthetic components within terrestrial lidar point cloud data of forest canopies“. In: *IEEE Transactions on Geoscience and Remote Sensing* 54.2, pp. 679–696.
- Maas, H-G, A Bienert, St Scheller, and E Keane (2008). „Automatic forest inventory parameter determination from terrestrial laser scanner data“. In: *International Journal of Remote Sensing* 29.5, pp. 1579–1593.
- Marcot, Bruce G, J Douglas Steventon, Glenn D Sutherland, and Robert K McCann (2006). „Guidelines for developing and updating Bayesian belief networks applied to ecological modeling and conservation“. In: *Canadian Journal of Forest Research* 36.12, pp. 3063–3074.
- Martinuzzi, Sebastián, Lee A Vierling, William A Gould, et al. (2009). „Mapping snags and understory shrubs for a LiDAR-based assessment of wildlife habitat suitability“. In: *Remote Sensing of Environment* 113.12, pp. 2533–2546.
- Matérn, Bertil (1956). „On the geometry of the cross-section of a stem“. In: *Meddelanden från Statens Skogsforskningsinstitut* 46.11, p. 28.
- Mitchard, Edward TA, Sassan S Saatchi, Iain H Woodhouse, et al. (2009). „Using satellite radar backscatter to predict above-ground woody biomass: A consistent relationship across four different African landscapes“. In: *Geophysical Research Letters* 36.23.
- Moskal, L Monika and Guang Zheng (2011). „Retrieving forest inventory variables with terrestrial laser scanning (TLS) in urban heterogeneous forest“. In: *Remote Sensing* 4.1, pp. 1–20.
- Mücke, Werner, Balázs Deák, Anke Schroiff, Markus Hollaus, and Norbert Pfeifer (2013). „Detection of fallen trees in forested areas using small footprint airborne laser scanning data“. In: *Canadian Journal of Remote Sensing* 39.sup1, S32–S40.
- Muja, Marius and David G Lowe (2014). „Scalable nearest neighbor algorithms for high dimensional data“. In: *IEEE transactions on pattern analysis and machine intelligence* 36.11, pp. 2227–2240.

- Návar, José (2009). „Biomass component equations for Latin American species and groups of species“. In: *Annals of Forest Science* 66.2, pp. 1–21.
- Nord-Larsen, Thomas and Johannes Schumacher (2012). „Estimation of forest resources from a country wide laser scanning survey and national forest inventory data“. In: *Remote Sensing of Environment* 119, pp. 148–157.
- Olofsson, Kenneth, Johan Holmgren, and Håkan Olsson (2014). „Tree stem and height measurements using terrestrial laser scanning and the ransac algorithm“. In: *Remote Sensing* 6.5, pp. 4323–4344.
- Papon, Jeremie, Alexey Abramov, Markus Schoeler, and Florentin Wörgötter (2013). „Voxel cloud connectivity segmentation-supervoxels for point clouds“. In: *Computer Vision and Pattern Recognition (CVPR), 2013 IEEE Conference on*. IEEE, pp. 2027–2034.
- Park, Min Ki, Seung Joo Lee, and Kwan H Lee (2012). „Multi-scale tensor voting for feature extraction from unstructured point clouds“. In: *Graphical Models* 74.4, pp. 197–208.
- Peng, Bo, Lei Zhang, and David Zhang (2011). „Automatic image segmentation by dynamic region merging“. In: *IEEE Transactions on image processing* 20.12, pp. 3592–3605.
- Pfeifer, N and G Mandlbürger (2008). „LiDAR data filtering and DTM generation“. In: *The Oxford Handbook of Innovation*. Ed. by Shan Jie and Toth K. Charles. Topographic Laser Ranging, Scanning: Principles, and Processing. Chap. 11, pp. 307–334.
- Pfeifer, N, G Mandlbürger, J Otepka, and W Karel (2014). „OPALS—A framework for Airborne Laser Scanning data analysis“. In: *Computers, Environment and Urban Systems* 45, pp. 125–136.
- Pfeifer, Norbert and Daniel Winterhalder (2004). „Modelling of tree cross sections from terrestrial laser scanning data with free-form curves“. In: *International Archives of the Photogrammetry, Remote Sensing and Spatial Information Sciences* 36.8/W2, pp. 76–81.
- Pfennigbauer, Martin and Andreas Ullrich (2010). „Improving quality of laser scanning data acquisition through calibrated amplitude and pulse deviation measurement“. In: *SPIE Defense, Security, and Sensing*. International Society for Optics and Photonics, 76841F–76841F.
- Plomion, Christophe, Grégoire Leprovost, and Alexia Stokes (2001). „Wood formation in trees“. In: *Plant Physiology* 127.4, pp. 1513–1523.
- Pöchtrager, Markus, Gudrun Styhler-Aydin, Marina Döring-Williams, and Norbert Pfeifer (2017). „Automated reconstruction of historic roof structures from point clouds - development and examples“. In: *ISPRS Annals of the Photogrammetry, Remote Sensing and Spatial Information Sciences* IV-2/W2, pp. 195–202.
- Price, Martin, Georg Gratzler, Lalisa Alemayehu Duguma, Thomas Kohler, and Daniel Maselli (2011). *Mountain Forests in a Changing World: Realizing Values, Addressing Challenges*. Food and Agriculture Organization of the United Nations (FAO): Rome, Italy.
- Pueschel, Pyare, Glenn Newnham, Gilles Rock, et al. (2013). „The influence of scan mode and circle fitting on tree stem detection, stem diameter and volume extraction from terrestrial laser scans“. In: *ISPRS journal of photogrammetry and remote sensing* 77, pp. 44–56.

- Puttonen, Eetu, Matti Lehtomäki, Harri Kaartinen, et al. (2013). „Improved sampling for terrestrial and mobile laser scanner point cloud data“. In: *Remote Sensing* 5.4, pp. 1754–1773.
- Puttonen, Eetu, Christian Briese, Gottfried Mandlburger, et al. (2016). „Quantification of overnight movement of birch (*Betula pendula*) branches and foliage with short interval terrestrial laser scanning“. In: *Frontiers in plant science* 7, pp. 222.1–222.13.
- Qi, Charles R, Hao Su, Kaichun Mo, and Leonidas J Guibas (2017). „Pointnet: Deep learning on point sets for 3d classification and segmentation“. In: *Proc. Computer Vision and Pattern Recognition (CVPR), IEEE* 1.2, p. 4.
- Rabbani, Tahir, Frank Van Den Heuvel, and George Vosselmann (2006). „Segmentation of point clouds using smoothness constraint“. In: *International archives of photogrammetry, remote sensing and spatial information sciences* 36.5, pp. 248–253.
- Raumonen, Pasi, Mikko Kaasalainen, Markku Åkerblom, et al. (2013). „Fast automatic precision tree models from terrestrial laser scanner data“. In: *Remote Sensing* 5.2, pp. 491–520.
- Razak, Khamarrul A, Alexander Bucksch, Michiel Damen, et al. (2013). „Characterizing tree growth anomaly induced by landslides using LiDAR“. In: *Landslide Science and Practice*. Springer, pp. 235–241.
- Reitberger, J, PI Krzystek, and U Stilla (2008). „Analysis of full waveform LIDAR data for the classification of deciduous and coniferous trees“. In: *International journal of remote sensing* 29.5, pp. 1407–1431.
- Repola, Jaakko (2008). „Biomass equations for Birch in Finland“. In: *Silva Fennica* 42.4, pp. 605–624.
- (2009). „Biomass equations for Scots pine and Norway spruce in Finland“. In: *Silva Fennica* 43.4, pp. 625–647.
- Rodríguez-Veiga, Pedro, James Wheeler, Valentin Louis, Kevin Tansey, and Heiko Balzter (2017). „Quantifying forest biomass carbon stocks from space“. In: *Current Forestry Reports* 3.1, pp. 1–18.
- Rosenqvist, Ake, Masanobu Shimada, Norimasa Ito, and Manabu Watanabe (2007). „ALOS PALSAR: A pathfinder mission for global-scale monitoring of the environment“. In: *IEEE Transactions on Geoscience and Remote Sensing* 45.11, pp. 3307–3316.
- Roy, David P, MA Wulder, Thomas R Loveland, et al. (2014). „Landsat-8: Science and product vision for terrestrial global change research“. In: *Remote sensing of Environment* 145, pp. 154–172.
- Russell, Robin E, Victoria A Saab, and Jonathan G Dudley (2007). „Habitat-suitability models for cavity-nesting birds in a postfire landscape“. In: *Journal of Wildlife Management* 71.8, pp. 2600–2611.
- Schmaltz, Elmar, Stefan Steger, Rainer Bell, et al. (2016). „Exploring possibilities of including detailed ALS derived biomass information into physically-based slope stability models at regional scale“. In: *Proceedings of the 12th International Symposium on Landslides (Napoli, Italy, 12-19 June 2016)*. Informa UK Limited, pp. 1807–1815.

- Schmaltz, Elmar M, Stefan Steger, and Thomas Glade (2017). „The influence of forest cover on landslide occurrence explored with spatio-temporal information“. In: *Geomorphology* 290, pp. 250–264.
- Spehn, Eva M, Katrin Rudmann-Maurer, and Christian Körner (2011). „Mountain biodiversity“. In: *Plant Ecology & Diversity* 4.4, pp. 301–302.
- Spracklen, DV and R Righelato (2014). „Tropical montane forests are a larger than expected global carbon store“. In: *Biogeosciences* 11.10, pp. 2741–2754.
- Stängle, Stefan M, Aaron R Weiskittel, Carsten F Dormann, and Franka Brüchert (2015). „Measurement and prediction of bark thickness in *Picea abies*: assessment of accuracy, precision, and sample size requirements“. In: *Canadian Journal of Forest Research* 46.1, pp. 39–47.
- Steger, Stefan, Thomas Glade, Markus Hollaus, et al. (2015). „Quantifying the effect of biomass and its change on landslide activity at regional scale“. In: *EGU General Assembly 2015*. Ed. by Geophysical Research Abstracts. Vol. 17, EGU2015–13587.
- Sun, Hua, Guangxing Wang, Hui Lin, et al. (2015). „Retrieval and Accuracy Assessment of Tree and Stand Parameters for Chinese Fir Plantation Using Terrestrial Laser Scanning“. In: *Geoscience and Remote Sensing Letters, IEEE* 12.9, pp. 1993–1997.
- Tao, Shengli, Qinghua Guo, Yanjun Su, et al. (2015a). „A geometric method for wood-leaf separation using terrestrial and simulated lidar data“. In: *Photogrammetric Engineering & Remote Sensing* 81.10, pp. 767–776.
- Tao, Shengli, Fangfang Wu, Qinghua Guo, et al. (2015b). „Segmenting tree crowns from terrestrial and mobile LiDAR data by exploring ecological theories“. In: *ISPRS Journal of Photogrammetry and Remote Sensing* 110, pp. 66–76.
- Taubin, Gabriel (1991). „Estimation of planar curves, surfaces, and nonplanar space curves defined by implicit equations with applications to edge and range image segmentation“. In: *IEEE Transactions on Pattern Analysis & Machine Intelligence* 11, pp. 1115–1138.
- Thies, M and H Spiecker (2004). „Evaluation and future prospects of terrestrial laser scanning for standardized forest inventories“. In: *Forest* 2.2.2, p. 1.
- Thies, Michael, Norbert Pfeifer, Daniel Winterhalder, and Ben GH Gorte (2004). „Three-dimensional reconstruction of stems for assessment of taper, sweep and lean based on laser scanning of standing trees“. In: *Scandinavian Journal of Forest Research* 19.6, pp. 571–581.
- Valente, Clara, Raffaele Spinelli, Bengt Gunnar Hillring, and Birger Solberg (2014). „Mountain forest wood fuel supply chains: Comparative studies between Norway and Italy“. In: *Biomass and Bioenergy* 71, pp. 370–380.
- Vapnik, V.N. (1995). *The Nature of Statistical Learning Theory*. Springer: New York, USA.
- Vauhkonen, Jari, Ilkka Korpela, Matti Maltamo, and Timo Tokola (2010). „Imputation of single-tree attributes using airborne laser scanning-based height, intensity, and alpha shape metrics“. In: *Remote Sensing of Environment* 114.6, pp. 1263–1276.
- Vauhkonen, Jari, Teemu Hakala, Juha Suomalainen, et al. (2013). „Classification of spruce and pine trees using active hyperspectral LiDAR“. In: *IEEE Geoscience and Remote Sensing Letters* 10.5, pp. 1138–1141.

- Véga, Cédric, A Hamrouni, S El Mokhtari, et al. (2014). „PTrees: A point-based approach to forest tree extraction from lidar data“. In: *International Journal of Applied Earth Observation and Geoinformation* 33, pp. 98–108.
- Vosselman, George (2013). „Point cloud segmentation for urban scene classification“. In: *International archives of photogrammetry, remote sensing and spatial information sciences* 1, pp. 257–262.
- Vosselman, George, Maximilian Coenen, and Franz Rottensteiner (2017). „Contextual segment-based classification of airborne laser scanner data“. In: *ISPRS journal of photogrammetry and remote sensing* 128, pp. 354–371.
- Wagner, Wolfgang, Andreas Ullrich, Vesna Ducic, Thomas Melzer, and Nick Studnicka (2006). „Gaussian decomposition and calibration of a novel small-footprint full-waveform digitising airborne laser scanner“. In: *ISPRS journal of Photogrammetry and Remote Sensing* 60.2, pp. 100–112.
- Wagner, Wolfgang, Markus Hollaus, Christian Briese, and Vesna Ducic (2008). „3D vegetation mapping using small-footprint full-waveform airborne laser scanners“. In: *International Journal of Remote Sensing* 29.5, pp. 1433–1452.
- Wang, Di, Markus Hollaus, Eetu Puttonen, and Norbert Pfeifer (2016a). „Automatic and self-adaptive stem reconstruction in landslide-affected forests“. In: *Remote Sensing* 8.12, pp. 974.1–974.23.
- (2016b). „Fast and robust stem reconstruction in complex environments using terrestrial laser scanning“. In: *International Archives of the Photogrammetry, Remote Sensing and Spatial Information Sciences*. Vol. XLI-B3, pp. 411–417.
- Wang, Di, Markus Hollaus, and Norbert Pfeifer (2017a). „Feasibility of machine learning methods for separating wood and leaf points from terrestrial laser scanning data“. In: *ISPRS Annals of the Photogrammetry, Remote Sensing and Spatial Information Sciences* IV-2/W4, pp. 157–164.
- Wang, Di, Ville Kankare, Eetu Puttonen, Markus Hollaus, and Norbert Pfeifer (2017b). „Reconstructing stem cross section shapes from terrestrial laser scanning“. In: *IEEE Geoscience and Remote Sensing Letters* 14.2, pp. 272–276.
- Wang, Di, Jasmin Brunner, Zhenyu Ma, et al. (2018). „Separating Tree Photosynthetic and Non-Photosynthetic Components from Point Cloud Data Using Dynamic Segment Merging“. In: *Forests* 9.5, pp. 252–1–252–23.
- Watson, Geoffrey S (1967). „Linear least squares regression“. In: *The Annals of Mathematical Statistics*, pp. 1679–1699.
- Watt, PJ and DNM Donoghue (2005). „Measuring forest structure with terrestrial laser scanning“. In: *International Journal of Remote Sensing* 26.7, pp. 1437–1446.
- Weinmann, M, Steffen Urban, Stefan Hinz, Boris Jutzi, and Clément Mallet (2015). „Distinctive 2D and 3D features for automated large-scale scene analysis in urban areas“. In: *Computers & Graphics* 49, pp. 47–57.
- Weinmann, Martin, Boris Jutzi, and Clément Mallet (2013). „Feature relevance assessment for the semantic interpretation of 3D point cloud data“. In: *ISPRS Annals of the Photogrammetry, Remote Sensing and Spatial Information Sciences* II-5/W2, pp. 313–318.

- Weinmann, Martin, Boris Jutzi, and Clément Mallet (2014). „Semantic 3D scene interpretation: a framework combining optimal neighborhood size selection with relevant features“. In: *ISPRS Annals of the Photogrammetry, Remote Sensing and Spatial Information Sciences* 2.3, p. 181.
- Weinmann, Martin, Michael Weinmann, Clément Mallet, and Mathieu Brédif (2017). „A Classification-Segmentation Framework for the Detection of Individual Trees in Dense MMS Point Cloud Data Acquired in Urban Areas“. In: *Remote Sensing* 9.3, pp. 277.1–277.28.
- Wezyk, P, K Koziol, M Glista, and M Pierzchalski (2007). „Terrestrial laser scanning versus traditional forest inventory. First results from the Polish forests“. In: *Proceedings of the ISPRS Workshop 'Laser Scanning*, pp. 12–14.
- Wieser, Martin, Markus Hollaus, Gottfried Mandlburger, Norbert Pfeifer, and Philipp Glira (2016). „ULS LiDAR supported analyses of laser beam penetration from different ALS systems into vegetation“. In: *ISPRS Annals of the Photogrammetry, Remote Sensing and Spatial Information Sciences*. Vol. III-3, pp. 233–239.
- Wulder, Michael A, Nicholas C Coops, Andrew T Hudak, et al. (2013). „Status and prospects for LiDAR remote sensing of forested ecosystems“. In: *Canadian Journal of Remote Sensing* 39.sup1, S1–S5.
- Xia, Shaobo, Cheng Wang, Feifei Pan, et al. (2015). „Detecting stems in dense and homogeneous forest using single-scan TLS“. In: *Forests* 6.11, pp. 3923–3945.
- Xu, Y, L Hoegner, S Tuttas, and U Stilla (2017a). „Voxel-and graph-based point cloud segmentation of 3d scenes using perceptual grouping laws“. In: *ISPRS Annals of the Photogrammetry, Remote Sensing and Spatial Information Sciences* 4, p. 43.
- Xu, Yusheng, Wei Yao, Ludwig Hoegner, and Uwe Stilla (2017b). „Segmentation of building roofs from airborne LiDAR point clouds using robust voxel-based region growing“. In: *Remote Sensing Letters* 8.11, pp. 1062–1071.
- Yao, Tian, Xiaoyuan Yang, Feng Zhao, et al. (2011). „Measuring forest structure and biomass in New England forest stands using Echidna ground-based lidar“. In: *Remote Sensing of Environment* 115.11, pp. 2965–2974.
- You, Lei, Shouzheng Tang, Xinyu Song, et al. (2016). „Precise measurement of stem diameter by simulating the path of diameter tape from terrestrial laser scanning data“. In: *Remote Sensing* 8.9, p. 717.
- Yun, Ting, Feng An, Weizheng Li, et al. (2016). „A novel approach for retrieving tree leaf area from ground-based LiDAR“. In: *Remote Sensing* 8.11, pp. 942.1–942.21.
- Zhang, Wuming, Jianbo Qi, Peng Wan, et al. (2016). „An easy-to-use airborne LiDAR data filtering method based on cloth simulation“. In: *Remote Sensing* 8.6, p. 501.
- Zheng, Guang, L Monika Moskal, and Soo-Hyung Kim (2013). „Retrieval of effective leaf area index in heterogeneous forests with terrestrial laser scanning“. In: *IEEE Transactions on Geoscience and Remote Sensing* 51.2, pp. 777–786.
- Zhu, Xi, Tiejun Wang, Roshanak Darvishzadeh, Andrew K Skidmore, and K Olaf Niemann (2015). „3D leaf water content mapping using terrestrial laser scanner backscatter intensity with radiometric correction“. In: *ISPRS journal of photogrammetry and remote sensing* 110, pp. 14–23.

Zhu, Xi, Andrew K Skidmore, Roshanak Darvishzadeh, et al. (2018). „Foliar and woody materials discriminated using terrestrial LiDAR in a mixed natural forest“. In: *International Journal of Applied Earth Observation and Geoinformation* 64, pp. 43–50.

